Neue Elemente in einer Erweiterung der Suche nach supersymmetrischen skalaren top quarks mit dem ATLAS Detektor in LHC Run 2

New elements to extend the search for supersymmetric scalar top quarks with the ATLAS detector in LHC Run 2

Masterarbeit an der Fakultät für Physik
der
Ludwig-Maximilians-Universität München

vorgelegt von
Michael Holzbock
geboren in München

München, den 5. Mai 2016

Gutachterin: Prof. Dr. Dorothee Schaile

Abstract

Supersymmetry is a promising extension of the Standard Model as it provides mathematically elegant solutions to several of its shortcomings. This thesis presents studies in the search for a supersymmetric partner of the top quark in Run 2 of the LHC with the ATLAS detector. The search is based on a class of models in which the scalar top decays via a three-body decay into a scalar tau, neutrino and b-quark. The adequate modeling of the signal of interest with a new Monte-Carlo generator setup with respect to the Run 1 analysis has been validated. The good performance of single-lepton triggers was studied by analyzing the gain of additional combined triggers and a $E_{\mathrm{T}}^{\mathrm{miss}}$ trigger, respectively. Two signal enriched regions have been designed to represent scenarios in which the scalar tau is either light or heavy with respect to the scalar top. These Signal Regions have been optimized for an integrated luminosity of 10 fb^{-1} to balance sensitivity and background uncertainty. In conjunction with preliminary background enriched regions, the Signal Regions show for 10 fb^{-1} already a discovery reach up to 700 GeV for scalar top masses, which is beyond the Run 1 exclusion limit. Even in the absence of signal, the expected exclusion range for scalar top masses increases up to 800 GeV, which makes the search a promising candidate at the summer conferences for high-energy physics in 2016.

Contents

1 Introduction

On 3 June 2015 the hunt for physics beyond the Standard Model entered the second round: The Large Hadron Collider started to deliver data again. During the two-year shutdown countless efforts in all fields have been made to enhance sensitivity for new physics at elementary particle level. Now particles in the accelerator collide at the unprecedented center of mass energy $\sqrt{s} = 13$ TeV. The detectors have been upgraded substantially to improve reconstruction of physical objects. Algorithms, especially at trigger level, used in the reconstruction have been revised to match the new conditions at the interaction points. Grid computing technology, needed to process the huge amount of incoming data, got upgraded in terms of performance. Theorists adjusted their models (or proposed new ones) according to the Run 1 results and refined the prediction of the Standard Model processes. Experimentalists checked promising models for sensitivity long before the first event was even recorded.

All these efforts raise a natural question: Why do so many theorists, experimentalists, engineers and people from the IT still invest so much time and knowledge in particle physics? Particularly with regard to the (most likely) discovery of the Higgs boson in 2012 that was the last missing Standard Model component. With the Standard Model completed and successfully describing nearly all phenomena on the elementary particle level, at the first glance there does not seem to be much need for accessing physics at such a small scale that it is irrelevant for our everyday's world.

There is actually more than one answer to the question above. And the spectrum of answers is probably as diverse as the community of particle physics itself: Ranging from personal inclination to face all kinds of technical challenges to the common point of view, that the Standard Model is a—very successful—low-energy approximation of a deeper theory. In this sense a rather surprisingly facet is that the results of particle physics are not only relevant on the smallest, but also on the largest scales. Since a long time it is known from astronomical observations that only a small fraction of the universe consists of matter and to a lesser extent anti-matter, whose interactions are well-understood. The rest is still unknown, but at least named: Dark Matter and Dark Energy. As astronomical observations cannot determine the nature of Dark Matter [1], its origin and structure have to be studied in collider experiments. Statements about this unknown components of our universe will definitely aid to set up cosmological models, explaining the origin of the universe. This intrinsic link of particle physics to the origin of the universe, one of the oldest questions in human history, makes all the huge efforts well motivated.

2 Concepts of Supersymmetry

Originally supersymmetric theories have not been developed directly to extend the Standard Model (SM) but for quite different reasons, including purely aesthetic ones [2]. When it turned out that SUSY can actually address quite successfully many shortcomings of the SM in a mathematical elegant way, its application in particle physics was elaborated to a point which makes it one of the best studied beyond Standard Model (BSM) candidates. This chapter will motivate BSM theories and summarize the main features of SUSY, its mathematical implementation and the particle content of the Minimal Supersymmetric Standard Model (MSSM).

2.1 Motivation

Besides the great success of the SM for describing phenomena at the reachable subatomic scale, it is generally viewed as just the first step towards a more fundamental theory. Such a "theory of everything", capable of modeling all known physics to arbitrary precision in a common framework, is indeed a very appealing idea. An approach to get there is to understand the shortcomings of the SM and to eliminate them with extensions so that a new, more complete description emerges. The nature of these shortcomings is quite diverse, ranging from the theoretical unattractive need for fine-tuning in the SM to the more obvious lack of a proper Dark Matter candidate and thus a lack of the origin of a good amount of the mass in the universe. As Supersymmetry can address quite a lot of these shortcomings, the subsequent sections will shortly review the most striking ones.

2.1.1 Naturalness

Besides providing an elegant solution for the masses of the gauge bosons via spontaneous symmetry breaking, the Higgs field leads to a well known problem that generally occurs for fundamental scalar fields: quadratic divergences when defining a cut-off scale Λ [3]. To see this, one can take a look at the 4-boson self interaction resulting from the ϕ^4 term in the Higgs potential [4]

$$V = -\mu^2 \phi^\dagger \phi + \frac{\lambda}{4}(\phi^\dagger \phi)^2 \tag{2.1}$$

where $\mu^2 > 0$, the Higgs self interaction $\lambda > 0$ and ϕ is the SU(2) doublet field. This self interaction will contribute to the $\phi^\dagger \phi$ term as

$$\delta\mu^2 = \lambda \int^\Lambda \frac{\mathrm{d}^4 k}{(2\pi)^4} \frac{1}{k^2} \propto \frac{\lambda}{16\pi^2}\Lambda^2 \tag{2.2}$$

Although the renormalizibility of the SM grants finite results even when Λ goes to infinity, the cut-off scale reflects often the energy scale where new physics are about to happen, i.e. the description of the SM will not be valid anymore. This will be for sure when the gravitational force cannot be neglected, which will ultimately be the case at the Planck scale $M_P \sim 10^{19}$ GeV†. The 1-loop correction in Equation 2.2 leads to a replacement of the parameter $-\mu^2$ in the Higgs potential by $-\mu^2_{\text{phys}} = -\mu^2 + \delta\mu^2$ or equivalently and neglecting numerical factors [4]

$$\mu^2_{\text{phys}} = \mu^2 - \lambda\Lambda^2 \tag{2.3}$$

From experiment it is known that μ^2_{phys} is of the order (100 GeV)^2. For the Planck scale Λ^2 would be of order (10^{19} GeV)^2 and therefore forces μ^2 to be of the same magnitude. To end up at μ^2_{phys} there have to be large cancellations over several orders of magnitude. This is the so called and unpleasant fine-tuning that furthermore contradicts the concept of naturalness. This states that the observable properties of a theory (e.g. masses) should be stable under small variations of the fundamental parameters [3]. If the cut-off Λ is at a lower value, i.e. new physics happens already at a lower energy the fine-tuning problem will be less severe. The SM is commonly viewed to be natural until the TeV scale, so when this scale is reached in experiment, new physics should happen from a "natural" point of view.

Not only self-interactions will lead to loop corrections for μ but also fermion loops will contribute to the Higgs self-energy. The problem of quadratic divergences affects only scalar particles as the other particles in the SM are protected by gauge and chiral symmetries [4]. The idea of SUSY is to impose a symmetry between fermions and bosons so that scalars get a similar protection. Practically, SUSY gives rise to a bunch of new particles and hence even more terms that contribute to the corrections. But as fermionic and bosonic loops contribute with a different sign, the contributions of fermions and bosons related by SUSY will cancel exactly if SUSY is an unbroken symmetry. This would even hold for arbitrary large Λ, so that SUSY provides a elegant solution to the fine-tuning problem and ensures naturalness on all scales.

2.1.2 Dark Matter

One of the most astounding observations in the last century has been that the universe is not formed by ordinary matter alone. Baryonic matter does by far not even contribute the most as there is roughly about five times more of some unknown kind of matter, denoted as Dark Matter.

The first astronomical observations of missing mass date back to the 1930s [5]. The visible mass, extracted from mass to luminosity ratios, could not explain all observed phenomena, e.g. the motion of stars. Another very instructive evidence had been made in the study of rotation curves of isolated galaxies. The rotational profile was deduced by the spectral lines of hot stars using surrounding clouds of hydrogen and helium as tracers. Assuming a "Keplerian" behavior, the orbits of the stars in the galaxy will

† In this theses natural units are used, so that $c = \hbar = 1$.

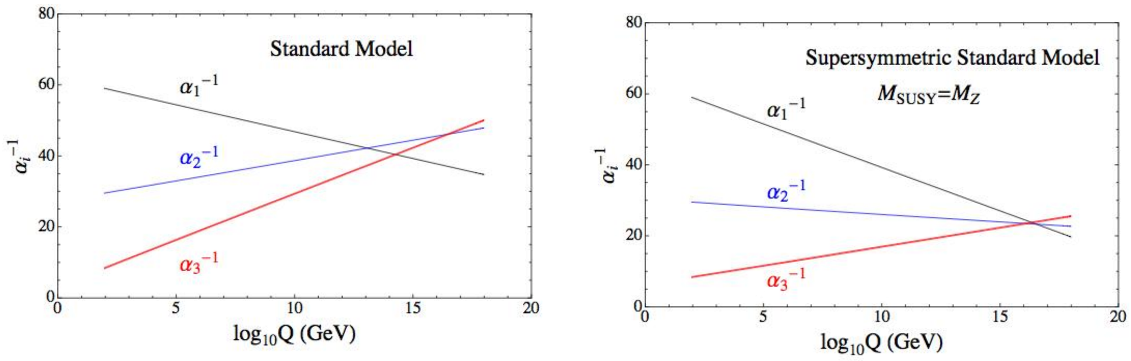

Figure 2.1: Running of the gauge couplings in the SM (left) and in a SUSY model (right). Figure taken from [6].

be similar to the motion of the planets in the solar system and thus their velocity should decrease with the radius as $v(r) \propto 1/\sqrt{r}$. However, observation pointed out an increase of v with the radius from the center until reaching a limit. This deviation from expectation showed that the picture of a luminous galaxy center containing the bulk of the galaxy's mass has to be abandoned in favor of a model in which there is additional, invisible mass somehow distributed across the galaxy. The discovery of gravitational lensing further increased the evidence. According to General Relativity light will follow its geodesic in space time with a curvature determined by the mass in the universe. That means light emitted from a distant source will bend around closer, massive objects (e.g. a cluster of galaxies) and be visible as a (partial) ring around the close object. The actual observation of such arclets and that the luminating mass cannot account for this phenomenon confirmed the existence of Dark Matter.

While the creation of Dark Matter during the hot expansion of the universe and its relic abundance can be modeled in terms of statistical thermodynamics, its exact nature is still unknown. Generally Dark Matter candidates are referred to as WIMPs (weakly interacting massive particles) ruling out every particle of the SM except the neutrino. However neutrinos are commonly disregarded due to their relativistic nature that would contradict some cosmological observations. Many SUSY models provide a natural Dark Matter candidate, the lightest supersymmetric particle (LSP). It fulfills all requirements and, in case of a neutralino as LSP, fits well into the explanations for the current relic abundance.

2.1.3 Unification of coupling Constants

A very appealing idea is that the three "running", i.e. scale dependent, gauge couplings α_1, α_2 and α_3 of the SM gauge group $\mathrm{SU}(2)_c \times \mathrm{SU}(2)_L \times \mathrm{U}(1)_Y$ will converge at some high energy scale Q_U. This would be the Grand Unification of the SM interactions. The running of the couplings is described with the renormalization group equation and, to 1-loop order, has the form [4]

$$\frac{\mathrm{d}\alpha_i}{\mathrm{d}t} = -\frac{b_i}{2\pi}\alpha_i^2 \tag{2.4}$$

where $t = \ln Q$ with Q the running energy scale and the coefficients b_i reflecting the kind of gauge group and the particle multiplets it couples to. Equation 2.4 can be reformulated for the inverse couplings and integrated to give

$$\alpha_i^{-1} = \alpha_i^{-1}(Q_0) + \frac{b_i}{2\pi}\ln\frac{Q}{Q_0} \tag{2.5}$$

where Q_0 is the scale where the running starts. In the SM the three couplings will come quite close, but do not really converge as it is shown in the left plot of Figure 2.1. In SUSY models, especially the well studied Minimal Supersymmetric Standard Model, the couplings may show a clear unification point and mark a scale for new physics (see the right plot of Figure 2.1). This scale is of course far larger than any accessible energy for collider experiments, e.g. in the MSSM $Q_U \approx 2.2 \times 10^{16}$ GeV. The remarkable point is, however, that the unification arises naturally out of the theory, which illustrates why SUSY is such a favored SM extension.

2.2 Implementation of Supersymmetry

In physics a symmetry is understood as a transformation of a physical object that keeps the object invariant. An often mentioned example is a sphere, that is invariant under rotations. Mathematically, the set of transformations of a certain kind form a group. The Poincaré group contains all space-time symmetries, namely invariance under translations, rotations and boosts. The basic idea of SUSY is to impose a new symmetry relating bosons and fermions and thus to enlarge the Poincaré group. That means a bosonic state can be transformed into a fermionic state and vice versa. Such a transformation is performed by a fermionic operator Q (carrying spin 1/2) so that schematically

$$Q\,|\mathrm{Boson}\rangle = |\mathrm{Fermion}\rangle\,, \qquad Q\,|\mathrm{Fermion}\rangle = |\mathrm{Boson}\rangle \tag{2.6}$$

holds. This is only possible if Q is an anti-commuting spinor as otherwise the Coleman-Mandula theorem forbids any nontrivial combination of space-time and internal symmetries [7]. As spinors are intrinsically complex, $Q^\dagger$ will also generate such transformations [2].

2.2.1 SUSY Algebra

The SUSY algebra is a set of commutation and anti-commutation relations that defines how the generators of SUSY transformations are embedded in the generators of the space-time symmetries, e.g.the generator of translations P_μ, with $\mu = 0, 1, 2, 3$. The

chiral supermultiplets

Names	spin 0	spin 1/2
squarks, quarks	$(\tilde{u}_L\ \tilde{d}_L)$ $\tilde{u}_R^*$ $\tilde{d}_R^*$	$(u_L\ d_L)$ $u_R^\dagger$ $d_R^\dagger$
sleptons, leptons	$(\tilde{\nu}\ \tilde{e}_L)$ $\tilde{e}_R^*$	$(\nu\ e_L)$ $e_R^\dagger$
Higgs, higgsinos	$(H_u^+\ H_u^0)$ $(H_d^0\ H_d^-)$	$(\tilde{H}_u^+\ \tilde{H}_u^0)$ $(\tilde{H}_d^0\ \tilde{H}_d^-)$

gauge supermultiplets

Names	spin 1/2	spin 1
gluino, gluon	$\tilde{g}$	g
Winos, W bosons	$\tilde{W}^\pm\ \tilde{W}^0$	$W^\pm\ W^0$
Bino, B boson	$\tilde{B}^0$	B^0

Table 2.1: Chiral and gauge supermultiplets for a minimal supersymmetric extension of the SM. Only the first matter generation for the lepton and quark sector is shown. The contents of the chiral supermultiplets are combined as $\mathrm{SU}(2)_L$ doublets and singlets, respectively, according to their transformation properties [2].

possible forms of this algebra are highly restricted [2] as features like chiral fermions enabling parity-violating interactions from the SM have to be kept. From the anti-commutation relations results that loosely speaking a combination of the SUSY generators Q and $Q^\dagger$ transforms like P_μ, i.e. translations. This illustrates the extension of the space-time symmetries.

2.2.2 Supermultiplets

In SUSY, the particles are arranged in the so-called supermultiplets, which are the irreducible representations of the SUSY algebra. As a supermultiplet contains boson and fermion states, these are known as superpartners of each other. In a supermultiplet the numbers of fermionic (n_F) and bosonic (n_B) degrees of freedom have to be the same [2] so that the simplest supermultiplet—called chiral supermultiplet—contains a single Weyl fermion ($n_F = 2$ because of the two spin helicity states) and a complex scalar field (real and imaginary part, so $n_B = 2$). As the SUSY generators Q and $Q^\dagger$ commute with the gauge transformation generators, a supermultiplet cannot contain different representations of the gauge group. This means that left- and right-handed states cannot be in the same supermultiplet.

All SM quarks and leptons, and their superpartners will reside in chiral supermultiplets. In addition there will also be the scalar Higgs sector. It turns out that at least two Higgs supermultiplets (each containing a weak isodoublet with weak hypercharge $Y = 1/2$ and $Y = -1/2$, respectively) are needed to avoid gauge anomalies and provide Yukawa couplings necessary to give mass to all particles. The neutral scalar corresponding to the SM Higgs boson is then a linear combination of the neutral parts of the doublets (namely H_u^0 and H_d^0). The left part of Table 2.1 gives an overview of the chiral supermultiplets needed for a phenomenologically consistent extension of the SM. As usual, the new fields are donated with a ~ above the associated symbol for the SM counterpart. In written text the superpartners of the fermions are referred to as sfermions, where the s stands for scalar. So the new particles are called scalar quarks and scalar leptons or short squarks and sleptons. In contrast, the superpartners of bosons will get the suffix “ino”.

The SM gauge bosons reside in gauge supermultiplets, which are arrangements of a massless spin 1 vector boson and a massless spin 1/2 Weyl fermion (a spin 3/2 fermion would not be renormalizable). The fermionic superpartners are called gauginos and summarized in the right part of Table 2.1.
The chiral and gauge supermultiplets in Table 2.1, complemented by the other fermion generations and the corresponding antiparticles, form the particle content of the MSSM. So far all SUSY particles would have the same mass as their SM counterparts. As not a single one of the SUSY particles has been observed, the symmetry has to be broken.

2.2.3 Symmetry Breaking

Although it is clear that SUSY must be a broken theory, the exact nature of the symmetry breaking and its mechanism is still unknown. In principle there are two ways for symmetry breaking in a theory: by explicit non-symmetric terms in the Lagrangian and via spontaneous symmetry breaking [4]. As there is no consensus how to break SUSY spontaneously, the first approach is mainly used in practice. The additional SUSY breaking terms are however heavily constrained, as they should not give rise to quadratic divergences, e.g. in the couplings, which would spoil the elegant solution to the fine-tuning problem of the SM. So the Lagrangian $\mathcal{L}$ will have the form

$$\mathcal{L} = \mathcal{L}_{\text{SUSY}} + \mathcal{L}_{\text{soft}}$$

where $\mathcal{L}_{\text{SUSY}}$ contains all of the gauge and Yukawa interactions [2] and $\mathcal{L}_{\text{soft}}$ violates SUSY assuming that the (unknown) breaking mechanism operates on a large energy scale and parametrizes its low-energy effects. As nevertheless over 100 parameters are needed for characterization the theory is quite variable and thus predictions are challenging. Furthermore soft symmetry breaking should also give rise to superpartner masses that differ not too much from the SM particles to maintain the cancellations between boson and fermion loop contributions. In fact the masses of SUSY particles should not be much above the TeV scale and thus accessible for the LHC.

2.3 Minimal Supersymmetric Standard Model

The SUSY Lagrangian consists of terms reflecting the free bosons and fermions, auxiliary fields that make the corresponding action invariant under SUSY transformations and a term which fixes the interactions and thus basically fixes the model. This term is called superpotential W and in the MSSM defined as [4]

$$W = y_u^{ij} \bar{u}_i Q_j H_u - y_d^{ij} \bar{d}_i Q_j H_d - y_e^{ij} \bar{e}_i L_j H_d + \mu H_u H_d \tag{2.7}$$

where the y_{ij} are 3×3 matrices in generation space and contain exactly the same Yukawa couplings as in the SM. The fields in Equation 2.7 are the superfields of the chiral multiplets in Table 2.1 indexed by their family. The first three terms give masses to the quarks and leptons while the "μ term" describes the coupling of the two different Higgs superfield doublets.

2.3.1 Particle Content

In principle Table 2.1 lists all fields of the MSSM. However the gauge eigenstates have not to be the mass eigenstates, so that the mass spectrum of the MSSM looks slightly different. After the electroweak symmetry breaking the eight degrees of freedom in the Higgs sector will form the three longitudinal modes of the massive vector bosons (Z^0 and $W^{\pm}$) and five scalars: the neutral h^0, H^0 (both CP-even) and A^0 (CP-odd) as well as the oppositely charged H^+ and H^- [2].
Due to effects of the electroweak symmetry breaking, the higgsinos and the gauginos can mix with each other. In particular the neutral higgsinos will mix with the neutral gauginos to form four mass eigenstates called neutralinos $\tilde{\chi}_i^0$ with $i = 1, 2, 3, 4$. Similarly the charged higgsinos and gauginos can mix to form the charginos $\tilde{\chi}_i^{\pm}$ with $i = 1, 2$. The indexing is ascending with respect to mass, so for example $m(\tilde{\chi}_1^0) < m(\tilde{\chi}_2^0)$. Many SUSY searches consider the lightest neutralino χ_1^0 as the LSP, as it is a very good candidate for Dark Matter.

Via soft symmetry breaking terms scalars with same electric charge, R-parity (see next chapter) and color quantum numbers can mix with each other across families [4]. For the first and second generation the mixing angles are predicted to be very small and thus suppressing inter-family mixing. This is not the case, however, for the third generation so that e.g. $(\tilde{t}_L, \tilde{t}_R)$ will form the mass eigenstates $\tilde{t}_1$ and $\tilde{t}_2$ (similarly for $\tilde{b}$ and $\tilde{\tau}$).

2.3.2 *R*-parity

The superpotential in Equation 2.7 could also be extended by other gauge-invariant and renormalizable terms that however violate lepton and baryon number conservation. Such processes have never been observed in nature and would also give rise to decay channels of the proton like $e^+\pi^0$ [4]. As the proton is stable, the corresponding terms in the Lagrangian have to be forbidden. For this purpose a new, multiplicatively conserved symmetry called R-parity is defined as

$$R = (-1)^{3B+L+2s} \tag{2.8}$$

where B is the baryon number, L the lepton number and s the spin of the particles. Thus R is always $+1$ for SM particle and -1 for their SUSY counterparts. In summary R-parity conservation forbids the additional terms excluded by experiment while allowing all MSSM interactions and has some further important consequences on phenomenology:

- the LSP is absolutely stable as there is no other SUSY particle it can decay into
- each SUSY particle except the LSP must decay into a state with an odd number of SUSY particles
- in collider experiments SUSY particles will be produced in pairs

A stable and neutral LSP will not be visible for a detector as it does interact with the detector material only weakly. Thus the LSP will carry away momentum and disequilibrate the vector sum of all momenta in an event. This missing energy can then be associated with the LSPs and will consequently play a significant role in most R-parity conservative SUSY searches.

2.3.3 Mechanism for SUSY breaking

An open question is still how the the symmetry is actually broken. Concepts based on spontaneous symmetry breaking have been developed but these theories are not compatible with the field content of the MSSM as they typically assign a vacuum expectation value to an appropriate field. As the MSSM lacks such a field, the soft terms are thought to emerge indirectly or radiatively [2]. The breaking of SUSY is modeled to occur in a hidden sector that couples not or just very weakly with the visible sector of the MSSM, the chiral supermultiplets. The soft breaking terms are then obtained by some messenger fields, that “communicate” the symmetry breaking from the hidden to the visible sector. There are multiple proposals for the nature of these messaging interactions.

One proposal is that the interactions are associated with new physics, including gravity that becomes relevant at the Planck scale, called Planck-scale-mediated supersymmetry breaking (PMSB) scenario. The significant feature of this proposal is that the LSP is the lightest neutralino.

Another popular assumption is that the messaging is performed by the electroweak and strong gauge interactions from the SM. In this gauge-mediated supersymmetry breaking (GMSB) model the communication is done via new messenger particles that couple to the supersymmetry breaking vacuum expectation value in the hidden sector and provide connection to the visible sector via the ordinary gauge interactions. In this scenario the LSP would be the gravitino, originating from supergravity (see next section).

Another interesting feature is that according to the Goldstone theorem one or more massless particles (“Goldstone bosons”) must be present when a symmetry is spontaneously broken. As the generators for the transformations are fermionic the emerging particle is a fermion called goldstino. This particles is important in the details of the symmetry breaking [3] and also plays the role of the LSP in some SUSY models.

2.4 Supergravity

Gravity can be included in SUSY by making the supersymmetric transformations local, i.e. dependent on space-time. The resulting theory is called supergravity and enlarges the particle content of the MSSM by two particles arranged in a gravity supermultiplet [4]: the spin-2 graviton G and its spin-3/2 fermion superpartner $\tilde{G}$, the gravitino. Both are massless unless SUSY is spontaneously broken. Then the gravitino acquires mass by "eating" the goldstino. The gravitino has now four helicity states, namely two transverse (helicity $\pm 3/2$) and two longitudinal ($\pm 1/2$) from the goldstino [2]. These longitudinal modes allow the gravitino to interact non-gravitationally so that it may actually be relevant for collider physics.

3 Experimental Setup

This chapter gives an overview of the accelerators and detectors located at CERN (Conseil Européen pour la Recherche Nucléaire). It summarizes the main features of the Large Hadron Collider (LHC) and its accelerator chain. Furthermore the concepts and technical realization of the ATLAS (A Toroidal LHC ApparatuS) detector and its trigger system are given.

3.1 Accelerators and detectors at CERN

Established in 1954, CERN is a research organization with its head office and an accelerator and detector complex near Geneva in Switzerland. The contributions of scientists from around the world have lead to remarkable progress in elementary particle physics like the recent discovery of a new boson, which matches the predictions of the Higgs particle of the SM.

Over the years, many different kinds of accelerators have delivered data for research. It started with the linear proton accelerators (LINAC 1 & 2) before moving over to synchrotron accelerators (e.g. LEP) step by step. Currently, data come from the LHC with four main experiments recording the collision data: ALICE, ATLAS, CMS and LHCb. While ALICE is specialized on heavy-ion collisions, the latter three are targeting especially proton-proton collisions. LHCb searches the answer for the question why there is more matter than antimatter in the universe analyzing the decays of b and $\bar{b}$ quarks [8]. ATLAS and CMS are general-purpose detectors to cover a wide range of SM and BSM physics. Both detectors have a very similar layout but the technical implementation of the components is different. This enables a quite useful mutual check: If one experiment sees something interesting, what about the other one? Figure 3.1 shows a schematic illustration of the CERN accelerator and detector complex.

3.2 The Large Hadron Collider

The LHC was built into the same 26.7 km long circular tunnel as the LEP accelerator and is a synchrotron collider as well. Their design implies that two particle beams run against counter-clock wise and collide with each other at certain interaction points (usually the place where the detectors are). In general, a variety of particle exists which can be used for the beams. There is however a limiting factor: the synchrotron radiation emission. As charged particles radiate when accelerated, they lose energy in every turn. This leads to another important task for the accelerator (besides accelerating): when

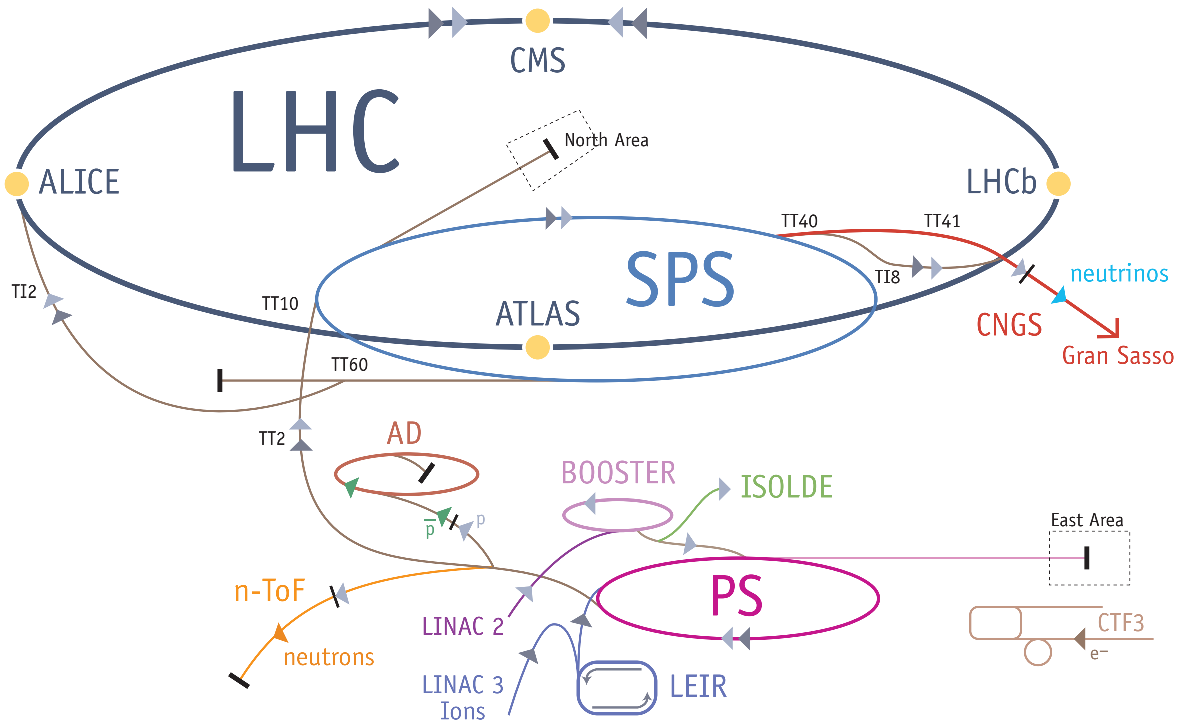

Figure 3.1: The LHC accelerator chain (elipsis) and experiements (yellow dots). Figure taken from [9].

the final energy is reached, the beams need to be provided constantly with energy. The energy loss per turn U_0 of a particle with charge e and mass m scales as [10]

$$U_0 = \frac{e^2}{3\epsilon_0}\frac{\gamma^4}{\rho} \propto \frac{1}{\rho}\frac{E^4}{m^4}$$

where E is the beam energy, ϵ_0 the vaccum permittivity, $\gamma = E/m$ the Lorenzfactor and ρ the radius of the circuit. As the proton mass is approximately 2000 times the electron mass, proton-proton synchrotrons like the LHC suffer significantly less from synchrotron radiation losses than lepton storage rings (like LEP) and therefore enable higher beam energies. As the major limitation of energy for this accelerator type remains the strength of the magnetic field that forces the particle on a circular motion. Hadron collider are complementary to leptonic ones: Due to their high center of mass energy the first ones are often called discovery machines [1] while the latter enable precision measurements as there are no hadronic remnants in the event.

The protons cannot be injected directly into the LHC. They need to be pre-accelerated before step by step. For economic reasons, the older accelerators at CERN are used for this purpose. First the protons (originating from a bottle of hydrogen atoms) are accelerated to 50 MeV with LINAC 2. Then, they are injected subsequently into the PS Booster, the Proton Synchrotron (PS) and Super Proton Synchrotron (SPS) until they are finally filled into the LHC at an energy of 450 GeV [9]. The protons do not enter the two parallel, vacuumized beam pipes continuously but arranged in bunches. After injection the particles are accelerated by 8 radiofrequency (RF) cavities per beam to their full energy of currently 6.5 TeV. These cavities also compensate the energy loss due to synchrotron radiation by oscillating at a frequency of 400 MHz[†]. The magnetic field that keeps the particles on track is provided by 1232 dipole magnets. These magnets are able to generate fields up to 8.3 T by using NbTi cables which become superconductive under 10 K. Only superconductivity enables currents up to 12000 A which are needed for such strong magnetic fields [9]. To achieve these low temperatures the LHC uses a gigantic cryogenic system. The temperature in the magnets is lowered to 1.9 K with helium, which is cooled down in multiple steps using refrigerator turbines. Vacuum-insulation of the magnets helps to preserve these low temperatures. Finally, quadruple magnets at the interaction points focus the bunches to maximize the instantaneous luminocity.

During the 2-year shutdown after Run 1 the LHC got substantially upgraded. The most obvious enhancement is the increase of the beam energies from 4 to 6.5 TeV, resulting in a center of mass energy of 13 TeV. To (re)achieve the needed magnetic field strength the magnets have been (re)trained by repeating the following procedure: the current in the magnet is slowly increased until small amounts of heat stops it from being superconductive ("quenching"). Then the current has to be extracted safely to avoid damaging the magnet [11]. For the higher beam energies also the RF cavities operate at higher voltages. Another notable change concerns the bunches: a bunch contains now less particles but the time between two bunches, the bunch spacing, is reduced by half to 25 ns. This helps to keep the interactions per bunch-crossing and hence the in-time pileup on a managable- and the luminosity at a high level. The disadvantage is the increase of out-time pileup from preceding collisions when the bunches are closer to each other. Many more "behind the scene" improvements of the LHC have been made like narrower beams or more secure vacuum [12]. All these efforts form the basis of a hopefully insightful Run 2.

3.3 The ATLAS detector

One design goal of the ATLAS detector was to allow research for many different experimental signatures. This means the instrumental coverage has to be as large as possible: "dead" space occupied by readout electronics or support structures like pedestals should be minimized while particle detection with adequate resolution should cover a solid angle as large as possible. For that purpose, ATLAS adapted the "barrel–endcaps" concept, so that many components consist of a cylindrical barrel covering the central region and endcaps for the forward (i.e. beam) direction.

In general the detector can be divided into four subsystems: the Inner Detector (ID), the electromagnetic calorimeter (Ecal), the hadronic calorimeter (Hcal) and the muon spectrometer. Percolation by magnetic fields enable momentum measurements

[†] cavities are also responsible for the bunch structure, as particles get accelerated or decelerated depending on whether they are too slow or too fast

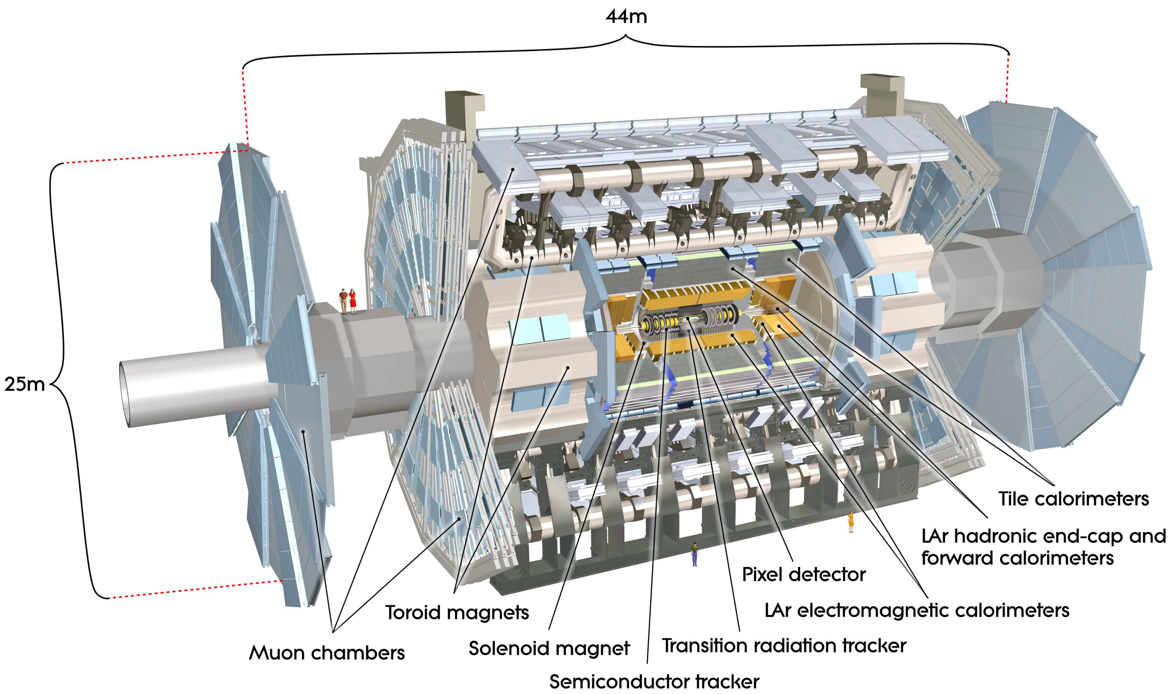

Figure 3.2: A schematic drawing of the ATLAS detector and its main components. Figure taken from [13].

of charged particles in the ID and muon spectrometer. All subsystems are linked to the ATLAS trigger and data acquisition system, which has to select interesting events for writing out. The geometrical layout of the components are shown in Figure 3.2.

3.3.1 The magnetic system

The ID is immersed in a magnetic field of strength 2 T, produced by a thin, superconducting solenoid [14]. For the outer components three (one barrel and two endcap) superconducting toroids, each consisting of 8 coils arranged in a azimuthal symmetric way, provide magnetic deflection. This configuration leads to magnetic fields of approximately 1 or 0.5 T in the barrel region and in the endcaps, respectively. To reach the superconducting state, all magnets are connected to a cryogenic system for cooling.

3.3.2 The Inner Detector

The ID provides pattern recognition, momentum and vertex measurements, and electron identification [14]. However, as the ID is closest to the interaction point, it has to face special challenges: high particle rates, radiation tolerance and as a consequence the aging of the detector [1]. The ID consists of three complementary subsystems: a silicon pixel detector, a silicon strip tracker and transition radiation tracker (TRT). The pixel detector and the strip tracker have cylindrical layers in the barrel region and multiple disc-layers at the endcap. New in Run 2 is an additional layer of the pixel detector in the barrel region called Insertable B-Layer (IBL) that now is the innermost layer. The IBL improves the tracking performance significantly [15] and thus algorithms depending on spatial information like b-tagging profit in particular. The two subsystems provide momentum resolution at inner radii of about 10 μm (in the r–ϕ plane[‡]) and cover a range $|\eta| < 2.5$. The TRT consists of gaseous straw tubes interleaved with transition radiation material [14]. The tubes are arranged along the beam in the barrel and radially in wheels at the endcaps. At larger radii the TRT significantly enhances the track-following in the range up to $|\eta| < 2.0$ by contributing with many additional hits per track.

3.3.3 The calorimeters

Calorimeters absorb electrons, photons (in the Ecal) and hadrons (Hcal) and measure their energy deposits. Usually they follow an "accordion"-like design: passive (absorbing) layers of high density are interleaved with active material. In total, the ATLAS calorimeters cover a range up to $|\eta| < 4.9$ with varying granularity over the $|\eta|$-range. Geometrically first comes the electromagnetic calorimeter, which is divided into a barrel part and two endcaps as well, covering the range up to $|\eta| < 3.2$. It uses lead for absorption and liquid Argon (LAr) as active material. The outer hadronic calorimeter is comprised by the Tile calorimeter, the Hadronic End-cap Calorimeter (HEC) and the Forward calorimeter (Fcal). The Tile calorimeter consists of a central and two extending barrels, all using steel and scintillating tiles for measurements. It covers the $|\eta|$-range up to 1.7. To extend coverage the HEC (copper/LAr) and the Fcal (copper-tungsten/LAr) so that energy deposits can be measured up to $|\eta| < 4.9$.

3.3.4 The muon spectrometer

The muon system surrounds the calorimeters and is embedded in the magnetical field produced by the coils. As all detectable particles except muons are absorbed in the Hcal at the latest, hits in this detector generally are caused by muons. In principle, the detectors are large-area gaseous chambers. For precision measurements Monitored Drift Tube (MDT) chambers in the barrel and the endcaps are used, arranged as concentric cylindrical layers or as wheels, respectively. Cathode-Strip Chambers (CSC) in the forward region (commonly refered to as "small wheels") help to withstand the high particle rates and grant good time resolution [14]. Together the MDTs and CSCs cover a range up to $|\eta| < 2.7$. As their time response is too slow for triggering, dedicated trigger chambers are installed: Resistive Plate Chambers(RPC) in the barrel and Thin Gap Chambers (TGC) at the endcaps (also grouped as wheels) provide muon triggering

[‡] ATLAS uses a right-handed coordinate system with its origin at the nominal interaction point (IP) in the centre of the detector and the z-axis along the beam pipe. The x-axis points from the IP to the centre of the LHC ring, and the y-axis points upward. Cylindrical coordinates (r, ϕ) are used in the transverse plane, ϕ being the azimuthal angle around the z-axis. The pseudorapidity is defined in terms of the polar angle θ as $\eta = -\ln\tan\big(\theta/2\big)$ [16] .

for $|\eta| < 2.4$. Due to their geometry the MDTs in the endcaps and the TGCs are called "big wheels" and govern the enormous size of ATLAS.

3.3.5 The ATLAS trigger system

Every second about 40 million times bunches collide with each other and over one billion interactions leave their marks in the detector. As the final write-out capacity is limited to about 1 kHz, there has to be an overall reduction of several orders of magnitude. For that purpose triggers use a subset of the detector information to search for promising signatures in the event. In Run 2 this is performed by a two level trigger system [17]. The Level 1 (L1) trigger reduces the rate from 40 MHz to 100 kHz by scanning relatively coarse signals from the calorimeters and the muon trigger systems. It determines geometrical Regions of Interests (RoI) and can calculate topological quantities e.g. if isolation criteria are fulfilled. The High Level Trigger (HLT) refines the L1 trigger decisions by running more sophisticated algorithms on the RoIs or offline-like algorithms on the full-event data. This leads to a final event rate of about 1 kHz, which reaches the output storage.

4 Search for scalar Top Quarks

This chapter introduces the search for scalar tops with two taus in the final state. First a short overview of the general, and in the search for new particles common, analysis strategy is given. Second the motivation and the details of the benchmark model are presented.

4.1 General Analysis Strategy

The main challenge in the hunt for new particles is their small production cross section compared to SM processes. So in ordinary kinematic distributions their potential signal is superimposed by large amounts of background. There are several ways to address this challenge and design a search for new physics. One of the most common approaches is to define Signal Regions (SR), which represent signal enriched regions in the phase space of the final state. If the recorded data significantly exceeds the background expectation in these regions, this might be a hint for BSM physics. For reliable statements, the analysis team has to show that their background expectations for the particular SM processes are correct. Usually Control Regions (CR) are defined, which are regions in phase space enriched with one specific background process and negligible signal contamination. The expectation for this process is fitted to data in the corresponding CR, resulting in a normalization factor. This factor can be transfered into the SR to take into account any over- or underestimation of the unfitted background estimation. The validity of this extrapolation is usually checked in Validation Regions (VR) that are designed to be in between the CRs and the SRs. This procedure is schematically drawn in Figure 4.1. The dashed lines indicate that regions can consist of multiple bins. This way also information about the shape of an observable in a certain range is used in the fit and thus enhances the statistical analysis.

If events from Monte Carlo generators are used as background estimation, this semi-data-driven method shows another important feature. Let P be a specific background process then the extrapolation from its CR to a SR takes the following form [18]

$$N_P^{\mathrm{est}}(\mathrm{SR}) = N_P^{\mathrm{obs}}(\mathrm{CR}) \times \frac{MC_P^{\mathrm{pred}}(\mathrm{SR})}{MC_P^{\mathrm{pred}}(\mathrm{CR})} = \mu_P \times MC_P^{\mathrm{pred}}(\mathrm{SR}) \tag{4.1}$$

where $N_P^{\mathrm{est}}(\mathrm{SR})$ is the SR background estimate, $N_P^{\mathrm{obs}}(\mathrm{CR})$ the number of observed events in the CR, μ_P the normalization factor and $MC_P^{\mathrm{pred}}(\mathrm{SR/CR})$ the Monte Carlo prediction of process P in the SR and CR, respectively. Due the ratio of Monte Carlo predictions in Equation 4.1 systematical uncertainties caused by non-optimal modeling can cancel.

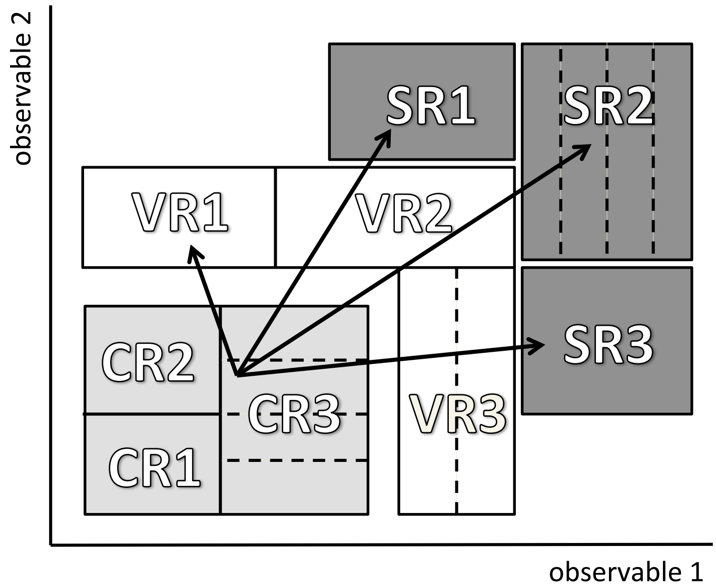

Figure 4.1: Extraploation from Control Regions to Validation- and Signal Regions as a schematic drawing. Figure taken from [18].

4.2 Benchmark Model

For designing the selections that define the CRs and SRs typically a benchmark model is used. As described in section 2.3 superpartners of left- and right-handed SM fermions can mix and form two mass eigenstates. The search described in this thesis considers a class of R-parity conserving MSSM models, in which the superpartners of the third generation SM fermions are light to achieve natural stabilization of the higgs mass. That means the masses of the lighter eigenstates ($\tilde{t}_1$ and $\tilde{\tau}_1$, herein after referred to as scalar top and scalar tau, respectively) are in the order of the electroweak symmetry breaking energy scale.

In a simplified scenario a scalar top (stop) pair is produced in the proton–proton (pp) collisions and each stop decays via a virtual chargino into a b-quark, a scalar tau (stau) and a tau neutrino. Like the other SUSY particles not entering the decay chain, the chargino is assumed to be very heavy so that the decay can be modeled as an effective three-body decay. Each stau decays then into a tau and the LSP. In general there are two candidates for this particle depending on the model of symmetry breaking: The lightest neutralino and the gravitino (via its longitudinal component that has spin 1/2). As this search assumes GMSB, the gravitino takes the role of the LSP and is assumed to be nearly massless. The decay topology is shown in Figure 4.2. Taus can decay either into a light lepton (electron or muon) or hadronically. This thesis will focus on only one case: one tau decaying into a lepton and the other tau into hadrons, denoted as lepton-hadron channel. The other channels are analyzed separately and will be combined later to maximize sensitivity. As it is a simplified model, the branching ratios (BR)

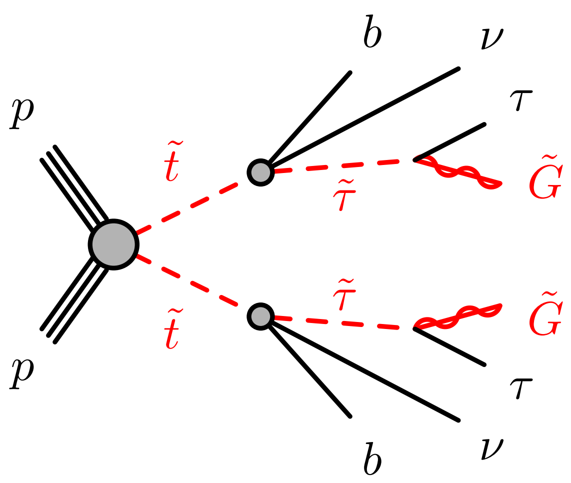

Figure 4.2: Diagram for the direct stop to stau search. Figure taken from [19]

BR($\tilde{t} \rightarrow b\nu\tilde{\tau}$) and BR($\tilde{\tau} \rightarrow \tau\tilde{G}$) are set to 1 and the other SUSY particles not entering the decay chain are decoupled†. This means, there are only two free parameters in the model: the stop and stau masses.

Previous analyses considering the same (ATLAS Run 1) or a comparable model (LEP) have already set exclusion limits on the stop and stau masses up to 650 GeV [20] and 87 GeV [21] respectively.

To sum up, the search presented here targets final states with one light lepton, one hadronically decaying tau, two jets containing a b-hadron (b-jets) and large missing transverse energy through particles escaping the detector (neutrinos and LSPs).

4.3 Prospects for Run 2

The presentation of first results for this analysis is planned to be at the summer conferences for high energy physics in 2016. By this time, it is expected to record in total around 10 fb^{-1} data, which is about half of the amount that was available for the Run 1 analysis. So the question arises if this amount of data is already sufficient for new results, e.g an extension of the exclusion limits.

The analysis will definitely benefit from the higher center-of-mass energy with respect to Run 1 and the consequently larger parton luminosities. These describe basically the probability that during a hadron collision, two partons interact that have enough energy to produce a particle of a certain mass. The ratio of the parton luminosities for the center-of-mass energy in Run 2 and Run 1 is shown in the left plot of Figure 4.3. It is clearly visible that they increase significantly for higher masses. In other words, the

† In principle, also the two-body decay $\tilde{t} \rightarrow t\tilde{G}$ is possible. Its partial width depends on the LSP mass whereas in the case of the three-body decay it depends on the chargino mass and the mixing of chargino and stop. Either mode can dominate, but this search focuses on a MSSM parameter space in which the latter one contributes the most.

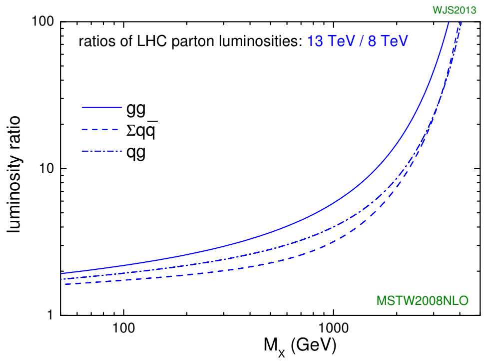

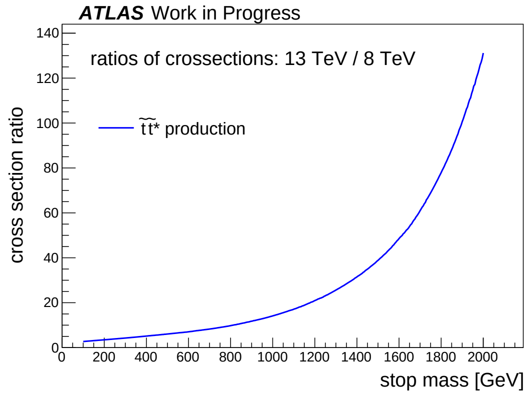

Figure 4.3: Ratio of parton luminosities (Figure taken from [22]) at the LHC (left) and of cross sections (taken from [23]) for the signal model (right) from Run 2 to Run 1

probability to produce heavier particles increases drastically with respect to Run 1. This directly translates into the production cross section for the benchmark model (see right plot of Figure 4.3).

The relevant mass spectrum for first results is beyond the exclusion limits of Run 1, so about 650 to 800 GeV. In this range the production cross section will rise roughly by a factor of 10, so that for the same amount of data 10-times more signal events are expected. On the contrary, the cross sections for the background processes will not rise that much. Taking top–anti-top production as an example, its cross section rises according to [24] roughly by a factor of 4. Estimating the sensitivity Z with the formula $Z = S/\sqrt{B}$ (see section 7.1) and considering that S and B will increase by factors of 5 and 2 (10-times more signal and 4-times more background but only half of the data), respectively, the analysis is already 3.5-times more sensitive for the mass spectrum above though only half the amount of data that was available in Run 1 is used.

5 Signal Grid Validation

Before simulated events can be used for analysis they have to be validated in a sense that they model the process under consideration correctly. The signal grid validation procedure for the direct stop to stau search is described in this chapter, preceded by an introduction how events are simulated in ATLAS.

5.1 Monte Carlo Generation at ATLAS

In particle physics events from a certain process will not always look the same but are distributed continuously over the kinematically allowed phase space, following a probability density function (p.d.f.). These p.d.f.s can be calculated from theory and are naturally quite complex. However, to model an event in a way how it finally would look like in the detector takes numerous steps more. On the one hand, there are many features of *pp* collisions that have to be treated with special methods like the signature of the partons that do not take part in the hard scattering process (underlying event) or the other interactions within the bunch crossing (pile up). On the other hand the detector response of the generated particles has to be simulated. The whole generation chain is very complex and will thus just be outlined here.

5.1.1 The Monto Carlo Method

In general the term Monte Carlo method refers to numerical techniques that make use of random numbers to calculate probability-related quantities [25]. Typically it maps a series of random numbers that is uniformly distributed in the range $[0, 1]$ into a series of numbers following the desired p.d.f. $f(x)$. There are a number of different approaches for this transformation (e.g. the acceptance-rejection method). Treating the values of x as simultaneous measurements and deducing from them the probability for x to be in a certain region, one effectively calculates the integral of $f(x)$ which may not be feasible with other methods when the p.d.f. is high dimensional. As a simple example, one can consider the scattering of an electron at a fixed target [25]. The scattering is described by the scattering angle θ. Theory predicts the probability for an electron being scattered in a certain θ-range (the differential cross-section $\frac{\mathrm{d}\sigma}{\mathrm{d}\cos\theta}$). The MC generator then maps the set of random numbers into a set of scattering angles distributed according to the differential cross section. Afterwards the final momentum vectors can be constructed from the scattering angles and the initial momentum.

5.1.2 Event Generation Flow

A typical event in *pp* collisions contains several hundreds of particles. The underlying theory for these processes is the strong interaction described by Quantum Chromodynamics (QCD). The interaction of gluons and quarks caused by their color charge can be calculated in principle to arbitrary precision at high energy. However, due to the non-abelian nature of the associated gauge theory, the gluons couple to each other. This leads to an increasing strong coupling constant for low energies, so that the perturbation ansatz breaks down. To handle these cases, models not relying on perturbation theory have been developed, e.g. Lattice QCD.

For an adequate modeling of an event, a variety of components have to be considered [26]:

- **hard scattering matrix element $\mathcal{M}$**
  They define the process under study as its cross section is proportional to $|\mathcal{M}|^2$.
- **structure functions**
  As protons are composite particles, the actual hard scattering interaction is done by their constitutions, the partons. Structure functions are p.d.f.s describing the momentum distribution of the partons and thus govern how much energy is available in the interaction
- **final state radiation**
  Partons in the final state may radiate in the form of gluons. This leads to additional jets in the final state.
- **initial state radiation**
  Before the hard interaction, the incoming partons may radiate as well. This mechanism adds jets in the forward direction, close to the incoming protons.
- **beam jets**
  Only one parton from each hadron takes part in the hard scattering. The remnants of the protons will also hadronize and form jets along the beam direction.
- **fragmentation and decays**
  The partons will form stable hadrons in the fragmentation process. This can take multiple steps, leading to the jet-characteristic of partons.

The separation above is not distinct in a sense that e.g. an additional gluon in the final state can be incorporated in the matrix element or in the description of the initial and final state radiation, respectively. A critical task is to merge the descriptions above in a consistent manner (often referred to as “parton matching”), that means to avoid any double-counting. This challenge leads to two somewhat complementary approaches of MC programs: using parton showering or matrix elements.

The parton shower approach usually implements only the lowest order matrix elements and adds the initial and final state radiation as showers. The showers are universal as they do not depend on the details of the hard process but of course on main features like energy and color of the associated partons. When finally beam jets and fragmentation models are added, all phenomenological important features of hadron collisions are taken into account in the event modeling.

In the matrix element (ME) approach the main focus lies on precision by calculating exactly the matrix elements up to higher orders. As the computation can take several hundreds of CPU hours, usually only a small amount of additional partons is generated. As exact calculation is only possible for high energies, the soft terms are then also attached via the shower approach.

A common method is to combine these two approaches and benefit from the strengths of both: a precise description of well separated, hard partons from ME generators and the good approximation of multiple soft, collinear partons from parton shower generators. However a correct parton matching implementation gets highly non-trivial when multiple generators are used for event generation.

After modeling the particle content of the event, the remaining question is how it will be visible in the detector. For that purpose GEANT has been developed. This software simulates the interaction of particles with the detector material also making use of MC methods. It provides information how particles will be visible in the tracking devices, how they will deposit their energy in the calorimeters and how the detector layout influences the measurements. A key feature is that GEANT uses different phenomenological models depending on the energy scale. Ideally the detector simulation and real data share the same output formats so that the same reconstruction algorithms can be used. After the conversion into ATLAS internal file formats the data and MC samples can be used in the analysis.

5.1.3 Reconstruction

Although reconstruction is more associated with the actual detector data, it is performed as well on the MC sample after the detector simulation. The aim is to convert the information of the different detector components like the tracking devices and calorimeters into physical objects. Reconstruction algorithms exploit the diversity in the signatures of particles to differentiate between them. These algorithms are not perfect, of course, and can misidentify or simply do not reconstruct a particle at all. For this purpose different working points are defined that reflect different purities and reconstruction efficiencies. In principle every analysis team has to check which working point provides the best balance with respect to statistical losses and classification power.

A common approach is to decorate the reconstructed objects with baseline and signal classifiers. The baseline criteria reflect some basic and rather loose standards, while the definition of signal objects often already incorporates signatures of the process under study. Objects that do not fulfill any of these criteria are not considered in the further analysis. The following gives a short overview of the reconstruction techniques for physical objects relevant for the analysis [27].

Jets As partons cannot exist freely they have to form colorless states by hadronization. This produces a cone of mainly hadronic particles, called jet, that originates from the parton. Topological calorimeter clusters (clustered energy deposits) are defined by the anti-k_t algorithm. Next the jets are corrected for various detector effects. In this search the reconstructed jets need to have a p_T larger than 20 GeV to fulfill the baseline requirement.

***b*-jets** The b-quark has some special features. One of them is its relatively long lifetime so that a secondary vertex can be reconstructed. Based on a neural network, the MV2C20 algorithm uses several spacial tagging algorithms that exploit this displacement as input to tag baseline jets as b-jets. A common working point grants 77% tagging efficiency and is used for this analysis.

Electrons Electron reconstruction in the central region uses information from calorimeter clusters in the EM calorimeter and requires a track in the ID originating from the primary vertex that is associated with the electron candidate. To separate the reconstructed candidates from background-like objects like converted photons the electron identification uses the so-called likelihood (LH) method. This is a multivariate technique that uses several properties of the candidates and provides multiple working points [28]. To refine the electron selection an isolation requirement, quantifying the density of particles around the electron can be applied. Based on two variables that are associated with the isolation at track and calorimeter level normalized to the electron p_T, multiple isolation working points are provided. This analysis uses the LooseLH working point for baseline electrons and an additional p_T requirement of at least 10 GeV. To fulfill the signal requirement TightLH electrons mainly need to satisfy a certain isolation criterion named GradientLoose [28] and have a p_T greater than 25 GeV.

Muons For muon reconstruction information from the tracking devices and the Muon Spectrometer is used, moderately enriched with calorimeter information [29]. Different types of muons are defined depending if tracks in the ID match to tracks in the MS and entries in the calorimeter cells. Based on these types and their specific features several working points are provided reflecting different balancing (quality) of reconstruction efficiency and purity. Similar to electrons, isolation requirements are defined quantifying the activity around muons in the tracking and calorimeter devices. In this analysis baseline muons need to be of medium quality and have a p_T larger than 10 GeV. In addition signal muons must fulfill an isolation requirement which is called GradientLoose as well.

Taus Due to their short lifetime taus decay mostly before they enter the active regions of the detector. So they can only be reconstructed via their decay products. If a tau decays leptonically, it will be reconstructed as an electron or muon. In the case of a hadronic decay the decay products are mainly one or three charged pions. Their subsequent decays involve in most scenarios charged kaons and neutral pions. This leads to similar cone structures like jets which makes it challenging to differentiate between these two. Electrons and to a lesser extend muons can also mimic hadronic tau signatures. The seed of the tau reconstruction are calorimeter energy deposits that have been reconstructed as jets with the anti-k_t algorithm [30]. After applying additional requirements on the associated tracks, the tau candidates are identified using variables based on the shower shape, the distinct number of charged particle tracks (prongs) and the displayed tau vertex as input for Boosted Decision Trees. Again different working points are defined representing varying balance of reconstruction efficiency and rejection of jets and electrons. The analysis uses taus of medium quality and p_{T} greater than 20 GeV.

Missing Transverse Momentum Weakly interacting particles like neutrinos are invisible to the detector. However they leave an indirect signature: due to momentum conservation, all transverse momenta of the particles in the final state should sum up to zero. Any imbalance may indicate particles that escape the detector. Missing transverse momentum is defined as the negative vector sum of the transverse momenta of all detected particles [31] with magnitude denoted as $E_{\mathrm{T}}^{\mathrm{miss}}$. It also contains a soft term representing all energy deposits not associated with a reconstructed object. As there is quite some freedom in the choice of reconstruction, the final $E_{\mathrm{T}}^{\mathrm{miss}}$ definition may vary from analysis to analysis. This search for example does not use photons in the calculation as they are not part of the signal model.

Overlap Removal The reconstruction routines run independent from each other. Thus it may occur that the same signature is reconstructed twice, which means as two different physical objects. For that purpose the Overlap Removal algorithm checks whether two reconstructed objects lie within a certain cone and decides which particle should be kept and which will be removed. The analyses considered here use the default settings for the removal as provided by ATLAS (see Appendix A.1 for details on the individual steps and a summary for the objects definitions used in this analysis).

5.2 Signal Grid in Run 2

Due to the decision to use a different MC generator setup with respect to Run 1 for stop searches, a detailed validation of the signal samples is needed. One reason for the migration from HERWIG++ to the now combined setup MADGRAPH and PYTHIA is the better simulation for initial state radiation of MADGRAPH. Initially, MADGRAPH simulates the hard scattering event and up to two additional partons. Then PYTHIA uses the output to model the three-body decay and the parton showering and subsequent decays. The question is if this new setup models the signal process properly.

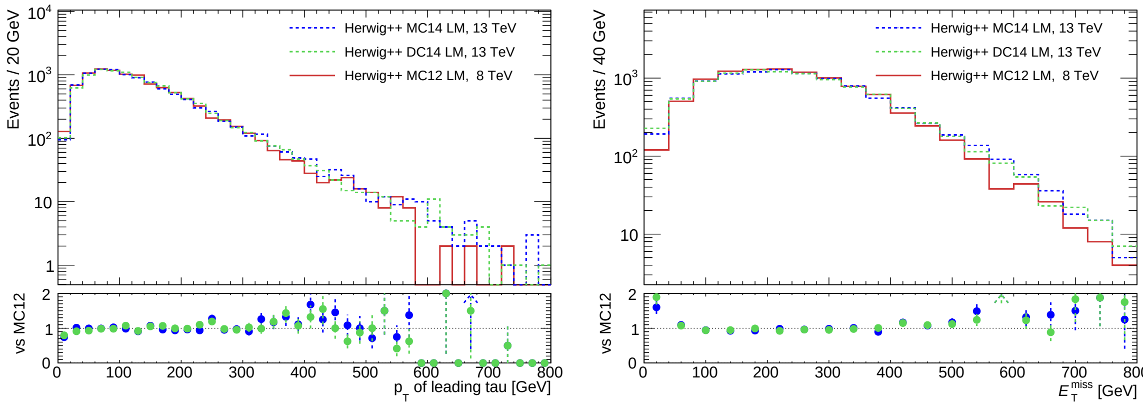

Figure 5.1: Distributions in the LM scenario of leading tau p_{T} (left) and $E_{\mathrm{T}}^{\mathrm{miss}}$ (right) of MC12 (solid red line), DC14 (dashed green line) and the locally produced MC14 (dashed blue line) sample. The ratio plot below shows the ratio of DC14 and MC14 with respect to MC12.

5.2.1 Validation Procedure

The general validation procedure makes use of former signal samples, in detail the MC files from Run 1 in 2012 ("MC12") and from a MC campaign in 2014 ("DC14"). Both samples were produced with HERWIG++, but at different center of mass energies: MC12 at $\sqrt{s} = 8$ TeV and DC14 at $\sqrt{s} = 13$ TeV. These samples from official, validated MC campaigns were compared in various kinematic distributions with locally produced samples that use the new setup. The use of rather general distributions like the transverse momentum (p_{T}) of particles or the missing transverse energy ($E_{\mathrm{T}}^{\mathrm{miss}}$) ensures that focus lies on an overall adequate modeling and not on generator specific details. Comparisons are done at truth-level, so no detector effects are included. Two different representative scenarios are used in the validation, one reflecting low, the other one reflecting high stau masses with respect to the stop mass. These scenarios are herein after referred to as LM and HM, respectively.

A technical issue is that MC12 and DC14 use an older version of the Analysis Release (the ATLAS intern framework) than the locally produced samples. To spot deviations caused by a more recent version a locally produced HERWIG++ sample ("MC14") was produced that uses the same Analysis Release as the new setup. So the first steps were to validate MC14 with respect to MC12 and DC14 and use it later for comparisons with the new setup.

5.2.2 Validation of locally produced MC14

The distribution at LM of $E_{\mathrm{T}}^{\mathrm{miss}}$ and the p_{T} of the leading tau[†] for the HERWIG++ samples MC12, DC14 and MC14 are shown in Figure 5.1. In both distributions the locally produced sample shows reasonable agreement with the "official" ones. There are some deviations at $E_{\mathrm{T}}^{\mathrm{miss}}$ in the bins representing small and large values, but there is no general mismodeling, as their is no slope in the ratio plot. An open question

[†] tau with the largest p_{T}

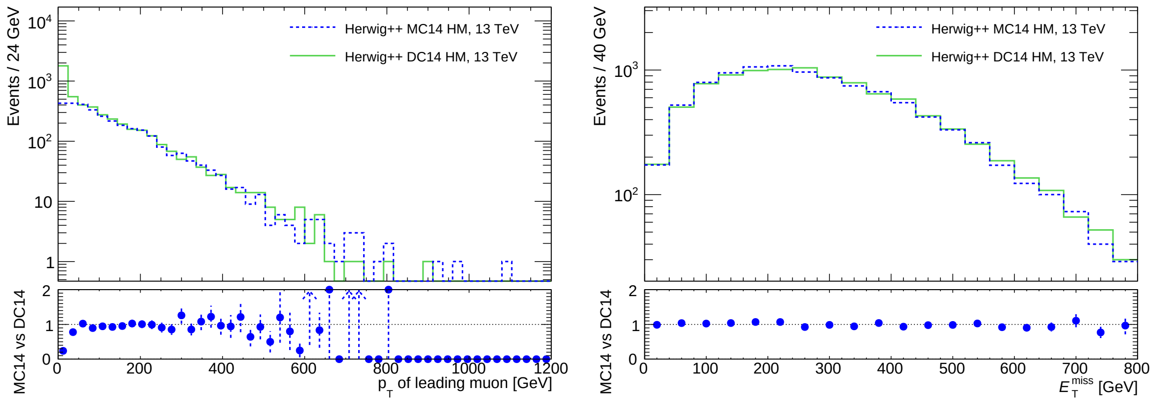

Figure 5.2: Distributions in the HM scenario of leading muon p_{T} (left) and $E_{\mathrm{T}}^{\mathrm{miss}}$ (right) of DC14 (solid green line) and the locally produced MC14 (dashed blue line) sample. The ratio plot below shows the ratio of MC14 with respect to DC14.

was, how reasonable the comparison of samples, simulated at different center of mass energies actually is. Intuitively, an increase in $\sqrt{s}$ affects in first place the longitudinal observables. Transversal observables like p_{T} and $E_{\mathrm{T}}^{\mathrm{miss}}$—that are more interesting for analysis anyway—should be less influenced if all samples are normalized to the same number of events to compensate the different cross sections. Figure 5.1 confirms this assumption, as the general shapes are not heavily influenced by $\sqrt{s}$, so the comparison is reasonable.

In the HM scenario the comparison can only be done with DC14 as there are no available matching files at event generation level for MC12. Figure 5.2 shows the distributions of the leading muon p_{T} and again $E_{\mathrm{T}}^{\mathrm{miss}}$. MC14 shows reasonable agreement with DC14 in both distributions. The discrepancy at low p_{T} muons, which is also visible for electrons (see Figure A.1), is most likely a consequence of the more recent Analysis Release framework. For some reason events in the older version of the framework seem to have much more low p_{T} light leptons. More relevant for this analysis are high-p_{T} leptons for which a good agreement is observed.

These observations validate the unofficial MC14 samples for HM and LM. As they show an adequate representation of the model under consideration, these samples will be used as future references for comparisons. That way any deviations caused by older reconstruction algorithms can be eliminated. This will also ease further checks for any substantial mismodeling of the signal process.

5.2.3 Validation of new Production Setup

So far only samples using HERWIG++ were compared. The new setup that uses MADGRAPH and PYTHIA8 will be herein after denoted as "MGP8". Figure 5.3 shows the distributions at LM of the leading tau p_{T} and $E_{\mathrm{T}}^{\mathrm{miss}}$. While there is an overall agreement in the latter, the former one clearly shows a shift towards higher p_{T} values of MGP8. This also visible as a slope in the ratio plot. Similar shifts are also present in the p_{T}

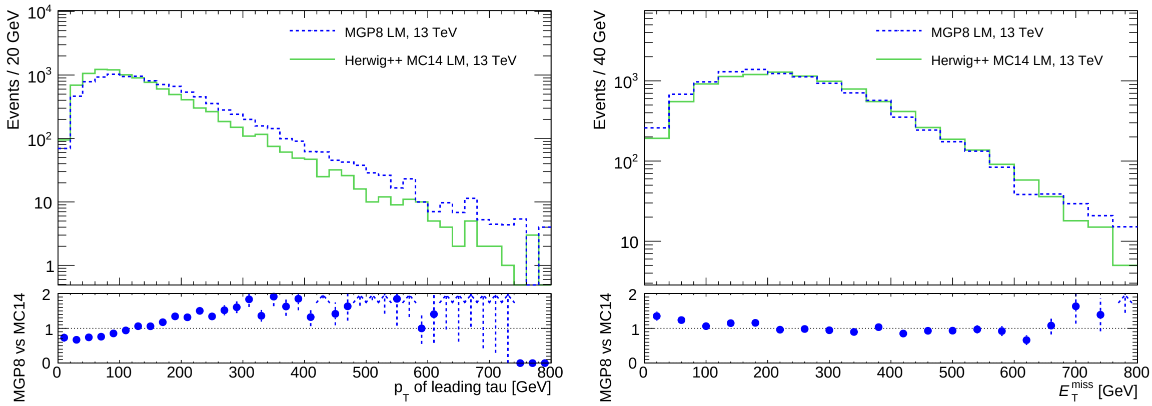

Figure 5.3: Distributions in the LM scenario of leading tau p_{T} (left) and $E_{\mathrm{T}}^{\mathrm{miss}}$ (right) of MC14 (solid green line) and MGP8 (dashed blue line). The ratio plot below shows the ratio of MGP8 to MC14.

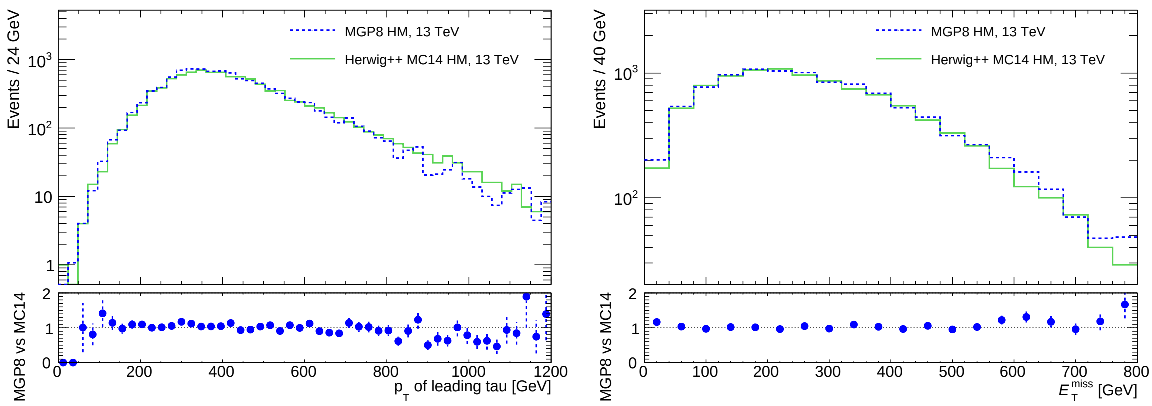

Figure 5.4: Distributions in the HM scenario of leading tau p_{T} (left) and $E_{\mathrm{T}}^{\mathrm{miss}}$ (right) of MC14 (solid green line) and MGP8 (dashed blue line). The ratio plot below shows the ratio of MGP8 to MC14.

distributions of electrons and muons (see Figure A.2).

At HM these slopes are not visible: Figure 5.4 shows the same distributions as before without any clear deviations at high stau masses. Nevertheless the mismodeling that happens at low mass staus has to be understood and resolved.

As taus, electrons and muons appear in the decay chain after the three-body decay a natural starting point is to consider a variable that is not influenced by it. A candidate for this is the p_{T} of the stops. In Figure 5.5 the distributions of the stop- and the stau p_{T} are plotted. While the former shows good agreement, the latter—directly influenced by the three-body decay—exhibits the same shift as the lepton distributions before. This implies that the origin of the mismodeling hides in the simulation of the three-body decay. To get an understanding what goes wrong there, Dalitz plots are very helpful as they visualize kinematics of all three decay products in one plot.

5.2.4 Dalitz Plots

Dalitz Plots exploit the concept that the whole kinematics can be contained in only two variables. Considering the decay $M \to 1 + 2 + 3$ one has three four-vectors in the final state: p_i^μ, where $i = 1, 2, 3$. So there are at first 12 components or degrees of freedom that are however linked by kinematical constraints [32]:

- energy and momentum conservation: $E_M = \sum E_i$ and $\mathbf{p}_M = \sum \mathbf{p}_i$
- particles obey $E^2 = m^2 + \mathbf{p}^2$
- particles decay in a plane, so that one can set $p_i^3 = 0$
- freedom to rotate system around x-y-plane

In principle the remaining two degrees of freedom can be chosen freely but usually the squared invariant masses of decay product pairs are used, so e.g. $m_{12}^2 = p_1 p_2$ and $m_{13}^2 = p_1 p_3$. These masses are plotted in a two-dimensional histogram against each other. As four-momentum conservation sets limits on the minimal and maximal values of the invariant masses [33] only a certain area in this phase space can be occupied. The distribution within the region then can give insight about special features of the decay.

5.2.5 Validation of adjusted Production Setup

Applying the concept of Dalitz plots, in Figure 5.6 the squared invariant mass of the b-quark–neutrino system is plotted versus the squared invariant mass of the b-quark–stau system. The occupation of the available phase space is modeled completely different in MC14 and MGP8: While in HERWIG++ the b-quark–neutrino system favors higher energies, the distribution in the MADGRAPH and PYTHIA8 setup is flat.

It is easy to see that the first setup models physics correctly: In the process a spin-0 particle (the scalar top) decays into two particles with spin 1/2 (b-quark and neutrino) and another scalar (the stau). So spin conservation demands the spins of b-quark and neutrino to compensate each other. The neutrino is left-handed and thus the spin direction will always be opposite to its momentum direction. Consequently configurations are favored in which the particles with spin 1/2 move in the same or the opposite direction. In the former case the stau gets due to momentum conservation a large momentum which is only realized in a small phase space and thus suppressed. Hence the b-quark and the neutrino end up being back-to-back which maximizes the invariant mass of their system.

In contrast to HERWIG++, PYTHIA8 does not handle spin-correlations so this feature is not reflected in the three-body decay modeled by it. At high stau masses this effect is also visible in Dalitz plots (see Figure A.3) but less obvious in the kinematic distributions because most energy of the decaying stop is needed for the stau. The available phase space is then rather small so that differences in its occupation are hidden in the p_T distributions of the daughter particles.

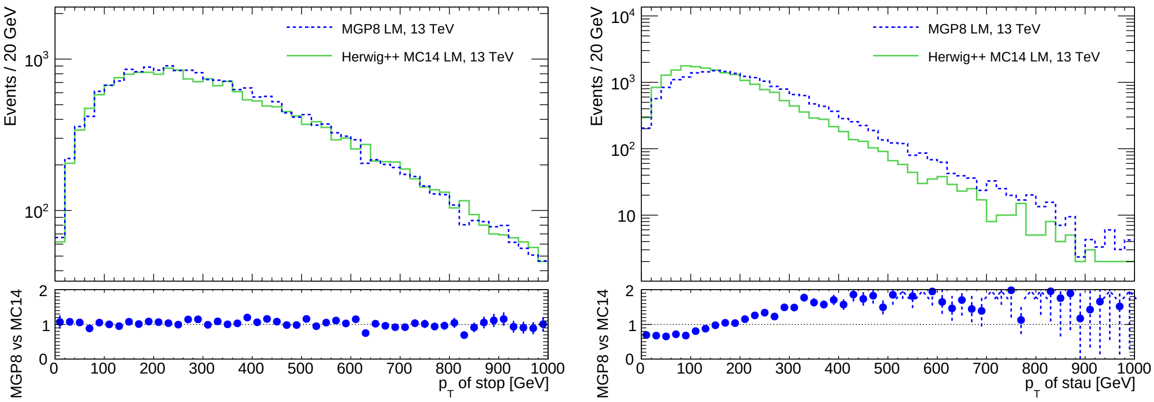

Figure 5.5: Distributions in the LM scenario of stop p_{T} (left) and stau p_{T} (right) of MC14 (solid green line) and MGP8 (dashed blue line). The ratio plot below shows the ratio of MGP8 to MC14.

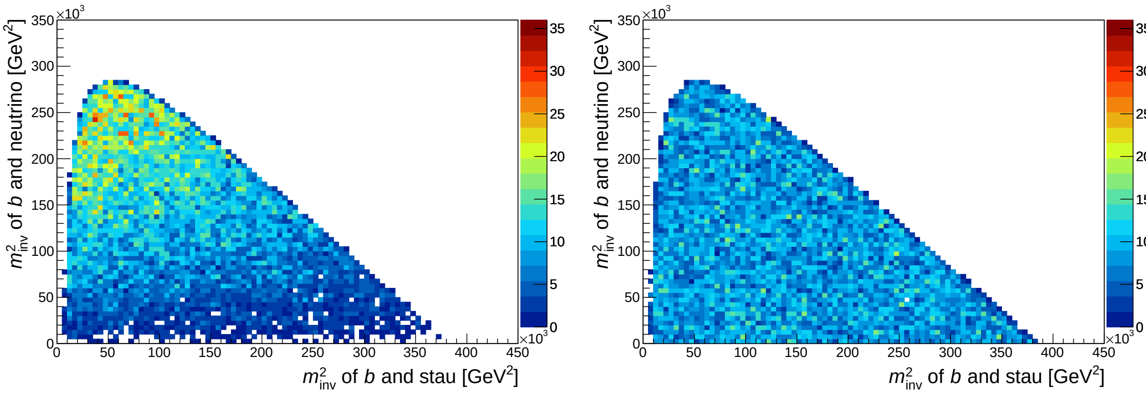

Figure 5.6: Two-dimensional scatter plots of the squared invariant mass of b-quark–neutrino system and the squared invariant mass of b-quark–stau system for MC14 (left, in HERWIG++) and MGP8 (right, in MADGRAPH and PYTHIA8).

An approach to solve this issue is to shift the three-body decay from PYTHIA8 to MADGRAPH that treats spin-correlations. This means MADGRAPH calculates matrix elements including the decay from stop to stau, b-quark and neutrino and delivers the output to PYTHIA8 which then handles the parton showering and subsequent decays. The Dalitz plot of this configuration in Figure 5.7 shows the same characteristics as the one of HERWIG++. Consequently the tau p_{T} distribution is in satisfying agreement. However, before this setup is accepted by ATLAS conveners, it has to pass some additional checks.

5.2.6 Check of Parton Matching

Using MADGRAPH for a three-body decay is a new and rather uncommon generator configuration in the search for stops at ATLAS. Although the configuration successfully

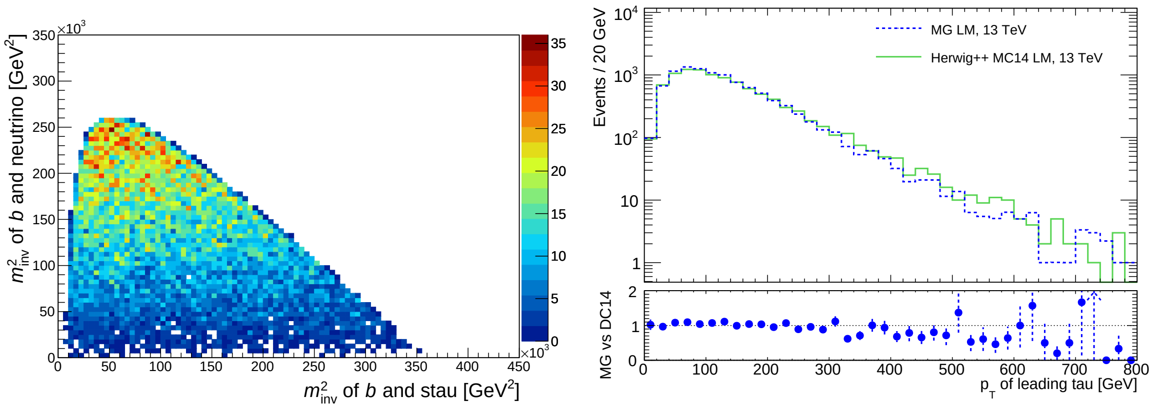

Figure 5.7: Dalitz plot for the setup in which MADGRAPH also handles the stop decay (left) and the $p_{\rm T}$ distribution of the leading tau for this sample.

reproduces the signal process in the variables relevant for the analysis, it has to be clarified if parton matching still works correctly. A way to check this is to produce multiple samples in which the number of additional partons varies. A distinction is made between "n-exclusive" samples, meaning exactly n additional partons and "n-inclusive" samples that contain n or more additional partons. Parton matching should influence only jets that are not part of the hard scattering decay chain in lowest order, in other words are not drawn in Figure 4.2. So the observable of interest is the $p_{\rm T}$ of the leading jet that does not originate from the stop decay ("non-stop jet"). To ensure this a ΔR-matching, where $\Delta R = \sqrt{(\Delta\phi)^2 + (\Delta\eta)^2}$, is applied: Only jets are considered if there is no b-quark, tau or gluon originating from a stop within a cone defined by $\Delta R < 0.2$. If parton matching works, the sum of a 0-exclusive and a 1-exclusive sample should give a similar distribution like a 0-inclusive sample assuming the maximum is one additional parton. The idea of the test is to study if low $p_{\rm T}$ jets come from the showering, large $p_{\rm T}$ jets from the matrix elements and the transition is smooth. Figure 5.8 indicates that this is the case as the sum of the exclusive samples follows the inclusive one, even though the fluctuations get pretty large at higher values.

Technically parton matching in MADGRAPH is governed by a variable called "xqcut" that defines the minimum distance in the phase space allowed between additional partons [34] and furthermore sets the scale of the phase space cut differentiating between PS and ME jets, i.e. the scale of the transition [34]. Naturally the setup should not depend on the exact value of this scale in a sense that the observables relevant for analysis are stable when varying xqcut. Figure 5.9 shows the $E_{\rm T}^{\rm miss}$ and $p_{\rm T}$ distribution of all jets for different values of xqcut. Its influence is rather small so the assumption that parton matching still works for the adjusted generator configuration is justified.

That completes the signal grid validation so that event generation and detector simulation for all grid points can start and the resulting signal samples are available in the main analysis.

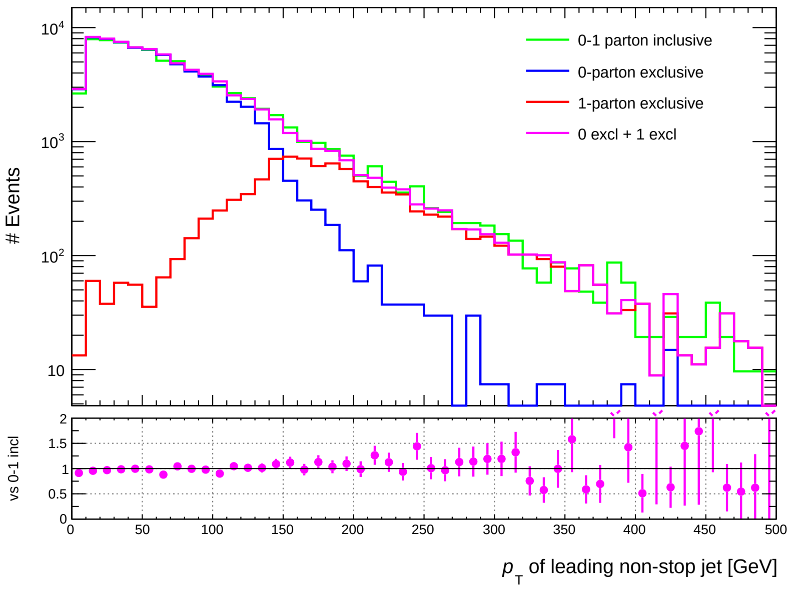

Figure 5.8: Distribution of the leading jet p_T that does not originate from the stop for samples in which the number of additional partons varies: no additional parton (blue), exactly one additional parton (red), the sum of both (magenta) and zero or more additonal partons (green). All processes have been normalized with respect to their cross section. The bottom plot shows the ratio of the sum of the 0-exlcusive and the 1-exclusive sample with respect to the 0-1 inclusive sample.

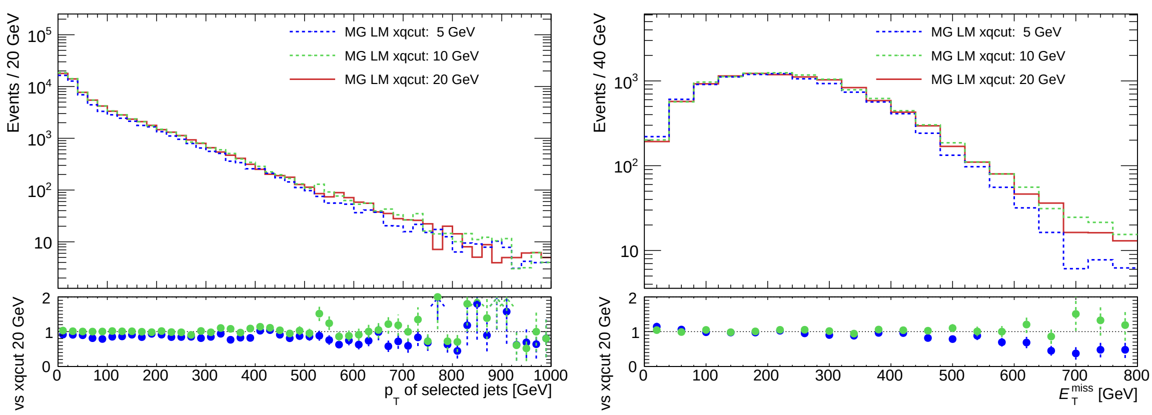

Figure 5.9: Distributions of jet p_T (left) and E_T^{miss} (right) for varying values of the xqcut variable.

6 Trigger Studies

The by far largest fraction of events occurring at particle colliders consists of well known and understood—and hence of minor interest—processes, e.g. simple scattering. Due to their lower cross section, a significant amount of data has to be recorded to store a reasonable amount of interesting events. Buffer- and write-out capacities are however limited, so there has to be some "online" decision whether an event should be kept or rejected. These selections are made by triggers, which form a critical part of any high-energy physics experiment. Triggers can respond ("fire") to different signatures, so the choice which ones are used in the analysis has to be well motivated and decided early. This can determine which class of events will be available for the future analysis. This chapter first introduces the basic concept of triggers and then compares single-lepton with combined and $E_{\mathrm{T}}^{\mathrm{miss}}$ triggers.

6.1 Basic Concepts

At first glance triggers represent a rather simple concept as they do fire or not. However trigger decisions have to be made on very short timescales so only a subset of the full detector information and fast reconstruction algorithms can be used for searching promising signatures in the event. This leads to a discrepancy between the online and the offline value of a certain reference, where time constraints are less of a concern. Triggers are characterized by their online threshold which corresponds to the minimum of the value associated with a certain signature that is needed to fire the trigger. As the online values can be larger or smaller than the offline ones, the following cases can occur: the trigger fires although it should not fire or it does not fire although it should. While the first situation leads to a waste of the available trigger rate (barren rate), the second one is maybe more unfavorable as potentially interesting events get rejected. Turn-on curves visualize the performance of triggers: the trigger efficiency, defined as the ratio of the number of events where the trigger should have fired and the number of events where it actually fired, is plotted against the offline reference. Figure 6.1 illustrates the shape of a typical turn-on curve. A perfect trigger would show a step-function while real triggers show a similar, but smeared out shape around the online threshold. The turn-on region is defined as the area in which the efficiency raises from zero to its maximum value (which does not have to be one) in the plateau region. Usually offline cuts are applied in the analysis to ensure that the trigger operates in the plateau region, as the steep rise in the turn-on region leverages discrepancies , i.e. mismodeling between the MC samples and data.

In general, the available trigger rates dictate the thresholds: The threshold is raised

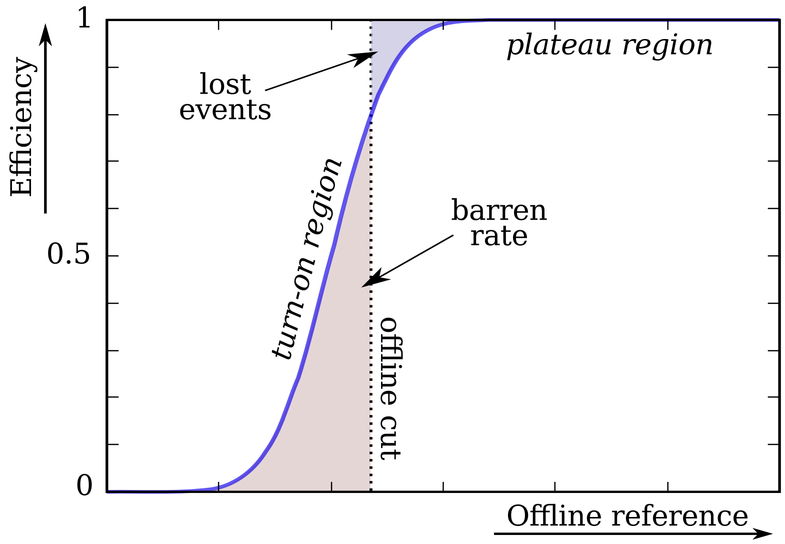

Figure 6.1: Schematic drawing of a turn-on curve that illustrates the terms used in the text. Figure taken from [35]

until the expected rate is manageable†. This would lead however to pretty high thresholds which is in many cases not desirable. There are two solutions to this problem. The first one is to add additional requirements to the trigger decisions, e.g. of topological kind. An example for this is an isolation cut: within a cone around the trigger object should be only a small amount of energy deposits. The other solution is to combine two or more triggers. This also enables lower thresholds for each single leg of such a composite trigger. The price for lower thresholds is in both cases an additional complexity of the trigger. Additional requirements lead in general to a lower efficiency in the plateau they simply provide another source for inefficiency. The legs of a combined trigger might be correlated, which has to be studied well before it should be used in an analysis.

6.2 Comparison of single-lepton with combined triggers

Commonly the trigger choice is motivated by special signatures of the benchmark model. In the lepton-hadron channel this is the appearance of a light lepton. So a natural choice would be the use of single-lepton triggers. This means using one trigger which fires on electron- and one that fires on muon signatures. One major advantage of this configuration is that single-lepton triggers are quite popular and hence easy to use: they are already well studied and scalefactors accounting for any mismodeling in the turn-on region are provided by the collaboration. The drawback is of course their higher

† Another approach is prescaling: events are skipped although the trigger fires. This way the rates can be reduced to account for the limited write-out capacities. Prescaling is less favored as it scales down signal and background democratically, i.e. by a common factor and does not perform a preliminary discrimination between those two.

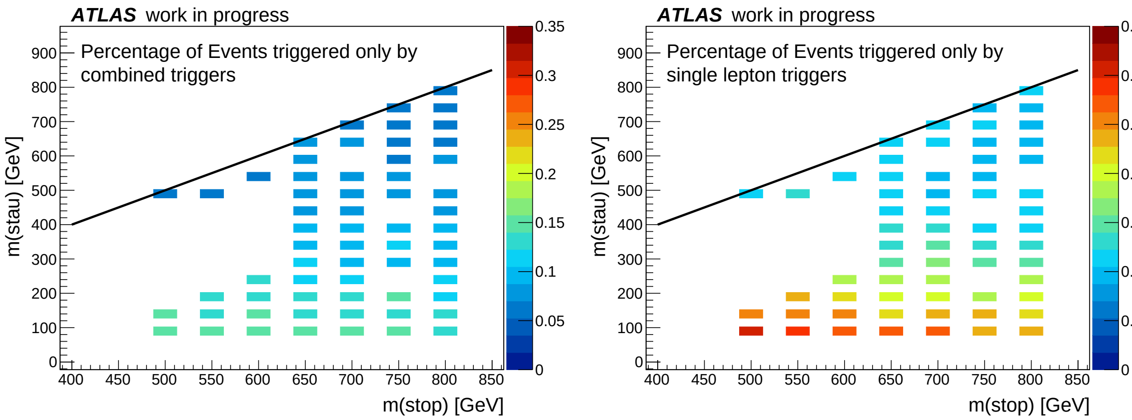

Figure 6.2: Performance of combined (left) and single-lepton trigger (right) after the preselection. Missing points in the grid are due to unavailability of the corresponding signal samples.

thresholds, so a lot of signal events will be rejected, if the leptons in the signal are too soft. Somewhat complementary triggers that also reflect the event topology, fire simultaneously on a tau and electron or muon, respectively. These combined triggers have lower thresholds for the lepton part than their single-lepton trigger counterparts. So they might give rise to another class of signal events containing rather soft leptons, that would otherwise be rejected. As this kind of triggers is rarely used, their drawback is that additional efforts are needed before they can be used in the analysis, e.g. to calculate scale factors. Furthermore these triggers will also be accompanied by larger systematical uncertainties than the well studied single-lepton triggers because time is limited to explore the origins of mismodeling.

The comparison procedure will be as follows. A preselection is introduced that reflects the signature of the particles in the final state. It consists of lepton, jet and trigger related cuts. The lepton cuts assure exactly one electron or muon and exactly one hadronic tau of medium quality in the event. The object quality for the leptons varies: in case of single-lepton triggers they have to be of signal, for combined triggers of baseline quality. The lepton cuts are exclusive, i.e. exactly one light lepton and tau is required, to make the lepton-hadron channel orthogonal to the lepton-lepton and hadron-hadron channels. Additionally, the event must contain at least two baseline jets ($p_{\mathrm{T}} > 20$ GeV) and its leading jet p_{T} has to be greater than 50 GeV to account for the jet signatures in the benchmark model. The trigger cuts check if the corresponding triggers have fired and that they operate in their plateau regions by applying p_{T} cuts one the associated physical object. To be on the safe side, these cuts are rather conservative: muons, electrons and taus need additional 3, 5 and 10 GeV to the online thresholds, respectively. The preselection is summarized in Table A.3.

Performing the comparison after this loose preselection assures that only events relevant for later analysis will enter it. As a measure of performance the number of events triggered only by single-lepton or $E_{\mathrm{T}}^{\mathrm{miss}}$ triggers is taken, normalized to the number of events triggered if both types would be used simultaneously. As the performance of

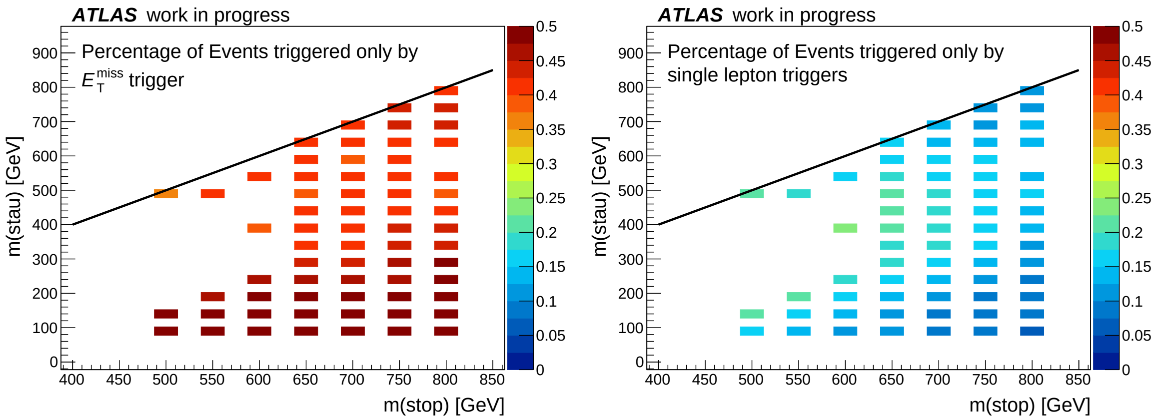

Figure 6.3: Performance of $E_{\mathrm{T}}^{\mathrm{miss}}$-trigger (left) and single-lepton trigger (right) after the preselection.

triggers may vary across the parameter space (here the stop and the stau mass) the ratio is plotted for the whole mass grid.

The results are shown in Figure 6.2. It is clearly visible, that single-lepton triggers perform better than combined triggers across the grid which makes them in conjunction with their simple usage by far the preferable option. Another consideration is to use both trigger types if the gain is worth the efforts. As anticipated, the main gain from combined triggers will be for low stau masses because the less energetic leptons profit from lower trigger thresholds. The gain is with around 10 to 15% however rather moderate. An explanation for the small increase are the comparably high thresholds of the tau-legs of the combined triggers. These are however needed because hadronic taus are difficult to separate from jets which are produced plenty in *pp* collisions. To avoid additional uncertainties that may as well spoil some of the rather small gains, only single-lepton triggers are used in the analysis.

6.3 Comparison of single-lepton with $E_{\mathrm{T}}^{\mathrm{miss}}$ Trigger

When designing the SRs it turns out that they benefit from high $E_{\mathrm{T}}^{\mathrm{miss}}$ cuts. These cuts would assure that a suitable $E_{\mathrm{T}}^{\mathrm{miss}}$ trigger is also in the plateau region. A natural question is if this trigger is an alternative to single-lepton triggers. To study that, the same comparison scheme as before is used.

The preselection for the $E_{\mathrm{T}}^{\mathrm{miss}}$ trigger is essentially the same as for the combined triggers. However there is no cut to ensure that the $E_{\mathrm{T}}^{\mathrm{miss}}$ trigger operates in its plateau region as this would be around 250 GeV (see Figure A.4). It would not be possible to design CRs with reasonable statistics from a preselection containing such a cut. One option is to use the trigger in its turn-on region for the analysis and calculate scalefactors and their associated uncertainties. For that reason the preselection contains a cut of 150 GeV on $E_{\mathrm{T}}^{\mathrm{miss}}$, which ensures that the trigger is well within its turn-on region. Figure 6.3 shows a gain of about 45% evenly across the grid. This gain is mainly due to the lower requirements on the leptons as they are in contrast to the signal lepton for single-lepton trigger just of baseline quality, i.e. the comparison is not fair. When also requiring signal leptons the gain shrinks to about 10% (see Figure A.5) which makes single-lepton triggers more preferable. This makes a final conclusion more difficult as the isolation requirement in the signal definition is physically motivated and hence should be kept.

Another idea is to use the single-lepton triggers in the CR and the $E_{\mathrm{T}}^{\mathrm{miss}}$ trigger in the SRs. Using different trigger for the regions is however unpleasant, as it has to be shown that the extrapolation is still valid. In any case it must be assured that the potential gain is worth this additional effort. So single-lepton triggers are still the preferable choice if consecutive studies will not show a significant gain.

7 Signal Region Optimization

This chapter covers the ideas behind and the results for the design of the SRs. It introduces the significance as an optimization measure and the variables under consideration. After the optimization procedure is discussed the results for single-lepton and $E_{\mathrm{T}}^{\mathrm{miss}}$ triggers will be presented.

7.1 The Significance

As their name implies, SRs should be designed as signal enriched regions, defined by a certain selection. The term signal enriched has however to be understood in a statistical sense. The aim of a search for new particles is to make clear, explicit statements about a potential discovery or exclusion limits on new physics. It is intuitive that the clearness of these statements are quantified by some kind of signal to the expected background ratio. A statistical concept for this is the p-value, defined as the probability to measure the observed value or something more extreme under a certain null hypothesis. This p-value can be turned into the "number of standard deviations (σ)" or significance Z via

$$Z = \Phi^{-1}(1 - p) \tag{7.1}$$

where Φ is the cumulative distribution of the standard Gaussian. When considering the background-only null hypothesis this is an estimate how unlikely it is that an observation can be explained by an upwards fluctuation of the background. An approximation in this scenario for the median significance is given by the "signal over noise" formula

$$Z = \frac{s}{\sqrt{b}} \tag{7.2}$$

where s and b are the number of signal and background events, respectively. It assumes that s and b are distributed according to a Gaussian and approximates the significance only well in the $s \ll b$ limit. As this often cannot be guaranteed, the more sophisticated RooStats function `BinomialExpZ` is used for the optimization. The statistical concept is the same as in Equation 7.2 but it provides a better approximation and also considers the uncertainty on the background expectation (for details see [36]).

In particle physics it is common to refer to two thresholds of the significance: 3σ and 5σ. A significance of 3σ allows to talk about an "evidence of an excess" as the probability of a background fluctuation is below 0.14% while 5σ are needed to claim a discovery.

Process	Subprocesses	MC generator
$t\bar{t}$	dileptonic, semileptonic, all-hadronic	POWHEG
single Top	tW-channel, t-channel, s-channel	POWHEG
W+jets	$W \to e\nu,\ W \to \mu\nu,\ W \to \tau\nu$	SHERPA
Z+jets	$Z \to ee,\ Z \to \mu\mu,\ Z \to \tau\tau,\ Z \to \nu\nu$	SHERPA
VV	WW, WZ, ZZ	POWHEG
$t\bar{t} + V$	$t\bar{t}W$, $t\bar{t}Z$	MADGRAPH
$t\bar{t} + H$	dileptonic, semileptonic, all-hadronic	HERWIG++

Table 7.1: Overview of the SM processes and their MC generators that have been considered in the optimization. A complete list of all samples can be found in Appendix A.10.

7.2 Background

In general background can be divided into two subgroups: reducible and irreducible background. Irreducible background processes have the same final state as the signal process and therefore can not be suppressed even with a perfect detector. Reducible background contributes because of detector effects. In that case for example a particle is not reconstructed or reconstructed as a different particle and thus the background event passes the selection. Final states with hadronic taus are quite susceptible to that because jets have a tendency to be reconstructed wrongly as taus ("fake") due to their similar detector signature. In this manner multi-jet events produced by QCD interactions can contribute to the background estimation: jets fake the physical objects in the selection and hence can make a contribution to the background. It would be computationally very expensive to model these interactions in MC with adequate statistics, so they are often estimated in a data-driven or semi-data-driven way. However one feature of multi-jet events is that they most likely do not contain any high energetic invisible particles that would give rise to significant $E_{\mathrm{T}}^{\mathrm{miss}}$. This means after a moderate $E_{\mathrm{T}}^{\mathrm{miss}}$ cut their contribution can be assumed to be negligible.

To verify this assumption, the appearance of two leptons in the final state allows an easy and quick estimation via the same-sign (SS) method. The basic assumption of this method is that the false reconstruction of a jet as an other object does not depend on the sign of the object's charge. In other words the multi-jet contribution for opposite sign (OS) events $N_{\text{multi-jet}}^{\mathrm{OS}}$ should be of the same order as the contribution for SS events $N_{\text{multi-jet}}^{\mathrm{SS}}$. These have to be produced mainly by QCD interactions faking the corresponding signatures as the SM does not give rise to many processes containing SS leptons. Taking the SS events from the SM (mainly due to a false reconstruction of the charge) into account with MC (without simulation of multi-jet events), the number of multi-jet events with OS can be estimated as

$$N_{\text{multi-jet}}^{\mathrm{OS}} \approx N_{\text{multi-jet}}^{\mathrm{SS}} \approx N^{\mathrm{SS}}(\mathrm{Data}) - N^{\mathrm{SS}}(\mathrm{MC}) \tag{7.3}$$

In Figure 7.1 the $E_{\mathrm{T}}^{\mathrm{miss}}$ distribution is plotted on the left side and contains a multi-jet estimate denoted as QCD (brown part of the stack) based on the method described

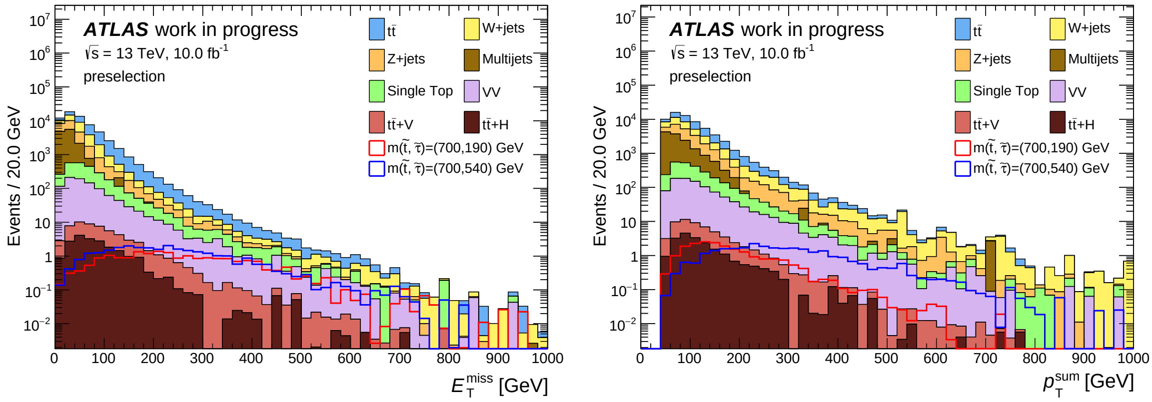

Figure 7.1: $E_{\mathrm{T}}^{\mathrm{miss}}$ (left) and $p_{\mathrm{T}}^{\mathrm{sum}}$ (right) distributions after the preselection with single-lepton triggers for HS (blue line) and LS (red line) samples plotted against the stacked background.

above. For this estimate 3.21 fb^{-1} of 2015 data are used and the resulting estimate is scaled to 10 fb^{-1}. It is clearly visible that multi-jet events do not contribute significantly for $E_{\mathrm{T}}^{\mathrm{miss}}$ values larger than 80 GeV. As the large number of invisible particles in the signal model suggests such a cut anyway, the multi-jet background is neglected in the optimization.

The background estimates for the SM processes have been taken completely from MC for the optimization. All considered background processes and their generators are listed in Table 7.1. The most dominant contributions are expected to come from $t\bar{t}$ events, and from $W \to \ell\nu$ processes in which the tau is faked.

7.3 Ideas for Signal Region design

When designing SRs, it is common to exploit some key features in the kinematics of the signal model. In the stop-to-stau search the general kinematics are governed by the stau mass (see Figure 4.2). When the stau is heavy (HS) the leptons that emerge from their decay will in general be high-energetic. In the case of light staus (LS) more energy is carried by the b-quarks, leading to high energetic b-jets in the event. This is illustrated in Figure 7.1 in which a sample representing a LS (red line) and HS (blue line) scenario are plotted against the stacked expected background. The distribution of the sum of the lepton and the tau p_{T} ($p_{\mathrm{T}}^{\mathrm{sum}}$) shows a rather fast decrease for LS while the HS sample has a wider shape covering a large range. On the other hand, a global variable like $E_{\mathrm{T}}^{\mathrm{miss}}$ shows a quite similar shape, suggesting a common cut for both cases. To account for these different kinematics and thus provide sensitivity across the whole mass grid it is natural to think of two SRs: one that is based on lepton cuts, targeting scenarios in which the stau is heavy (HS), and one using jet-based cuts in case of light staus (LS).

7.4 Optimization Procedure

The first steps for the design of SRs is to find a set of variables that discriminate between signal and background and are in the best case physically motivated. Discriminating means for example that the distributions for signal and background peak at different values, or the background falls off steeply while the signal has a flatter slope for larger values. To get an idea which cuts and corresponding values are reasonable, a brute-force algorithm scans the "cut space" by calculating the significance for each cut combination. The cut space is rather coarse, i.e. the cut values for a variable are not too close to each other and also includes the possibility not to cut on a certain variable. This way some variables can be removed, that do not show any further discrimination power, e.g. because they are highly correlated with another variable. Cut combinations that lead to a large significance give a hint in which way the SR definition may develop. As the brute-force scan only optimizes with respect to significance, one should not simply reduce the distance between the cut values and take the combinations leading to the largest significance as SR. It has to be assured that the MC description is still valid, especially for the main backgrounds. When systematical uncertainties are included single events may "slide" in or out of the regions. In case the corresponding background process is described only by a small number of raw MC events this may result in huge fluctuations, especially if the events have a large weight. Due to the limited MC statistic this is not possible to achieve for every background process. A satisfying statistical description should be assured however for the main backgrounds. If their systematic uncertainties get too large, the overall background estimation is not reliable anymore.

A way to visualize how the background composition behaves under a certain cut are N-1 plots. In these plots the cut of one variable in the cut combination is released, while keeping the other cuts. Next the distribution of the variable which cut was released is plotted. Plots of the significance and the cumulative background, resulting from a cut at the corresponding value of the variable, is applied are placed under the distribution for a better overview. The significance includes a relative uncertainty on the background b consisting of a statistical and systematical part that are combined via Gaussian error propagation as follows

$$\frac{\Delta b}{b} = \sqrt{\left(\frac{\Delta b_{stat}}{b}\right)^2 + \left(\frac{\Delta b_{sys}}{b}\right)^2} \tag{7.4}$$

where the statistical term Δb_{stat} is the square root of the sum of the squared event weights and the systematical term is estimated as a flat contribution: $\Delta b_{sys} = 0.25\ b$. This value represents experience from Run 1 analyses, as the systematical uncertainties were typically in that regime.

The plotting setup directly gives feedback when adjusting the cuts. When tightening a cut, the gain (or even loss) in significance and the influence on the background can be read directly from the plot (see for an example Figure 7.4). Another feature is to see if a certain cut can be loosened a bit for better background statistics and just a small loss in sensitivity. Iterating over all variables leads to a final selection in which the cuts are placed within a maximum of the significance and no further gains are possible without sacrificing too much MC statistics.

7.5 Promising Variables

As there has already been a SR definition in Run 1, an obvious step is to check the variables used there if they still show discrimination power under the new conditions.

7.5.1 Effective mass

The effective mass m_{eff} is defined as

$$m_{\mathrm{eff}} = E_{\mathrm{T}}^{\mathrm{miss}} + H_{\mathrm{T}} + p_{\mathrm{T}}^{\mathrm{sum}} \tag{7.5}$$

where H_{T} is the sum of the two leading jets and $p_{\mathrm{T}}^{\mathrm{sum}}$ the sum of the lepton and the hadronic tau p_{T}. The left plot in Figure 7.2 shows the distribution of m_{eff} for a HS (blue line) and LS (red line) signal. The signal events tend to have a broader m_{eff} shape that the SM background and might therefore discriminate between those two. As it consists of a lepton and jet term it is not influenced much by the varying kinematics across the signal grid and might thus be useful for all scenarios. It is however highly correlated with $E_{\mathrm{T}}^{\mathrm{miss}}$ and the optimization has to show if there are any gains in case both are used.

7.5.2 Transverse mass

The transverse mass m_{T} is defined for a scenario in which a particle with mass M decays into two particles with one of them being invisible. A direct reconstruction of M via the invariant mass of the daughter system is not possible in this case. Denoting the four momenta of the visible particle as p^{μ} and of the invisible particle as q^{μ}, a lower bound on M^2 is however given by [33]

$$m_{\mathrm{T}}^2 = m_p^2 + m_q^2 + 2(E_{\mathrm{T}}^p E_{\mathrm{T}}^q - \mathbf{p}_{\mathrm{T}}\mathbf{q}_{\mathrm{T}}) \leq M^2 \tag{7.6}$$

where E_{T} and $\mathbf{p}_T/\mathbf{q}_T$ are the transverse parts of the energy and of the momentum vector of the decay products, respectively. As there is just one visible particle it has to account for all the missing transverse energy and one can set $\mathbf{q}_{\mathrm{T}} = \mathbf{E}_{\mathrm{T}}^{\mathrm{miss}}$.

In the analysis m_{T} is calculated with the four momentum of the light lepton ℓ. In $W\ell\nu$ events this should lead to an upper bound of m_{T} at the W-boson mass. Detector effects are smearing this out but the right plot in Figure 7.2 shows that contributions of $W\ell\nu$ (yellow part of the stack) to the total background is significantly reduced for $m_{\mathrm{T}} > 100$ GeV. As this is not the case for the signal, which has a rather flat distribution in m_{T}, the variable might be useful to veto $W \to \ell\nu$ events

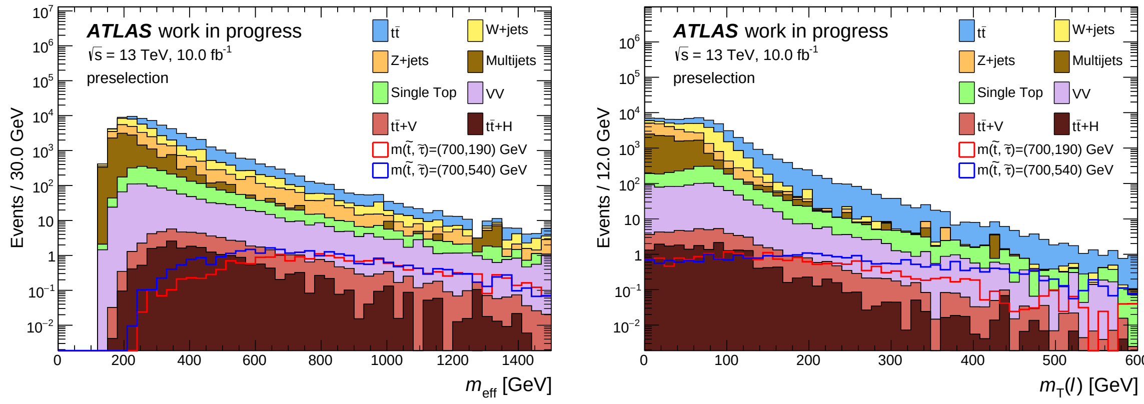

Figure 7.2: m_{eff} (left) and m_{T} (right) distributions after the preselection with single-lepton triggers for HS (blue line) and LS (red line) samples plotted against the stacked background.

7.5.3 The Stransverse Mass

The stransverse mass or m_{T2} can be viewed as a generalization of the transverse mass in case of two or more invisible particles in the final state. In this situation it is unknown how $\mathbf{E}_{\text{T}}^{\text{miss}}$ is distributed among the invisible particles. In the standard definition a particle pair is produced, where each particle decays into one visible and one invisible particle. The basic idea is to loop over all possibilities to distribute $\mathbf{E}_{\text{T}}^{\text{miss}}$ and calculate m_{T} for both decay chains. Denoting the four-momenta of the two visible particles as p_1^μ and p_2^μ, and of the invisible particles as q_1^μ and q_2^μ, m_{T2} has the following form [37]

$$m_{\text{T2}}^2 = \min_{\mathbf{q}_1+\mathbf{q}_2=\mathbf{E}_{\text{T}}^{\text{miss}}} \left[\max\left\{ m_T^2(\mathbf{p}_1,\mathbf{q}_1), m_T^2(\mathbf{p}_2,\mathbf{q}_2) \right\} \right] \leq M^2 \tag{7.7}$$

with the minimization performed over all possible two-momenta of the invisible particles. This variable is constructed to also represent a lower bound to M, the mass of the mother particles.

This analysis uses two variations of the variable. The first one, $m_{\text{T2}}\ (\ell,\tau)$, is calculated with the four-momenta of the lepton and the hadronic tau and assumes massless invisible particles. This definition targets events that contain W-bosons like $t\bar{t}$. Then $m_{\text{T2}}\ (\ell,\tau)$ has the W mass as an upper bound which is shown in the left plot of Figure 7.3. The signal is rather flat over the complete range and shows especially for HS samples a good discrimination. The other m_{T2} variant follows an asymmetric approach and is therefore denoted as $am_{\text{T2}}(b\ell,b)$. It is calculated from the lepton and the two jets with the largest b-tagging weight by pairing the lepton with one of the b-jets and take the four momentum of the resulting system. To solve the two-fold ambiguity, the pairing is taken whose invariant mass is closest to the top mass. This definition aims for dileptonic $t\bar{t}$ events in which one of the leptons is not reconstructed as in theory the variable should be bounded by the top mass for such events. In this picture the mother particles are the top quarks while the b-quarks represent the two visible particles. The invisible particles are on the one side formed by the neutrino from the W decay in the

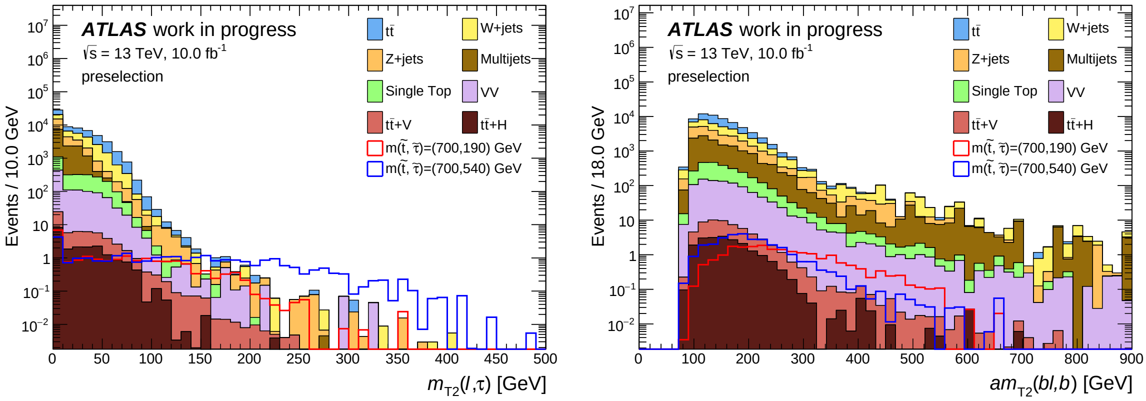

Figure 7.3: $m_{\mathrm{T2}}\ (\ell, \tau)$ (left) and $am_{\mathrm{T2}}(b\ell, b)$ (right) distributions after the preselection with single-lepton triggers for HS (blue line) and LS (red line) samples plotted against the stacked background.

decay chain in which the lepton is reconstructed. In the other decay chain, the not reconstructed lepton and the neutrino are both invisible. So it makes sense to define their mother particle, the W boson itself, as the other invisible particle. Consequently the masses of the neutrino and the W boson are used for the masses of the invisible particles. This assignment does not match the typology of the m_{T2} definition perfectly. However the distribution of am_{T2} (see right plot of Figure 7.3) shows that $t\bar{t}$ events contribute mostly below 170 GeV, so this variable might help to discriminate against top events as especially for LS samples the peak of the distribution is shifted towards higher values.

7.6 Optimization results

In general the optimization will produce a set of N-1 plots as shown in Figure 7.4 that represents the final cut combination. The plots illustrate that the cuts (marked as dashed red lines) are in the right place in a sense that the resulting significance and the quality of the background description with MC are in balance. The starting point are events that pass the preselection described in section 6.2, have $E_{\mathrm{T}}^{\mathrm{miss}} > 150$ GeV to veto multi-jet events and at least one b-jet to exploit the characteristic of the signal model and suppress events from $W \to \ell\nu$ processes.

7.6.1 Single-Lepton Triggers

The results for a SR targeting models of heavy staus using single-lepton triggers are shown as N-1 plots in Figure 7.4 and summarized in the second column of Table 7.2. Testing combinations of cuts, the variables $E_{\mathrm{T}}^{\mathrm{miss}}$, m_{T2} and the p_{T} of the tau lead to the most promising results. The resulting significance of above 6 is quite large, at the price of low MC statistics represented by an uncertainty on the background of about 25% . However, Figure 7.4 shows clearly that any loosening of the cuts would lead to

SRs for single-lepton triggers	heavy staus	light staus
basic cuts	$E_{\mathrm{T}}^{\mathrm{miss}} > 150$ GeV, $N_{b\text{-jet}} \geq 1$	
SR cuts	$E_{\mathrm{T}}^{\mathrm{miss}} > 200$ GeV $p_{\mathrm{T}}(\tau) > 90$ GeV $m_{\mathrm{T2}} > 100$ GeV	$m_{\mathrm{eff}} > 600$ GeV $p_{\mathrm{T}}(\text{ldg. } b\text{-jet}) > 125$ GeV $m_{\mathrm{T2}} > 100$ GeV $am_{\mathrm{T2}} > 150$ GeV
Total Background	1.02 ± 0.25	2.08 ± 0.44
Signal	13.79 ± 0.55	5.54 ± 0.35
Significance Z_0	6.35	2.45

Table 7.2: Results for the SR optimization using evens triggered by single-lepton triggers targeting scenarios of heavy and light staus. The contribution to the total background of each background sample is shown in Figure A.6.

a distinct loss of significance.

In the case of light staus a combination of the variables m_{eff} , m_{T2} , am_{T2} and the p_{T} of the leading b-jet leads to the best results (see Figure 7.5 for the N-1 plots and the third column of Table 7.2). However, it is not possible to raise the significance above 3 with the available set of variables as none of them discriminates signal from $t\bar{t}$ events good enough. This selection is also accompanied with a large statistical uncertainty on the background of about 25%.

7.6.2 $E_{\mathrm{T}}^{\mathrm{miss}}$ Trigger

As the SRs benefit from hard $E_{\mathrm{T}}^{\mathrm{miss}}$ cuts, the question arises if a $E_{\mathrm{T}}^{\mathrm{miss}}$ trigger would not be the better choice than single-lepton triggers. In contrast to them, the $E_{\mathrm{T}}^{\mathrm{miss}}$ trigger is fully efficient in its plateau at around 250 GeV. So its use could lead to some additional events in the selection. For that reason the optimization is redone starting at the same preselection as before but requiring that the $E_{\mathrm{T}}^{\mathrm{miss}}$ trigger has fired.

It has to be stated that this starting point is not optimal, as the preselection demands signal leptons with cuts of 25 and 10 GeV on the electron and muon p_{T}, respectively. However, these cuts are not required for the $E_{\mathrm{T}}^{\mathrm{miss}}$ trigger and can be loosened. This could lead to a gain of signal events, especially in the case of final states with an electron. On the other hand the signal definition also contains the isolation requirement which should definitely be kept. In the current background and signal samples available for this study it is technically not possible to extract the isolation information separately. So the preselection for the $E_{\mathrm{T}}^{\mathrm{miss}}$ trigger also uses signal leptons but one has to keep in mind that its performance in the SRs might be underestimated.

To summarize the starting point for this optimization is formed by events that fulfill the preselection, have $E_{\mathrm{T}}^{\mathrm{miss}} > 250$ GeV to be in the plateau of the trigger and again at least one b-jet.

For a HS Signal Region, any lepton based cuts surprisingly do not lead to the best

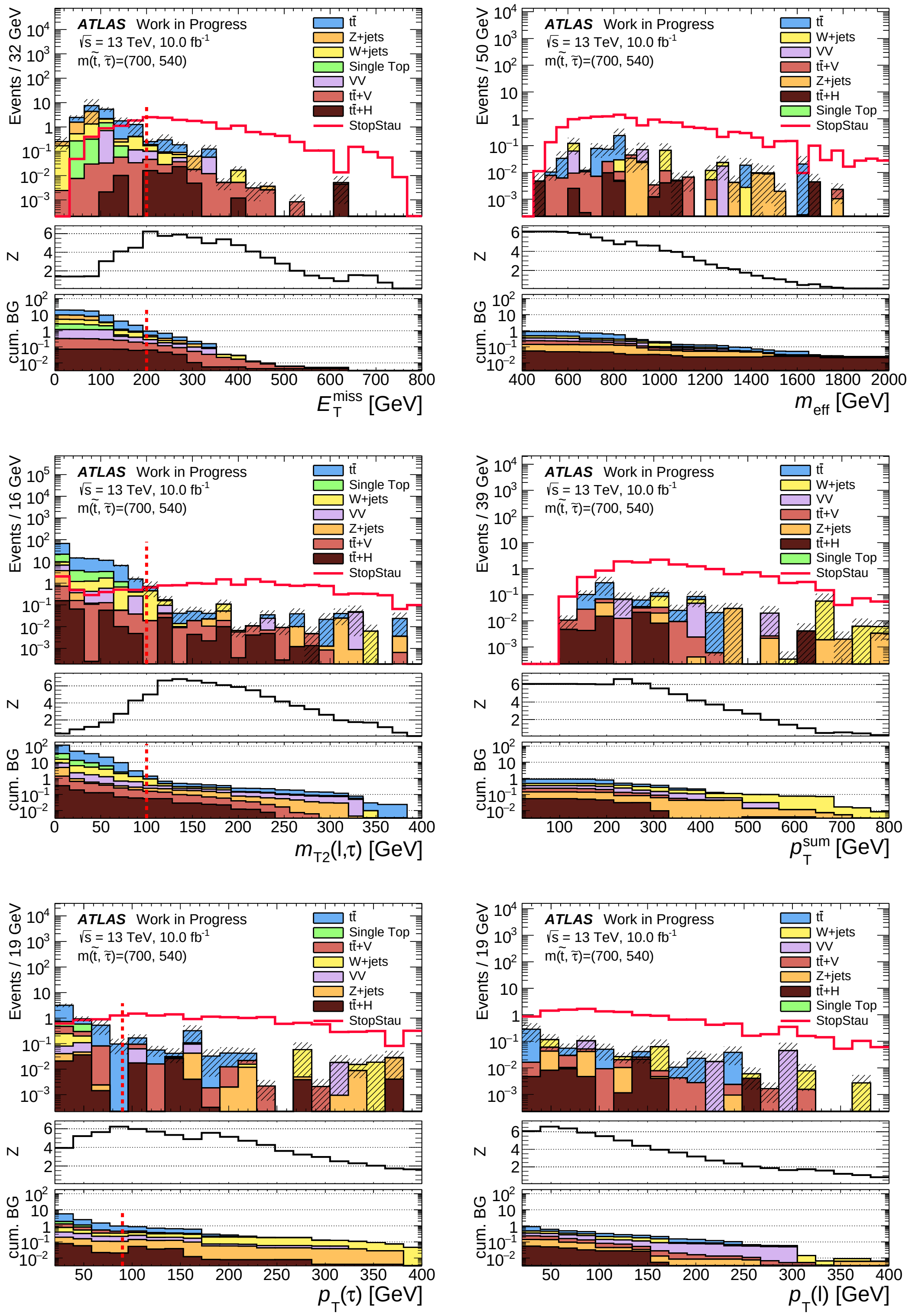

Figure 7.4: Set of N-1 plots representing the final cut combination in the optimization for a HS Signal Region based on single-lepton triggers. Each N-1 plot is formed by a plot of the distribution of the variable under consideration (top), the significance Z when cutting on the associated value (middle), and the remaining cumulative background for such a cut (bottom). The dashed bars in the distribution plots indicate the statistical error of the background in each bin.

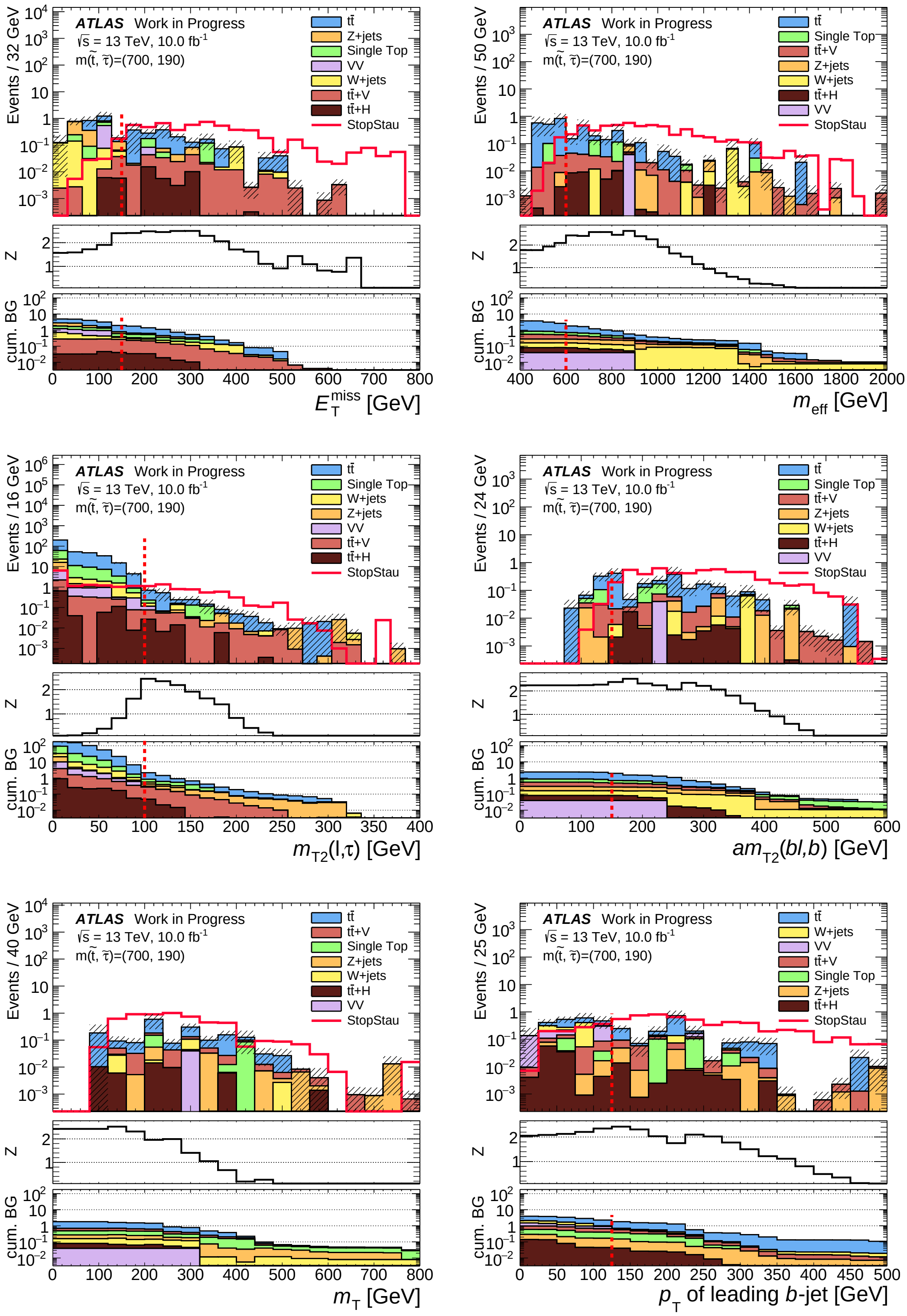

Figure 7.5: Set of N-1 plots representing the final cut combination in the optimization for a LS Signal Region based on single-lepton triggers. Current cuts are marked as dashed red lines.

SRs for $E_{\mathrm{T}}^{\mathrm{miss}}$ trigger	heavy staus	light staus
basic cuts	$E_{\mathrm{T}}^{\mathrm{miss}} > 150$ GeV, $N_{b\text{-jet}} \geq 1$	
SR cuts	$m_{\mathrm{T2}} > 150$ GeV	$H_{\mathrm{T}} > 200$ GeV p_{T}(ldg. b-jet) > 80 GeV $m_{\mathrm{T2}} > 90$ GeV $am_{\mathrm{T2}} > 190$ GeV
Total Background	1.15 ± 0.2	1.33 ± 0.22
Signal	12.4 ± 0.53	5.21 ± 0.34
Significance Z_0	5.73	2.81

Table 7.3: Results for the SR optimization using evens triggered by single-lepton triggers targeting scenarios of heavy and light staus.

result. On the contrary, a very simple SR definition of just one additional harsh m_{T2} cut gives a significance close to 6 and a total uncertainty on the background of about 17% (see Table 7.3). Figure 7.6 shows that the significance does not really benefit from additional cuts on lepton related variables.

The situation for a SR targeting light staus is different as in this case a combination of cuts has to be preferred, namely on H_{T}, the p_{T} of the leading b-jet and on the m_{T2} variables (N-1 plots in Figure 7.7). This configuration gives a significance just below 3 and an acceptable background uncertainty of about 16%.

7.7 Summary

All in all, the two trigger types give rise to quite similar SR definitions and the resulting sensitivity, especially in the LS scenarios. The $E_{\mathrm{T}}^{\mathrm{miss}}$ trigger tends to give less background uncertainty. This might occur because the single lepton triggers are not fully efficient in their plateaus (see Figure A.4). Consequently, some events are lost due to this effect, which does not happen when using a fully efficient trigger. Ideally, the next step would be to adjust the preselection for the $E_{\mathrm{T}}^{\mathrm{miss}}$ trigger, i.e. to lower the p_{T} requirements for the leptons, as additional events with low p_{T} leptons might improve the performance of $E_{\mathrm{T}}^{\mathrm{miss}}$ trigger SRs. After providing separate information on the lepton isolation—which was not available for this study—in the events samples, the fraction of events containing isolated low p_{T} leptons can be estimated and the optimization eventually redone.

Although the comparison is not optimal a first conclusion from this study can be drawn. So far the $E_{\mathrm{T}}^{\mathrm{miss}}$ trigger does not perform significantly better than the single-leptons counterparts. When the preselection is adjusted, more signal events will pass the selection. Otherwise this is also true for background events. So the significance, roughly a signal over background ratio, does not necessarily improve. Most likely a switch of the trigger type will not provide large gains in sensitivity which would

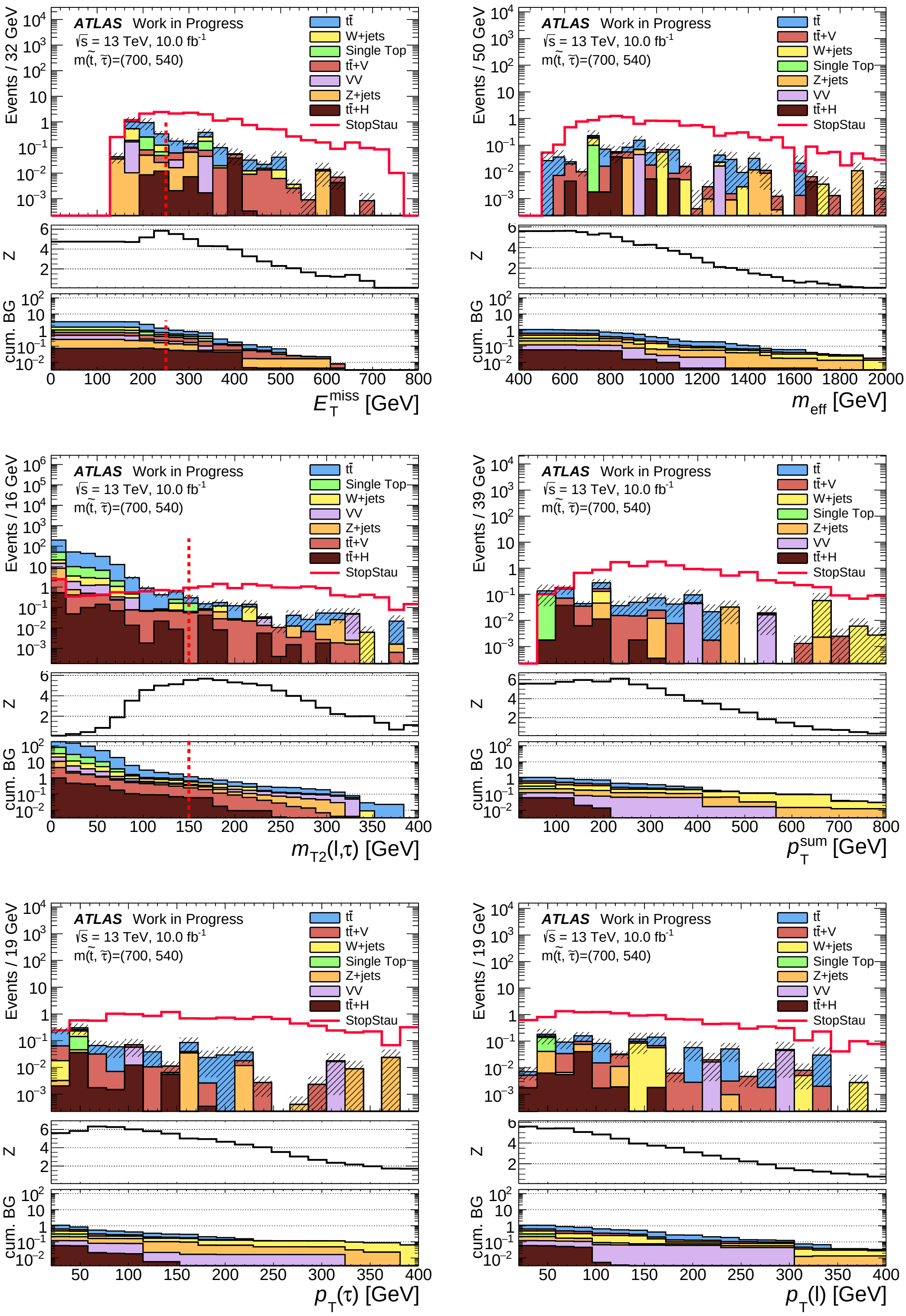

Figure 7.6: Set of N-1 plots representing the final cut combination in the optimization for a HS Signal Region using the E_T^{miss} trigger. Here a very simple SR definition, containing only E_T^{miss} and m_{T2} cuts, gives the best results.

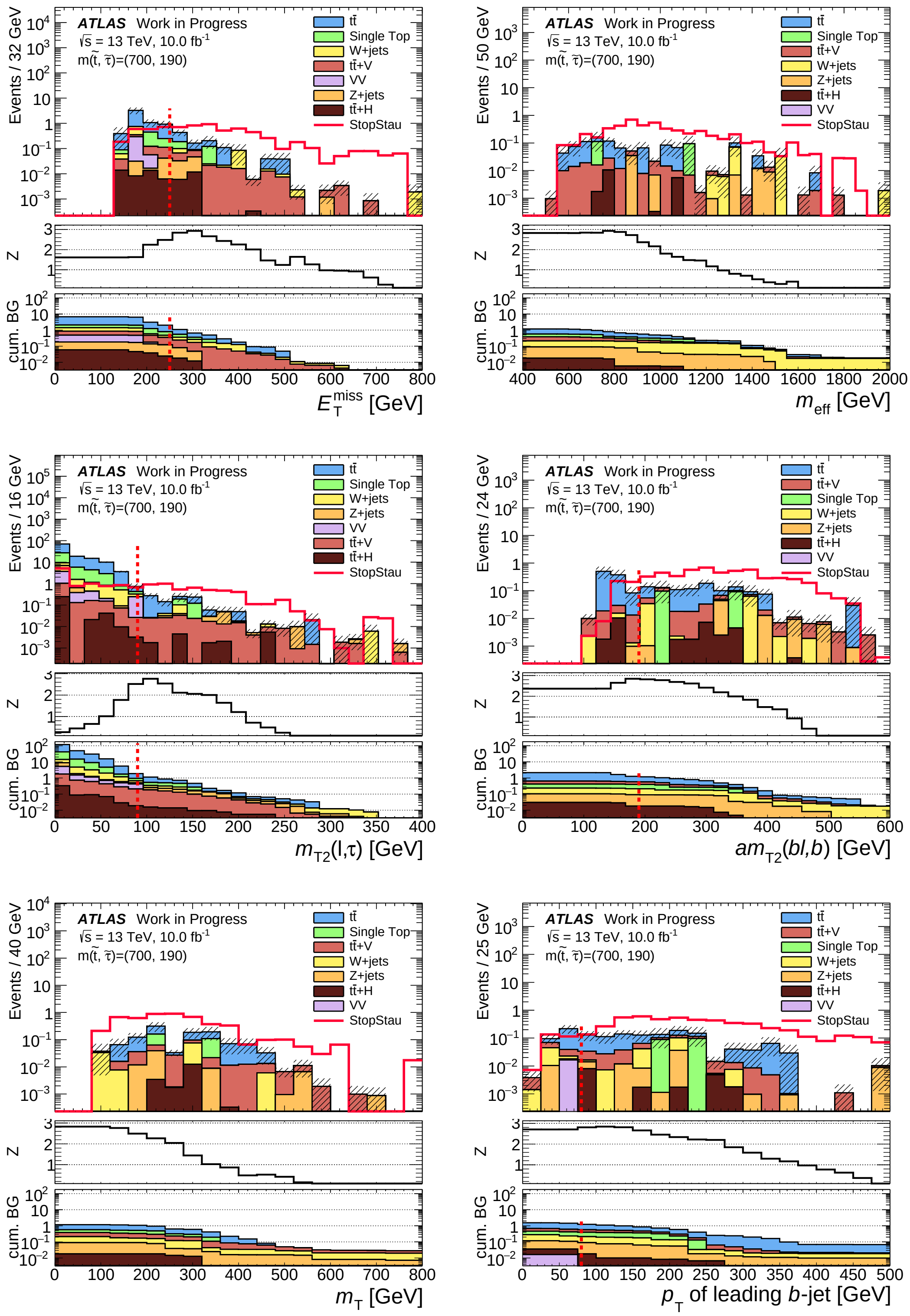

Figure 7.7: Set of N-1 plots representing the final cut combination in the optimization for a LS Signal Region based on the E_T^{miss} trigger.

outweigh the disadvantages. As discussed in section 6.3 this is mainly the necessity to use different triggers in CRs and SRs and hence to validate the extrapolation between them. Because of the large background uncertainty in either case, this extrapolation is definitely needed at least for the main backgrounds to support their estimates in a data-driven and reliable way. Regarding the other background processes the low MC statistics provided by MC have probably to be accepted. Low MC statistics is a common problem when cutting in areas of the phase space that is barely occupied by the SM.

8 Expected Discovery and Exclusion Limits

After the design of the SRs, a natural question is how they will perform, e.g. with respect to the Run 1 results, when they are embedded in the other parts of the analysis like the CRs. For that usually the expected limits for discovery and exclusion are plotted over the parameter space, which is in this analysis spanned by the masses of the stop and the stau. As this search is aiming for a presentation of first results at the summer conferences in 2016, the sensitivity and exclusion predictions are created for 10 fb^{-1}, which is the expected amount of total available integrated luminosity for that date. This chapter will also shortly review the statistical methods involved for the hypothesis tests before presenting the results produced with HistFitter, a framework for statistical analysis.

8.1 Statistical Data Analysis

Data analysis in high energy particle physics is essentially a reduction of the physical model formulated in group and quantum field theory to a statistical model. Only this kind of model can be treated with statistical methods which allow statements how well the model under consideration actually fits to the observed data and determine the values of its parameters. There are two “schools” that interpret the concept of probability differently: Bayesians and Frequentists. In the frequentist approach probability is interpreted as the fraction of outcomes for future, identical experiments [38]. For Bayesians probability is more related to a subjective degree of belief, for example how likely a hypothesis is. The study in this thesis make only use of the first approach, so mainly frequentist statistical methods are described here.

8.1.1 Fundamental Concepts

A hypothesis H is a statistical model that makes a statement about the probability $P(\mathbf{x}|H)^\dagger$ for a dataset $\mathbf{x}$ [33]. If the probability is interpreted as a function of H, it is called the likelihood L, i.e. $L(\mathbf{x}|H)$ is the probability to measure the data $\mathbf{x}$ assuming the model H. H usually specifies a p.d.f. $f(x)$ for some random variable x. If f depend on further free parameters, H is called a composite hypothesis. Usually the signal strength μ is set as a free parameter, so that $\mu = 0$ refers to the background only hypothesis H_0 and $\mu = 1$ to H_1, the hypothesis with the nominal signal as predicted by the benchmark model. The idea of statistical tests is to construct a critical region w_μ so that the probability for the data to be in w_μ and thus falsely reject H_μ is not

† Baysians would ask for $P(H \mid \mathbf{x})$, the degree of belief for H being true given the data greater than α, denoted as the size of the test [39]:

$$P(\mathbf{x} \in w_\mu | H_\mu) \leq \alpha \tag{8.1}$$

This is equivalent to the p-value concept introduced in section 7.1 when $p_\mu < \alpha$ defines the corresponding critical region. The confidence level CL for rejecting a hypothesis is then given by $1 - \alpha$. Instead of p-values one often constructs a test statistic q_μ that represents the compatibility of the data with the hypothesis H_μ. Usually higher values of q_μ reflects increasing incompatibility so that the connection to the p-value is as follows

$$p_\mu = \int_{q_{\mathrm{obs}}}^{\infty} f(q_\mu | H_\mu)\, \mathrm{d}q_\mu \tag{8.2}$$

where $f(q_\mu|H_\mu)$ is the p.d.f. of the test statistic assuming H_μ and q_{obs} its observed value. In other words, the signal-to-background discrimination is condensed into one single number [40]. The Neyman-Pearson lemma states that likelihood ratios form the most powerful discriminators. A variant of such a test statistic and commonly used at LHC related experiments, uses the profile likelihood ratio $\lambda(\mu)$ defined as

$$q_\mu = -2 \log \lambda(\mu) = -2 \log \frac{L(\mathbf{x}|\mu, \hat{\hat{\boldsymbol{\theta}}})}{L(\mathbf{x}|\hat{\mu}, \hat{\boldsymbol{\theta}})} \tag{8.3}$$

where $\boldsymbol{\theta}$ is a set of nuisance parameters related to systematic uncertainties, $\hat{\mu}$ and $\hat{\boldsymbol{\theta}}$ maximize the likelihood function and $\hat{\hat{\boldsymbol{\theta}}}$ maximize the likelihood for a given μ. Finally the modeling of L will make use of the assumption that the results of counting experiments in particle physics follow Poisson distributions. The likelihood for some observed event counts $\mathbf{n}$ and background predictions $\mathbf{b}$ in the CRs and SRs will have the form [18]

$$\begin{aligned} L(\mathbf{n}|\mu, \mathbf{b}, \boldsymbol{\theta}) &= P_{\mathrm{SR}} \times P_{\mathrm{CR}} \times C_{\mathrm{sys}} \\ &= P(n_S|\lambda_S(\mu, \mathbf{b}, \boldsymbol{\theta})) \times \prod_{i \in CRs} P(n_i|\lambda_i(\mu, \mathbf{b}, \boldsymbol{\theta})) \times C_{\mathrm{sys}} \end{aligned}$$

where P_{SR} and P_{CR} are the probabilities for measuring the number of observed events n_S and n_i in the SR and CRs, respectively, under the assumption of the Poisson expectations λ that depend on the background predictions $\mathbf{b}$, the nuisance parameters $\boldsymbol{\theta}$ and the signal strength μ. The term C_{sys} includes systematic uncertainties which are in case of independent uncertainties modeled as a product of Gaussians. The last missing ingredient is the distribution of the test statistic under a certain hypothesis, that is $f(q_\mu|H_\mu)$. It can be obtained by rendering pseudo experiments that randomize the observed event counts in the regions. This is however computational and time expensive when many systematic uncertainties are included and thus the statistical models get complicated. However, according to Wilks' theorem the distribution of q_μ is known when the statistic is large enough (the asymptotic regime). In this case q_μ follows a χ^2 distribution with one degree of freedom and can easily be approximated [18]. The p-value defined in Equation 8.2 can now be used for statistical tests reflecting the discovery and exclusion potential of the new physics under consideration.

8.1.2 Discovery Limits

When analyzing an excess over the SM predictions, the main question is how probable it is that the excess is caused by an upwards fluctuation of the background. If this probability is small enough, a significant excess or even a discovery can be claimed. In the statistical language the null hypothesis is the background only hypothesis H_0 and is tested against some alternative hypothesis including a signal component H_μ.

The expected discovery sensitivity is calculated by assuming an observation of the expected background plus the nominal signal. The probability of the background being responsible for the resulting higher event numbers is translated into the number of standard deviations (σ's). Repeating this for every point in the signal grid, the contours of particular σ-levels can provide information in which areas of the mass plane the analysis is already sensitive or not.

8.1.3 Exclusion Limits

In case of no significant excess above the SM the natural question arises which parts of the parameter space can be excluded with the observation. Here, one is interested in the probability that a model consisting of signal and background can account for the number of observed events or less. The roles of the hypothesis are inverted as H_μ is now the null hypothesis. Typically, exclusion statements in particle physics are made at 95% CL. This means the probability to falsely reject the signal plus background hypothesis is less than 5%. In case of low sensitivity, i.e. when the signal prediction is only slightly larger than the corresponding background prediction, the use of the p-value as discriminant is problematic. It might lead to exclusion caused by e.g. an under-fluctuation of the background. Exclusion of parameter subspaces with little to no sensitivity is generally an unfavored behavior that can be improved by using the CL_s statistic instead, defined as [33]

$$\mathrm{CL}_s = \frac{p_\mu}{1 - p_0} \tag{8.4}$$

where p_0 is the p-value of the background-only hypothesis. Both p-values are defined as the integral of a test statistic as stated above. Exclusion statements require now $\mathrm{CL}_s < \alpha$. This is in a sense more stringent than before because the denominator of Equation 8.4 is always smaller than one. If sensitivity is low, then not only p_μ decreases but also $1 - p_0$ in case of an under-fluctuation.

The expected exclusion limits are calculated assuming nominal signal strength and that exactly the background predictions are observed. Plotting the CL_s values for all signal points enables to check the exclusion performance e.g. with respect to Run 1 over the mass plane and gives somewhat complementary information to the discovery limits of the analysis status.

Variable	CR $t\bar{t}$	CR W
$N_{b\text{-jet}}$	≥ 1	0
$E_{\mathrm{T}}^{\mathrm{miss}}$	> 40 GeV	> 60 GeV
m_{eff}	> 200 GeV	> 300 GeV
m_{T} (ℓ)	> 100 GeV	40–120 GeV
H_{T} / m_{eff}	–	< 0.5
m_{T2} $(b\ell, b\tau)^{\ddagger}$	> 180 GeV	–
m_{T2} (ℓ, τ)	20–100 GeV	–

Table 8.1: Definitions for the $t\bar{t}$ and W Control Regions

8.2 Preliminary Control Regions

Preliminary CRs for $t\bar{t}$ and $W\ell\nu$ processes have been designed by Balthasar Schachtner and will be shortly summarized here. The CRs are based on the same preselection introduced in section 6.2 and the precise definitions are listed in Table 8.1. Their design reflects special signatures, e.g. the presence or absence of b-jets in top and W related processes, respectively. To suppress multi-jet background, moderate cuts on $E_{\mathrm{T}}^{\mathrm{miss}}$ are applied.

Figure 8.1 compares the 2015 data with the SM prediction in the cutflows for the CRs. The last bins show reasonable purities around 65%. For the W CR there is already agreement between data and MC within the statistical uncertainties. This is not the case for the $t\bar{t}$ CR, but the difference of data and prediction is less than 20% and hence acceptable for a preliminary CR. Furthermore the signal contamination is for most parts of the grid less than 1% (see Figure A.8) and hence negligible.

It is clear that the origins of the differences of observation and prediction have to be understood, but it can be concluded that the prediction of the MC is not completely off. Thus it can be expected that the final normalization factors will not differ much from 1. So when calculating the expected discovery and exclusion limits without them the results will still be reasonable.

8.3 HistFitter Setup

The HistFitter [18] framework provides an interface to the classes in RooFactory, RooFit and RooStats that build the statistic models for the predictions and perform the fits and hypothesis tests.

The two CRs and two SRs have been implemented such that the fit is better constrained as it is performed simultaneously in all regions. For a statistical correct calculation, the regions have to be orthogonal to each other which means to cover different phase spaces. The CRs are orthogonal to each other and the SRs via the b-jet veto and the inverted m_{T2} cut in the W and $t\bar{t}$ CR, respectively. To make the SR orthogonal to

‡ This m_{T2} variant originates from the Run 1 analysis and its exact definition can be found in [20]

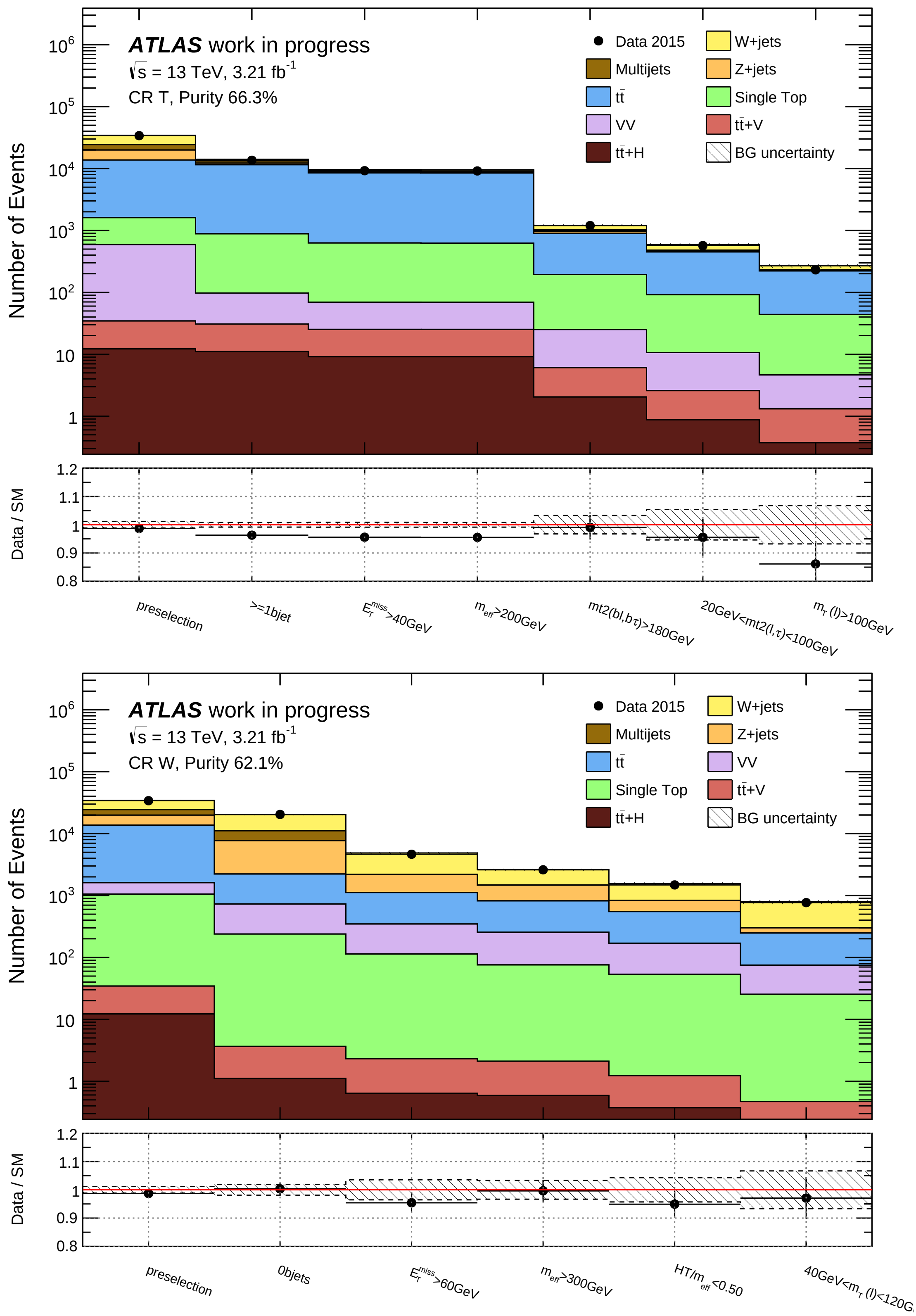

Figure 8.1: Cutflows for the $t\bar{t}$ (top) and W (bottom) Control Regions comparing the MC predictions of the background with 3.2 fb^{-1} of 2015 data.

each other an additional cut on the ratio of the sum of the transverse momenta of the two leptons ($p_{\mathrm{T}}^{\mathrm{sum}}$) and the sum of the transverse momenta of the two leading jets (H_{T}) is introduced. The SR targeting heavy staus requires $p_{\mathrm{T}}^{\mathrm{sum}}/H_{\mathrm{T}} > 0.45$ while for the LS Signal Region this cut is inverted.

This addition to the SR definitions (see Table 7.2) decreases again the MC statistic by a small amount, but the simultaneous combination of the SR will lead to additional constraints in the model and thus can improve the results. It is also possible to treat the SRs separately and calculate the expected limits for each SR and combine the results by taking the best limit for every grid point in the mass plane. As there is no need of additional cuts for orthogonalization, this approach has the advantages of less statistical uncertainties. In this study the former approach is used because it is simple to make the SR orthogonal with an acceptable loss of MC statistics.

To incorporate systematic uncertainties, which have not been implemented in detail in the available samples, all backgrounds are decorated with a 40% weight-based “dummy” systematic uncertainty. The magnitude is in the regime of the Run 1 uncertainties and a rather conservative estimate. Theoretical uncertainties on the signal cross section are usually taken into account in the observed limit, which cannot be done for this study. As an alternative, they are treated with a 20% systematic on the signal sample. This is again rather conservative, compared to the official uncertainties [23].

Systematic uncertainties can be implemented in a correlated or uncorrelated way. When a systematic uncertainty affects multiple samples, their statistical modeling contains the same nuisance parameter to reflect this correlation. On the contrary if a certain systematic uncertainty affects only one sample this will get its “own” systematic uncertainty which is not correlated with the others. The final analysis will contain an ensemble of correlated and uncorrelated systematic uncertainties. For this study, only uncorrelated dummy systematics are used, so each background sample has a separate systematic. In the case of one correlated systematic shared by all samples, a strong correlation up to 0.99, depending on the size of the uncertainty, between the normalization factors of the $t\bar{t}$ and W CR can be observed. The results of the hypothesis tests do not depend on the implementation of the dummy systematic so to avoid these unexpected correlations uncorrelated dummy systematics are used.

For the evaluation of the hypothesis test the asymptotic calculator is used. To check that the approximation of the asymptotic regime is valid, the hypotheses tests were run with toys as well for a couple of points. As both methods lead to very similar values for the expected p-values the asymptotic calculator is used throughout the grid. To test if the obtained results match with the fitted signal and background yields, another validation of the HistFitter setup was done with a very simple configuration file. This script takes only the signal and total background yields, and their associated errors as input. Then the hypothesis tests are performed using these numbers. Input are the yields after the fit, retrieved with a script contained in the HistFitter package (see Appendix A.9). Again the results are compared for a number of grid points. In general the simple setup gives similar but slightly less stringent limits. This is expected, as the simple configuration effectively uses only one SR, while the main setup uses two.

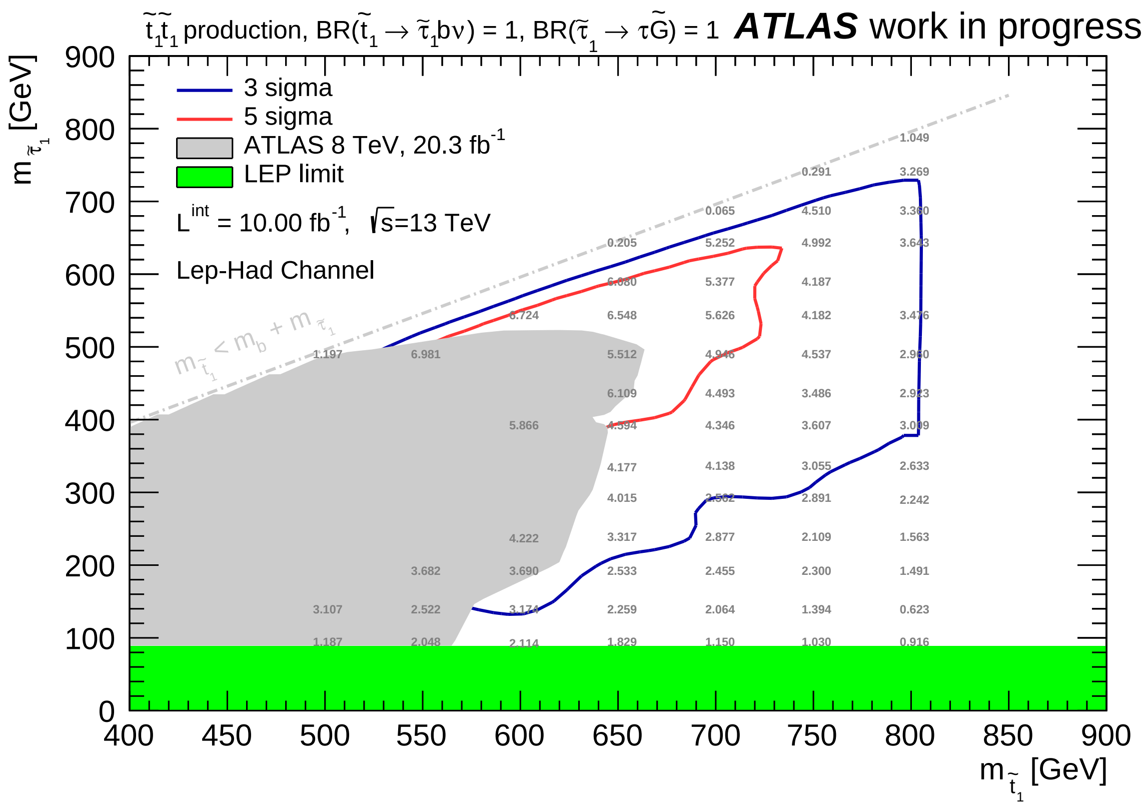

Figure 8.2: Expected Run 2 discovery limits for 10 fb^{-1} in the mass plane of the stop and the stau. The gray numbers are the associated σ values of the expected p-values for the background only hypothesis. The dark blue and the red line represent the 3σ and 5σ contours, respectively. The gray area marks the observed exclusion limit in the Run 1 analysis [20]. The green bar gives the limit on the stau mass observed in the LEP experiments [21].

Overall, the limits are similar enough to deduce that the setup produces correct results.

8.4 Results

The expected limits for discovery and exclusion are shown in Figure 8.2 and Figure 8.3, respectively. The main conclusion for both limits can be summarized as follows.

- **Good performance of the HS Signal Region**
  Both limits show excellent sensitivity in scenarios with heavy staus. This is also expected due to the good signal–background discrimination of the $m_{\mathrm{T2}}(\ell, \tau)$ variable in this case.

- **Loss of sensitivity at the borders**
  Close to the diagonal as well as towards the LEP limit, i.e. lower stau masses, the sensitivity decreases quite fast. At the diagonal, representing energy conservation in a sense that the stop cannot be lighter than its decay products, this loss is most

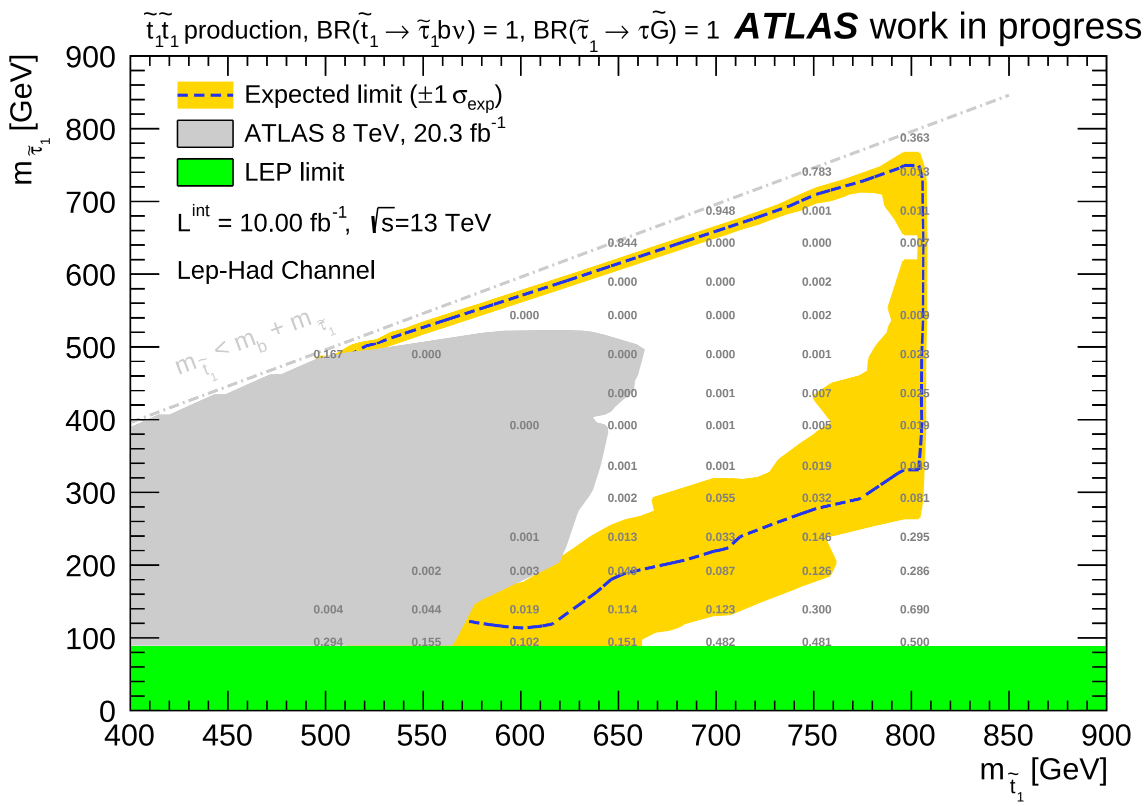

Figure 8.3: Expected Run 2 exclusion limits for 10 fb^{-1} in the mass plane of the stop and the stau at 95% CL. The gray numbers are the expected CL$_s$ for nominal signal strength. The dashed blue line represents the exclusion contour and the dark yellow area its 1σ error band. The gray area masks the observed exclusion limit in the Run 1 analysis [20]. The green bar reflects the limit on the stau mass observed in the LEP experiment [21].

likely due to the jet requirements. Compressed scenarios, in which the masses of the SUSY particles are close to each other, may change significantly in their signature. Here the stau gets so heavy, that there is hardly energy left for the b-quarks to leave a noticeable jet signature. The very narrow uncertainty bands in the exclusion limit plot illustrate that the sensitivity decreases quickly. The low sensitivity and exclusion power for low stau masses is a consequence of the signal model getting more and more similar to $t\bar{t}$ when the stau mass approaches the mass of the W boson and thus makes it more challenging to between these two processes. So far an effective top-discriminating variable is missing for this scenario.

- **Reaching the borders of the simulated grid**
  The exclusion limits already reach the border for HS scenarios. This is a clear hint to enlarge the simulated parameter space to not artificially limit the exclusion range.

The most important conclusion is, however, that the analysis in the current state shows already a discovery reach for stop masses up to 700 GeV which is beyond the exclusion limit of Run 1. In the absence of signal, the expected exclusion range increases to stau masses up to 800 GeV with 10 fb^{-1} of integrated luminosity, which is about half the data recorded in Run 1. This highly encourages a presentation during the summer conferences.

Improving the less sensitive regions will be another critical challenge. For the region close to the diagonal another SR loosening all jet cuts and focus completely on the resulting hard leptons is the most obvious solution. When neglecting the b-jet signature the model will look quite similar to other SUSY stop searches and thus potential overlap has to be avoided. To deal with the decreasing sensitivity towards low stau masses a top reconstruction algorithm can be considered. In a sense this is already done with the am_{T2} variable (see subsection 7.5.3) that in theory has a cutoff at the top mass. Tweaking this variable, e.g. how the two-fold ambiguity in defining the pairing is resolved, is a natural starting point for improving the discrimination against top background.

However, one has to keep in mind that there are also the lepton-lepton and hadron-hadron channel, that can contribute in a combination. In Run 1 these two channels already provided sensitivity at the diagonal and for light staus, where the lepton-hadron channel lost sensitivity like it is currently the case as well. As the different channels can be made orthogonal quite easily via tau vetos or requirements, their combination is possible with a moderate effort and an elegant way to maximize sensitivity across the mass grid.

9 Conclusion and Outlook

Although the way to a working MC generator configuration was full of technical challenges, the current setup produces signal events modeling the process under consideration correctly. With the produced signal samples, the question which triggers should be used in a search for direct stop-to-stau production is answered: single lepton triggers perform well and are easy to use as they are quite common in SUSY searches and thus well understood. Based on these kind of triggers, Signal Regions have been designed and optimized with respect to an optimal balance of sensitivity and MC statistic for the background description. In a extensively validated configuration of a statistical framework, they show, combined with preliminary Control Regions, excellent discovery potential and exclusion power beyond the Run 1 analysis at 10 fb^{-1}. This makes the analysis interesting for a presentation of first results during the summer conferences.

Even though the expected sensitivity is very promising, the analysis is in the middle of its research and development phase. Consequently, there is still much work left, which concerns roughly three categories. The first one is to improve the background predictions. The CRs have to be revised to improve the data to MC agreement. Origins of disagreement have to be studied and compensated with normalization factors. This semi-data driven approach has then to be tested with yet to be designed Validation Regions. Besides that, the estimate of the multi-jet background has to be improved as this may not be important in the SRs but in the CR as the $E_{\mathrm{T}}^{\mathrm{miss}}$ cuts there are significantly lower. The assumption of equal fake rates for same-sign and opposite-sign events may not be completely justified. To account for deviations in the reconstruction rates, an option is to define a CR dedicated to multi-jet processes and calculate a normalization factor in this region. The factor can then be applied on the multi-jet contribution in the other CRs.

Secondly, a major gain would be more sensitivity in the LS region. This could be achieved by either a possible contribution of the hadron-hadron channel or a new variable discriminating signal from top event better. Possible starting points are to improve in the implemented am_{T2} variable or even add a more sophisticated top reconstruction algorithm. Conceivable as well is to exploit “Fat-jets” [41]. These jets are for example produced when the top quark has a large boost. Then its decay products will be located within a cone due to momentum conservation. Everything might the be reconstructed as one fat jet that exhibits substructure. Algorithms using this substructure enable the reconstruction of boosted top quarks as the invariant mass of the resulting jet will be close to the top mass. Such events have large $E_{\mathrm{T}}^{\mathrm{miss}}$ and might contribute to the $t\bar{t}$ background notably. All this has of course to be studied in detail.

Another large effort will be to incorporate systematics like uncertainties on the jet energy scale and replace the dummy systematics that are currently in use. The systematics will lead to small variations in the variable values and will show how much the background predictions will fluctuate. As there are quite a lot of systematics to consider this will take a good amount of bookkeeping and computation time.

When the construction areas mentioned above can be closed in time, not too many new ones arise and new data is recorded as planned, the analysis team will definitely be able to present some new insights or maybe even some positive surprises in summer.

A Appendix

A.1 Object Definitions

Electrons	Baseline	Signal
p_T	$p_\mathrm{T} > 10$ GeV	$p_\mathrm{T} > 25$ GeV
η-acceptance	$\lvert\eta\rvert < 2.47$	$\lvert\eta\rvert < 2.47$
quality	LooseLH	TightLH
isolation	–	GradientLoose
Muons	Baseline	Signal
p_T	$p_\mathrm{T} > 10$ GeV	$p_\mathrm{T} > 10$ GeV
η-acceptance	$\lvert\eta\rvert < 2.5$	$\lvert\eta\rvert < 2.5$
quality	Medium	Medium
isolation	–	GradientLoose
Taus	Baseline	
p_T	$p_\mathrm{T} > 20$ GeV	
η-acceptance	$\lvert\eta\rvert < 2.47$	
n-prongs	1 or 3	
quality	Medium	
jet BDT	medium	
Jets	Baseline	b-jets
Collection	`AntiKt4EMTopo`	`AntiKt4EMTopo`
p_T	$p_\mathrm{T} > 20$ GeV	$p_\mathrm{T} > 20$ GeV
η-acceptance	$\lvert\eta\rvert < 2.8$	$\lvert\eta\rvert < 2.5$
JVT	0.64	0.64
b-tag	–	`MV2c20` 77% OP

Table A.1: Object definitions used in the search for direct sto-to-stau production.

Step	Object removed	Object compared against	Condition
1.	medium tau	baseline electron	$\Delta R < 0.2$
2.	medium tau	baseline muon	$\Delta R < 0.2$
3.	baseline electron	baseline muon	shared ID track
4.	jet	baseline electron	$\Delta R < 0.2$
5.	baseline electron	baseline jet	$\Delta R < 0.2$
6.	baseline muon	baseline jet	$\Delta R < 0.2$
7.	jet	medium tau	$\Delta R < 0.2$

Table A.2: Procedure of the overlap removal

A.2 Preselection Definitions

single-lepton triggers

- HLT_e24_lhmedium_iloose_L1EM20VH
- HLT_mu20_iloose_L1MU15

combined triggers

- HLT_e17_lhmedium_tau25_medium1_tracktwo
- HLT_mu14_tau35_medium1_tracktwo

$E_{\mathrm{T}}^{\mathrm{miss}}$ trigger

- HLT_xe70

preselection	single-lepton	combined	$E_{\mathrm{T}}^{\mathrm{miss}}$ trigger
	el/mu [GeV]	el/mu + tau [GeV]	$E_{\mathrm{T}}^{\mathrm{miss}}$ [GeV]
online threshold(s)	24/20	17/14 + 25/35	70
offline threshold(s)	29/23†	25/21 + 35/45	150
lepton cuts	1 signal el/mu 1 medium tau OS	1 baseline el/mu 1 medium tau OS	1 baseline el/mu‡ 1 medium tau OS
jet cuts	2 baseline jets ldg. jet $p_{\mathrm{T}} > 50$ GeV	2 baseline jets ldg. jet $p_{\mathrm{T}} > 50$ GeV	2 baseline jets ldg. jet $p_{\mathrm{T}} > 50$ GeV

Table A.3: Preselection definitions for single-lepton and combined triggers as well as for the $E_{\mathrm{T}}^{\mathrm{miss}}$ trigger.

† In the SR optimization no additional plateau cuts are necessary as scalefactors are provided for both single-lepton triggers so that they can be used in their turn-on regions. ‡ Due to the additional isolation requirement signal leptons are also used for the $E_{\mathrm{T}}^{\mathrm{miss}}$ trigger in the SR optimization

A.3 Additional Plots for the Signal Grid Validation

This chapter includes some additional information and plots for the signal grid validation.

Dataset IDs of signal samples in earlier MC campaigns

MC12

- LM: 186782

DC14

- LM: 204943
- HM: 204944

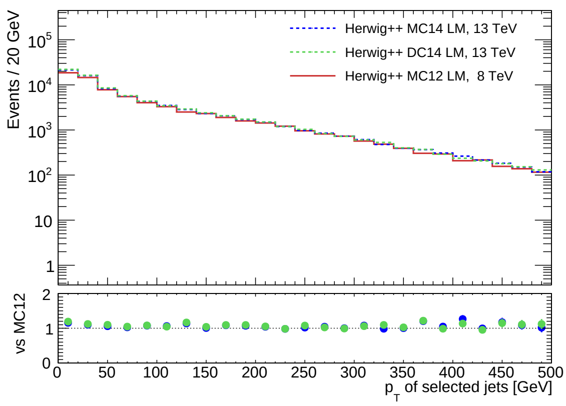

(a) p_{T} distribution for jets in LM.

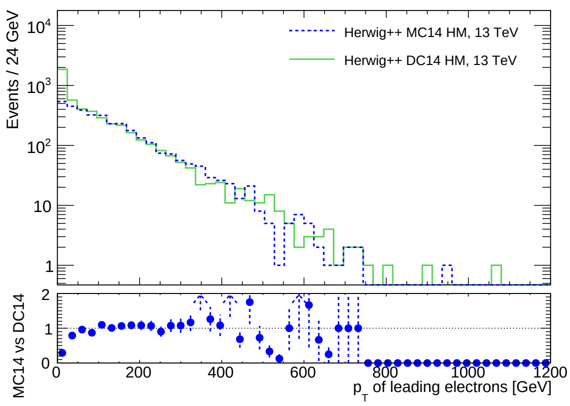

(b) p_{T} distribution for leading electrons in HM.

Figure A.1: Additional plots for the validation of the private MC14 sample (see subsection 5.2.2).

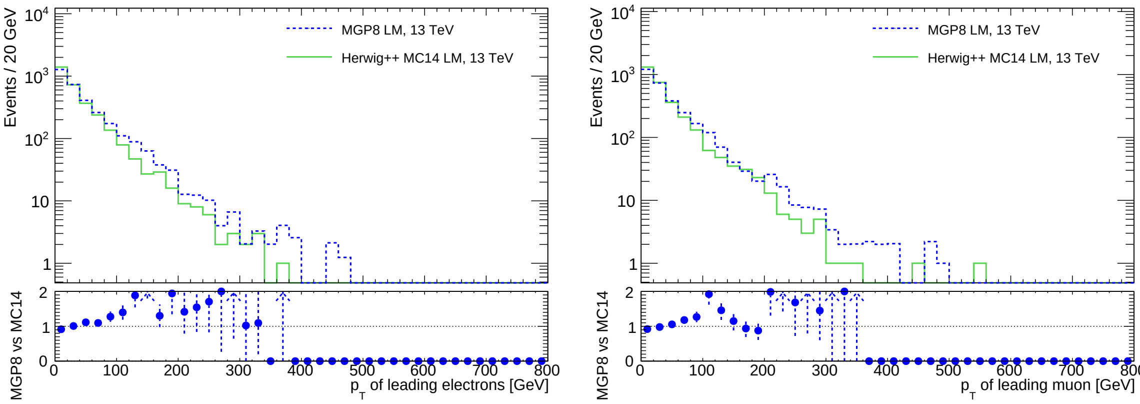

(a) p_{T} distribution for leading electrons in LM. **(b)** p_{T} distribution for leading muons in LM.

Figure A.2: Additional plots for the validation of the new MC configuration sample (see subsection 5.2.3).

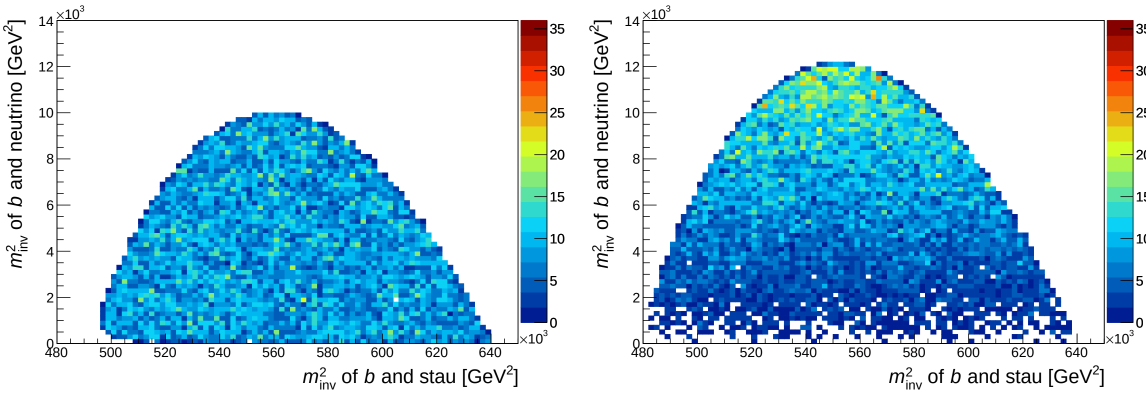

Figure A.3: Dalitz plots showing the invariant mass of the b–neutrino system versus the b–stau system in a HS scenario when the three-body decay is simulated in PYTHIA8 (left) and in MADGRAPH (right). The plots have been created with samples in which the parameters for stop and stau mass differ slightly from each other. This leads to the slight difference in the magnitude of the covered phase space.

A.4 Turn-on Curves for selected Triggers

The turn-curves in this chapter are produced with $t\bar{t}$ events from MC. For the muon and electron triggers a ΔR matching is applied: Only electrons that are matched to a trigger electron signature within a cone of ΔR < 0.2 are considered. These plots serve as an illustration for some features of the triggers which are discussed in the main text.

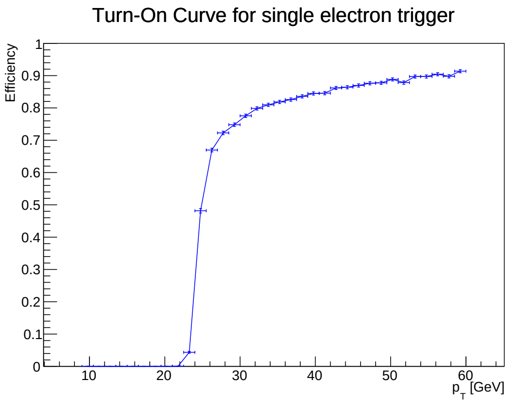

(a) `HLT_e24_lhmedium_iloose_L1EM20VH`

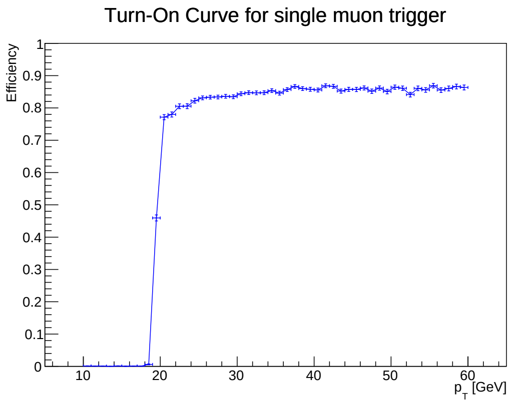

(b) `HLT_mu20_iloose_L1MU15`

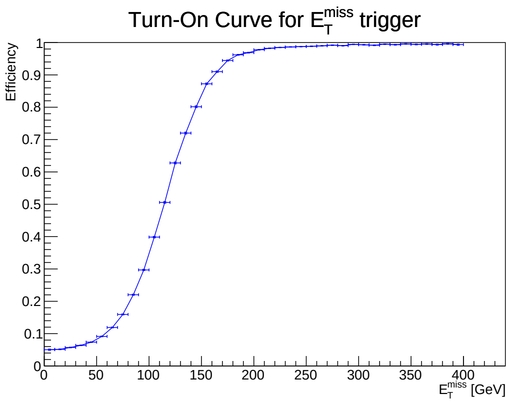

(c) `HLT_xe70`

Figure A.4: Turn-on curves for some of the triggers under consideration in this theses

A.5 Additional Plots for Trigger Studies

If in the comparison of the $E_{\mathrm{T}}^{\mathrm{miss}}$ trigger versus the single leptons triggers, the preselection of the $E_{\mathrm{T}}^{\mathrm{miss}}$ trigger is based on signal leptons as well, the number of additional events gained by it, reduces significantly.

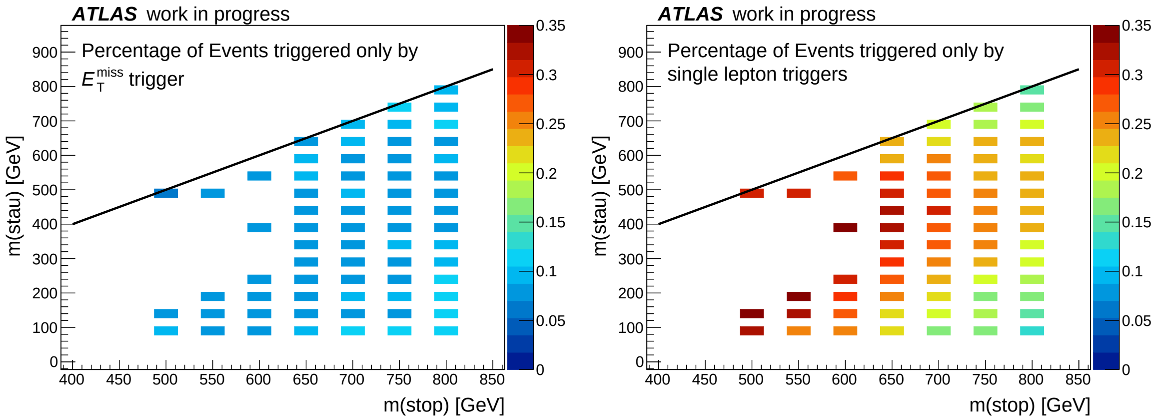

Figure A.5: Performance of $E_{\mathrm{T}}^{\mathrm{miss}}$ trigger (left, using now also signal leptons in its preselection) and single-lepton trigger (right) after the preselection

A.6 Background Composition of the SRs

The following pie charts illustrate how much each process contributes to the total background estimate. The numbers in the parenthesis behind the sample name are the absolute contribution with the associated statistical error and the number of raw MC events, respectively.

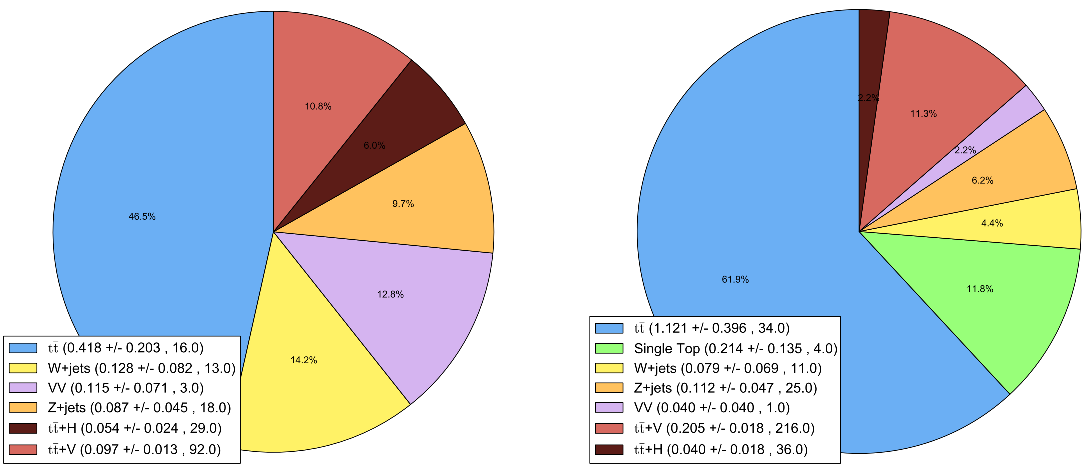

(a) SR for heavy staus (HS) **(b)** SR for light staus (LS)

Figure A.6: Background contributions for the final SR definitions based on single lepton triggers

A.7 Signal Yields for the Signal Regions

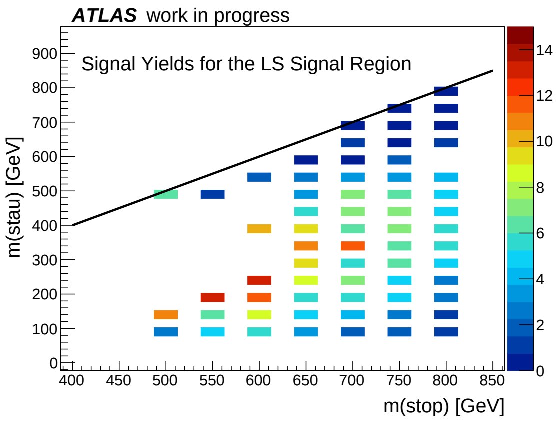

(a) LS Signal Region

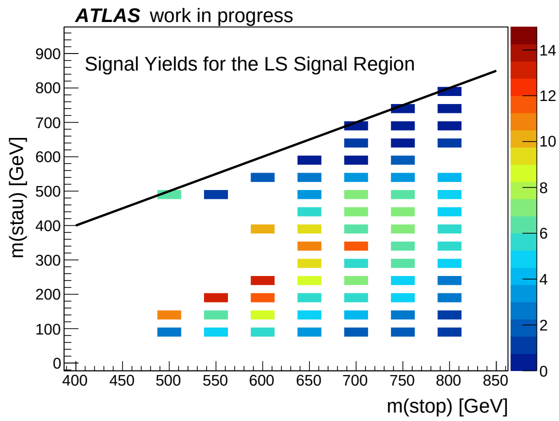

(b) HS Signal Region

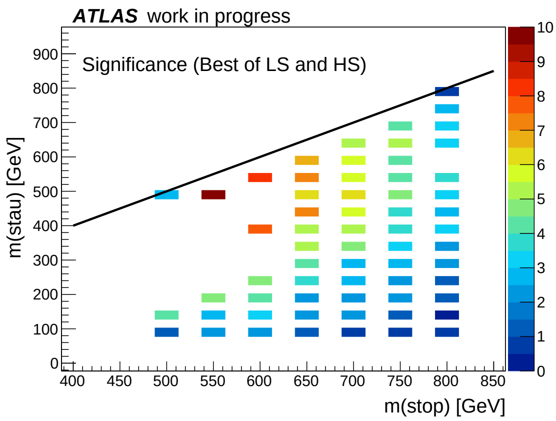

(c) Best significance of both SRs

Figure A.7: Signal yields of the two SRs (top) and the best significance of both for every point in the signal grid.

A.8 Signal Contamination of the CRs

The plots below show the fraction of signal in the sum of the expected signal and background yields for the CRs, called signal contamination. For grid points not within the existing exclusion range, it is less than 1% and hence negligible.

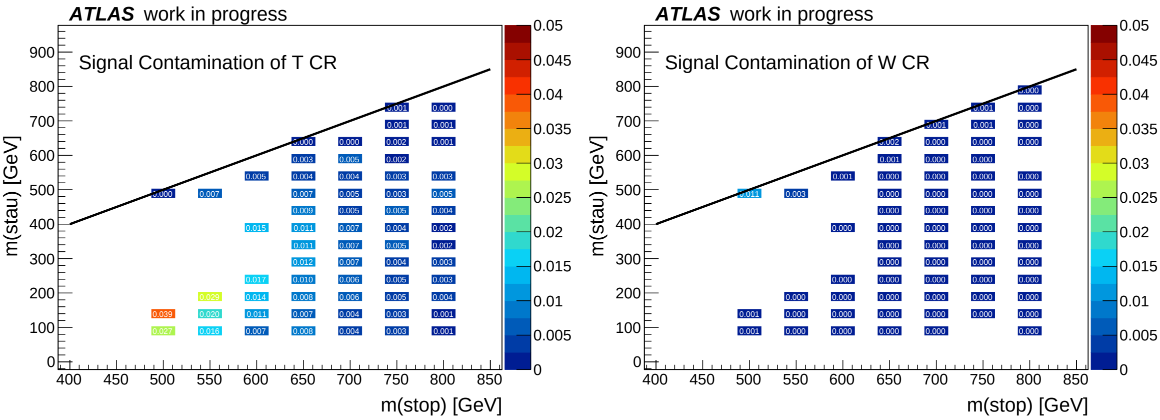

(a) Signal Contamination for the $t\bar{t}$ CR

(b) Signal Contamination for the W CR

Figure A.8: Signal contribution to the total SM background in the preliminary CRs

A.9 Event Yields in the CRs and SRS

The yields were retrieved with the script `YieldsTable.py` contained in the HistFitter package. There are large uncertainties on the signal expectation after the fit, but according to a HistFitter expert error estimation does not change hypothesis test results, so that if the error estimation is off the test results can still be fine.

Sample / Channel	CR W	CR $t\bar{t}$	SR LS	SR HS
Observed events	2465	815	1	0
Fitted bkg events	2466.42 ± 49.69	815.27 ± 28.48	1.68 ± 0.34	$0.48^{+1.67}_{-0.48}$
Fitted ttbar events	536.77 ± 61.58	537.62 ± 44.30	1.10 ± 0.20	0.12 ± 0.01
Fitted WJets events	1531.48 ± 91.44	133.60 ± 13.02	0.07 ± 0.01	0.13 ± 0.01
Fitted ttV events	1.06 ± 0.21	2.67 ± 0.55	0.17 ± 0.04	0.05 ± 0.01
Fitted singletop events	77.63 ± 15.41	120.20 ± 24.67	0.19 ± 0.05	0.00 ± 0.00
Fitted ttH events	0.41 ± 0.08	1.13 ± 0.23	0.04 ± 0.01	0.02 ± 0.00
Fitted Diboson events	154.75 ± 30.77	10.30 ± 2.12	0.04 ± 0.01	0.11 ± 0.02
Fitted ZJets events	164.33 ± 32.66	9.74 ± 2.00	0.06 ± 0.01	0.03 ± 0.01
Fitted Sig_TT_700_540 events	$0.00^{+0.06}_{-0.00}$	$0.01^{+0.51}_{-0.01}$	$0.00^{+0.21}_{-0.00}$	$0.03^{+1.67}_{-0.03}$
MC exp. SM events	2466.40	819.14	3.12	11.92
MC exp. ttbar events	537.54	538.25	1.10	0.12
MC exp. WJets events	1530.18	133.45	0.07	0.13
MC exp. ttV events	1.06	2.67	0.17	0.05
MC exp. singletop events	77.57	120.08	0.19	0.00
MC exp. ttH events	0.41	1.13	0.04	0.02
MC exp. Diboson events	154.90	10.31	0.04	0.11
MC exp. ZJets events	164.32	9.74	0.06	0.03
MC exp. Sig_TT_700_540 events	0.43	3.52	1.44	11.46

Sample / Channel	CR W	CR $t\bar{t}$	SR LS	SR HS
Observed events	2465	815	1	0
Fitted bkg events	2466.21 ± 49.70	815.47 ± 28.52	$1.71^{+3.26}_{-1.71}$	$0.46^{+0.56}_{-0.46}$
Fitted ttbar events	536.74 ± 61.80	537.79 ± 44.50	1.10 ± 0.16	0.12 ± 0.02
Fitted WJets events	1531.14 ± 91.60	133.62 ± 13.05	0.07 ± 0.01	0.13 ± 0.02
Fitted ttV events	1.06 ± 0.21	2.67 ± 0.55	0.17 ± 0.04	0.05 ± 0.01
Fitted singletop events	77.57 ± 15.41	120.15 ± 24.69	0.19 ± 0.04	0.00 ± 0.00
Fitted ttH events	0.41 ± 0.08	1.13 ± 0.23	0.04 ± 0.01	0.02 ± 0.00
Fitted Diboson events	154.94 ± 30.78	10.32 ± 2.12	0.04 ± 0.01	0.11 ± 0.03
Fitted ZJets events	164.36 ± 32.66	9.75 ± 2.00	0.06 ± 0.01	0.03 ± 0.01
Fitted Sig_TT_700_190 events	$0.00^{+0.21}_{-0.00}$	$0.04^{+3.47}_{-0.04}$	$0.04^{+3.28}_{-0.04}$	$0.01^{+0.56}_{-0.01}$
MC exp. SM events	2466.27	820.50	6.31	1.25
MC exp. ttbar events	537.54	538.25	1.10	0.12
MC exp. WJets events	1530.18	133.45	0.07	0.13
MC exp. ttV events	1.06	2.67	0.17	0.05
MC exp. singletop events	77.57	120.08	0.19	0.00
MC exp. ttH events	0.41	1.13	0.04	0.02
MC exp. Diboson events	154.90	10.31	0.04	0.11
MC exp. ZJets events	164.32	9.74	0.06	0.03
MC exp. Sig_TT_700_190 events	0.29	4.88	4.63	0.79

Table A.4: Expected Event Yields in the CRs and SRs for a HS (top) and a LS sample (bottom).

A.10 List of background samples

$t\bar{t}H$ samples

```
mc15_13TeV.341177.aMcAtNloHerwigppEvtGen_UEEE5_CTEQ6L1_CT10ME_ttH125_dil.merge.DAOD_SUSY5.e4277_s2608_s2183_r6869_r6282_p2436
mc15_13TeV.341270.aMcAtNloHerwigppEvtGen_UEEE5_CTEQ6L1_CT10ME_ttH125_semilep.merge.DAOD_SUSY5.e4277_s2608_s2183_r6869_r6282_p2436
mc15_13TeV.341271.aMcAtNloHerwigppEvtGen_UEEE5_CTEQ6L1_CT10ME_ttH125_allhad.merge.DAOD_SUSY5.e4277_s2608_s2183_r6869_r6282_p2436
```

Diboson samples

```
mc15_13TeV.361063.Sherpa_CT10_llll.merge.DAOD_SUSY5.e3836_s2608_s2183_r7267_r6282_p2452
mc15_13TeV.361064.Sherpa_CT10_lllvSFMinus.merge.DAOD_SUSY5.e3836_s2608_s2183_r7267_r6282_p2452
mc15_13TeV.361065.Sherpa_CT10_lllvOFMinus.merge.DAOD_SUSY5.e3836_s2608_s2183_r7267_r6282_p2452
mc15_13TeV.361066.Sherpa_CT10_lllvSFPlus.merge.DAOD_SUSY5.e3836_s2608_s2183_r7267_r6282_p2452
mc15_13TeV.361067.Sherpa_CT10_lllvOFPlus.merge.DAOD_SUSY5.e3836_s2608_s2183_r7267_r6282_p2452
mc15_13TeV.361068.Sherpa_CT10_llvv.merge.DAOD_SUSY5.e3836_s2608_s2183_r7267_r6282_p2452
mc15_13TeV.361069.Sherpa_CT10_llvvjj_ss_EW4.merge.DAOD_SUSY5.e3836_s2608_s2183_r7267_r6282_p2452
mc15_13TeV.361070.Sherpa_CT10_llvvjj_ss_EW6.merge.DAOD_SUSY5.e3836_s2608_s2183_r7267_r6282_p2452
mc15_13TeV.361081.Sherpa_CT10_WplvWmqq.merge.DAOD_SUSY5.e3836_s2608_s2183_r7326_r6282_p2470
mc15_13TeV.361082.Sherpa_CT10_WpqqWmlv.merge.DAOD_SUSY5.e3836_s2608_s2183_r7326_r6282_p2470
mc15_13TeV.361083.Sherpa_CT10_WlvZqq.merge.DAOD_SUSY5.e3836_s2608_s2183_r7326_r6282_p2470
mc15_13TeV.361084.Sherpa_CT10_WqqZll.merge.DAOD_SUSY5.e3836_s2608_s2183_r7326_r6282_p2470
mc15_13TeV.361085.Sherpa_CT10_WqqZvv.merge.DAOD_SUSY5.e3836_s2608_s2183_r6869_r6282_p2452
mc15_13TeV.361086.Sherpa_CT10_ZqqZll.merge.DAOD_SUSY5.e3926_s2608_s2183_r7326_r6282_p2470
mc15_13TeV.361087.Sherpa_CT10_ZqqZvv.merge.DAOD_SUSY5.e3926_s2608_s2183_r6869_r6282_p2452
```

W+jets samples

```
mc15_13TeV.361301.Sherpa_CT10_Wenu_Pt0_70_CFilterBVeto.merge.DAOD_SUSY5.e3651_s2586_s2174_r7326_r6282_p2470
mc15_13TeV.361302.Sherpa_CT10_Wenu_Pt0_70_BFilter.merge.DAOD_SUSY5.e3651_s2586_s2174_r7326_r6282_p2470
mc15_13TeV.361303.Sherpa_CT10_Wenu_Pt70_140_CVetoBVeto.merge.DAOD_SUSY5.e3651_s2586_s2174_r7267_r6282_p2452
mc15_13TeV.361304.Sherpa_CT10_Wenu_Pt70_140_CFilterBVeto.merge.DAOD_SUSY5.e3651_s2586_s2174_r7267_r6282_p2452
mc15_13TeV.361305.Sherpa_CT10_Wenu_Pt70_140_BFilter.merge.DAOD_SUSY5.e3651_s2586_s2174_r7267_r6282_p2470
mc15_13TeV.361306.Sherpa_CT10_Wenu_Pt140_280_CVetoBVeto.merge.DAOD_SUSY5.e3651_s2586_s2174_r7267_r6282_p2452
mc15_13TeV.361307.Sherpa_CT10_Wenu_Pt140_280_CFilterBVeto.merge.DAOD_SUSY5.e3651_s2586_s2174_r7267_r6282_p2452
mc15_13TeV.361308.Sherpa_CT10_Wenu_Pt140_280_BFilter.merge.DAOD_SUSY5.e3651_s2586_s2174_r7267_r6282_p2452
mc15_13TeV.361309.Sherpa_CT10_Wenu_Pt280_500_CVetoBVeto.merge.DAOD_SUSY5.e4133_s2608_s2183_r7326_r6282_p2470
mc15_13TeV.361310.Sherpa_CT10_Wenu_Pt280_500_CFilterBVeto.merge.DAOD_SUSY5.e4133_s2608_s2183_r7326_r6282_p2470
mc15_13TeV.361311.Sherpa_CT10_Wenu_Pt280_500_BFilter.merge.DAOD_SUSY5.e4133_s2608_s2183_r7326_r6282_p2470
mc15_13TeV.361312.Sherpa_CT10_Wenu_Pt500_700_CVetoBVeto.merge.DAOD_SUSY5.e4133_s2608_s2183_r7326_r6282_p2470
mc15_13TeV.361313.Sherpa_CT10_Wenu_Pt500_700_CFilterBVeto.merge.DAOD_SUSY5.e4133_s2608_s2183_r7326_r6282_p2470
mc15_13TeV.361314.Sherpa_CT10_Wenu_Pt500_700_BFilter.merge.DAOD_SUSY5.e4133_s2608_s2183_r7326_r6282_p2470
mc15_13TeV.361315.Sherpa_CT10_Wenu_Pt700_1000_CVetoBVeto.merge.DAOD_SUSY5.e4133_s2608_s2183_r7326_r6282_p2470
mc15_13TeV.361316.Sherpa_CT10_Wenu_Pt700_1000_CFilterBVeto.merge.DAOD_SUSY5.e4133_s2608_s2183_r7326_r6282_p2470
mc15_13TeV.361317.Sherpa_CT10_Wenu_Pt700_1000_BFilter.merge.DAOD_SUSY5.e4133_s2608_s2183_r7326_r6282_p2470
mc15_13TeV.361318.Sherpa_CT10_Wenu_Pt1000_2000_CVetoBVeto.merge.DAOD_SUSY5.e4133_s2608_s2183_r7326_r6282_p2470
mc15_13TeV.361319.Sherpa_CT10_Wenu_Pt1000_2000_CFilterBVeto.merge.DAOD_SUSY5.e4133_s2608_s2183_r7326_r6282_p2470
mc15_13TeV.361320.Sherpa_CT10_Wenu_Pt1000_2000_BFilter.merge.DAOD_SUSY5.e4133_s2608_s2183_r7326_r6282_p2470
mc15_13TeV.361321.Sherpa_CT10_Wenu_Pt2000_E_CMS_CVetoBVeto.merge.DAOD_SUSY5.e4133_s2608_s2183_r7326_r6282_p2470
mc15_13TeV.361322.Sherpa_CT10_Wenu_Pt2000_E_CMS_CFilterBVeto.merge.DAOD_SUSY5.e4133_s2608_s2183_r7326_r6282_p2470
mc15_13TeV.361323.Sherpa_CT10_Wenu_Pt2000_E_CMS_BFilter.merge.DAOD_SUSY5.e4133_s2608_s2183_r7326_r6282_p2470
mc15_13TeV.361324.Sherpa_CT10_Wmunu_Pt0_70_CVetoBVeto.merge.DAOD_SUSY5.e3651_s2608_s2183_r7267_r6282_p2470
mc15_13TeV.361325.Sherpa_CT10_Wmunu_Pt0_70_CFilterBVeto.merge.DAOD_SUSY5.e3651_s2586_s2174_r7267_r6282_p2470
mc15_13TeV.361326.Sherpa_CT10_Wmunu_Pt0_70_BFilter.merge.DAOD_SUSY5.e3651_s2608_s2183_r6869_r6282_p2452
mc15_13TeV.361327.Sherpa_CT10_Wmunu_Pt70_140_CVetoBVeto.merge.DAOD_SUSY5.e3651_s2586_s2174_r7267_r6282_p2452
mc15_13TeV.361328.Sherpa_CT10_Wmunu_Pt70_140_CFilterBVeto.merge.DAOD_SUSY5.e3651_s2586_s2174_r7267_r6282_p2452
mc15_13TeV.361329.Sherpa_CT10_Wmunu_Pt70_140_BFilter.merge.DAOD_SUSY5.e3651_s2586_s2174_r7267_r6282_p2452
mc15_13TeV.361330.Sherpa_CT10_Wmunu_Pt140_280_CVetoBVeto.merge.DAOD_SUSY5.e3651_s2586_s2174_r7267_r6282_p2452
mc15_13TeV.361331.Sherpa_CT10_Wmunu_Pt140_280_CFilterBVeto.merge.DAOD_SUSY5.e3651_s2586_s2174_r7267_r6282_p2452
mc15_13TeV.361332.Sherpa_CT10_Wmunu_Pt140_280_BFilter.merge.DAOD_SUSY5.e3651_s2586_s2174_r7267_r6282_p2452
mc15_13TeV.361333.Sherpa_CT10_Wmunu_Pt280_500_CVetoBVeto.merge.DAOD_SUSY5.e4133_s2608_s2183_r7326_r6282_p2470
mc15_13TeV.361334.Sherpa_CT10_Wmunu_Pt280_500_CFilterBVeto.merge.DAOD_SUSY5.e4133_s2608_s2183_r7326_r6282_p2470
mc15_13TeV.361335.Sherpa_CT10_Wmunu_Pt280_500_BFilter.merge.DAOD_SUSY5.e4133_s2608_s2183_r7326_r6282_p2470
mc15_13TeV.361336.Sherpa_CT10_Wmunu_Pt500_700_CVetoBVeto.merge.DAOD_SUSY5.e4133_s2608_s2183_r7326_r6282_p2470
mc15_13TeV.361337.Sherpa_CT10_Wmunu_Pt500_700_CFilterBVeto.merge.DAOD_SUSY5.e4133_s2608_s2183_r7326_r6282_p2470
mc15_13TeV.361338.Sherpa_CT10_Wmunu_Pt500_700_BFilter.merge.DAOD_SUSY5.e4133_s2608_s2183_r7326_r6282_p2470
mc15_13TeV.361339.Sherpa_CT10_Wmunu_Pt700_1000_CVetoBVeto.merge.DAOD_SUSY5.e4133_s2608_s2183_r7326_r6282_p2470
mc15_13TeV.361340.Sherpa_CT10_Wmunu_Pt700_1000_CFilterBVeto.merge.DAOD_SUSY5.e4133_s2608_s2183_r7326_r6282_p2470
mc15_13TeV.361341.Sherpa_CT10_Wmunu_Pt700_1000_BFilter.merge.DAOD_SUSY5.e4133_s2608_s2183_r7326_r6282_p2470
mc15_13TeV.361342.Sherpa_CT10_Wmunu_Pt1000_2000_CVetoBVeto.merge.DAOD_SUSY5.e4133_s2608_s2183_r7326_r6282_p2470
mc15_13TeV.361343.Sherpa_CT10_Wmunu_Pt1000_2000_CFilterBVeto.merge.DAOD_SUSY5.e4133_s2608_s2183_r7326_r6282_p2470
mc15_13TeV.361344.Sherpa_CT10_Wmunu_Pt1000_2000_BFilter.merge.DAOD_SUSY5.e4133_s2608_s2183_r7326_r6282_p2470
mc15_13TeV.361345.Sherpa_CT10_Wmunu_Pt2000_E_CMS_CVetoBVeto.merge.DAOD_SUSY5.e4133_s2608_s2183_r7326_r6282_p2470
mc15_13TeV.361346.Sherpa_CT10_Wmunu_Pt2000_E_CMS_CFilterBVeto.merge.DAOD_SUSY5.e4133_s2608_s2183_r7326_r6282_p2470
mc15_13TeV.361347.Sherpa_CT10_Wmunu_Pt2000_E_CMS_BFilter.merge.DAOD_SUSY5.e4133_s2608_s2183_r7326_r6282_p2470
mc15_13TeV.361348.Sherpa_CT10_Wtaunu_Pt0_70_CVetoBVeto.merge.DAOD_SUSY5.e3733_s2608_s2183_r7267_r6282_p2470
mc15_13TeV.361349.Sherpa_CT10_Wtaunu_Pt0_70_CFilterBVeto.merge.DAOD_SUSY5.e3733_s2608_s2183_r7267_r6282_p2470
mc15_13TeV.361350.Sherpa_CT10_Wtaunu_Pt0_70_BFilter.merge.DAOD_SUSY5.e3733_s2608_s2183_r7267_r6282_p2470
mc15_13TeV.361351.Sherpa_CT10_Wtaunu_Pt70_140_CVetoBVeto.merge.DAOD_SUSY5.e3733_s2608_s2183_r7267_r6282_p2470
mc15_13TeV.361352.Sherpa_CT10_Wtaunu_Pt70_140_CFilterBVeto.merge.DAOD_SUSY5.e3733_s2608_s2183_r7267_r6282_p2452
mc15_13TeV.361353.Sherpa_CT10_Wtaunu_Pt70_140_BFilter.merge.DAOD_SUSY5.e3733_s2608_s2183_r7267_r6282_p2452
mc15_13TeV.361354.Sherpa_CT10_Wtaunu_Pt140_280_CVetoBVeto.merge.DAOD_SUSY5.e3733_s2608_s2183_r7267_r6282_p2452
mc15_13TeV.361355.Sherpa_CT10_Wtaunu_Pt140_280_CFilterBVeto.merge.DAOD_SUSY5.e3733_s2608_s2183_r7267_r6282_p2452
mc15_13TeV.361356.Sherpa_CT10_Wtaunu_Pt140_280_BFilter.merge.DAOD_SUSY5.e3733_s2608_s2183_r7267_r6282_p2452
mc15_13TeV.361357.Sherpa_CT10_Wtaunu_Pt280_500_CVetoBVeto.merge.DAOD_SUSY5.e4133_s2608_s2183_r7326_r6282_p2470
mc15_13TeV.361358.Sherpa_CT10_Wtaunu_Pt280_500_CFilterBVeto.merge.DAOD_SUSY5.e4133_s2608_s2183_r7326_r6282_p2470
mc15_13TeV.361359.Sherpa_CT10_Wtaunu_Pt280_500_BFilter.merge.DAOD_SUSY5.e4133_s2608_s2183_r7326_r6282_p2470
mc15_13TeV.361360.Sherpa_CT10_Wtaunu_Pt500_700_CVetoBVeto.merge.DAOD_SUSY5.e4133_s2608_s2183_r7326_r6282_p2470
```

mc15_13TeV.361361.Sherpa_CT10_Wtaunu_Pt500_700_CFilterBVeto.merge.DAOD_SUSY5.e4133_s2608_s2183_r7326_r6282_p2470
mc15_13TeV.361362.Sherpa_CT10_Wtaunu_Pt500_700_BFilter.merge.DAOD_SUSY5.e4133_s2608_s2183_r7326_r6282_p2470
mc15_13TeV.361363.Sherpa_CT10_Wtaunu_Pt700_1000_CVetoBVeto.merge.DAOD_SUSY5.e4133_s2608_s2183_r7326_r6282_p2470
mc15_13TeV.361364.Sherpa_CT10_Wtaunu_Pt700_1000_CFilterBVeto.merge.DAOD_SUSY5.e4133_s2608_s2183_r7326_r6282_p2470
mc15_13TeV.361365.Sherpa_CT10_Wtaunu_Pt700_1000_BFilter.merge.DAOD_SUSY5.e4133_s2608_s2183_r7326_r6282_p2470
mc15_13TeV.361366.Sherpa_CT10_Wtaunu_Pt1000_2000_CVetoBVeto.merge.DAOD_SUSY5.e4133_s2608_s2183_r7326_r6282_p2470
mc15_13TeV.361367.Sherpa_CT10_Wtaunu_Pt1000_2000_CFilterBVeto.merge.DAOD_SUSY5.e4133_s2608_s2183_r7326_r6282_p2470
mc15_13TeV.361368.Sherpa_CT10_Wtaunu_Pt1000_2000_BFilter.merge.DAOD_SUSY5.e4133_s2608_s2183_r7326_r6282_p2470
mc15_13TeV.361369.Sherpa_CT10_Wtaunu_Pt2000_E_CMS_CVetoBVeto.merge.DAOD_SUSY5.e4133_s2608_s2183_r7326_r6282_p2470
mc15_13TeV.361370.Sherpa_CT10_Wtaunu_Pt2000_E_CMS_CFilterBVeto.merge.DAOD_SUSY5.e4133_s2608_s2183_r7326_r6282_p2470
mc15_13TeV.361371.Sherpa_CT10_Wtaunu_Pt2000_E_CMS_BFilter.merge.DAOD_SUSY5.e4133_s2608_s2183_r7326_r6282_p2470

Z+jets samples
mc15_13TeV.361372.Sherpa_CT10_Zee_Pt0_70_CVetoBVeto.merge.DAOD_SUSY5.e3651_s2586_s2174_r7267_r6282_p2470
mc15_13TeV.361373.Sherpa_CT10_Zee_Pt0_70_CFilterBVeto.merge.DAOD_SUSY5.e3651_s2586_s2174_r7267_r6282_p2470
mc15_13TeV.361374.Sherpa_CT10_Zee_Pt0_70_BFilter.merge.DAOD_SUSY5.e3651_s2586_s2174_r7267_r6282_p2470
mc15_13TeV.361375.Sherpa_CT10_Zee_Pt70_140_CVetoBVeto.merge.DAOD_SUSY5.e3651_s2586_s2174_r7267_r6282_p2470
mc15_13TeV.361376.Sherpa_CT10_Zee_Pt70_140_CFilterBVeto.merge.DAOD_SUSY5.e3651_s2586_s2174_r7267_r6282_p2452
mc15_13TeV.361377.Sherpa_CT10_Zee_Pt70_140_BFilter.merge.DAOD_SUSY5.e3651_s2586_s2174_r7267_r6282_p2470
mc15_13TeV.361378.Sherpa_CT10_Zee_Pt140_280_CVetoBVeto.merge.DAOD_SUSY5.e3651_s2586_s2174_r7267_r6282_p2470
mc15_13TeV.361379.Sherpa_CT10_Zee_Pt140_280_CFilterBVeto.merge.DAOD_SUSY5.e3651_s2586_s2174_r7267_r6282_p2470
mc15_13TeV.361380.Sherpa_CT10_Zee_Pt140_280_BFilter.merge.DAOD_SUSY5.e3651_s2586_s2174_r7267_r6282_p2470
mc15_13TeV.361381.Sherpa_CT10_Zee_Pt280_500_CVetoBVeto.merge.DAOD_SUSY5.e4133_s2608_s2183_r7326_r6282_p2470
mc15_13TeV.361382.Sherpa_CT10_Zee_Pt280_500_CFilterBVeto.merge.DAOD_SUSY5.e4133_s2608_s2183_r7326_r6282_p2470
mc15_13TeV.361383.Sherpa_CT10_Zee_Pt280_500_BFilter.merge.DAOD_SUSY5.e4133_s2608_s2183_r7326_r6282_p2470
mc15_13TeV.361384.Sherpa_CT10_Zee_Pt500_700_CVetoBVeto.merge.DAOD_SUSY5.e4133_s2608_s2183_r7326_r6282_p2470
mc15_13TeV.361385.Sherpa_CT10_Zee_Pt500_700_CFilterBVeto.merge.DAOD_SUSY5.e4133_s2608_s2183_r7326_r6282_p2470
mc15_13TeV.361386.Sherpa_CT10_Zee_Pt500_700_BFilter.merge.DAOD_SUSY5.e4133_s2608_s2183_r7326_r6282_p2470
mc15_13TeV.361387.Sherpa_CT10_Zee_Pt700_1000_CVetoBVeto.merge.DAOD_SUSY5.e4133_s2608_s2183_r7326_r6282_p2470
mc15_13TeV.361388.Sherpa_CT10_Zee_Pt700_1000_CFilterBVeto.merge.DAOD_SUSY5.e4133_s2608_s2183_r7326_r6282_p2470
mc15_13TeV.361389.Sherpa_CT10_Zee_Pt700_1000_BFilter.merge.DAOD_SUSY5.e4133_s2608_s2183_r7326_r6282_p2470
mc15_13TeV.361390.Sherpa_CT10_Zee_Pt1000_2000_CVetoBVeto.merge.DAOD_SUSY5.e4133_s2608_s2183_r7326_r6282_p2470
mc15_13TeV.361391.Sherpa_CT10_Zee_Pt1000_2000_CFilterBVeto.merge.DAOD_SUSY5.e4133_s2608_s2183_r7326_r6282_p2470
mc15_13TeV.361392.Sherpa_CT10_Zee_Pt1000_2000_BFilter.merge.DAOD_SUSY5.e4133_s2608_s2183_r7326_r6282_p2470
mc15_13TeV.361393.Sherpa_CT10_Zee_Pt2000_E_CMS_CVetoBVeto.merge.DAOD_SUSY5.e4133_s2608_s2183_r7326_r6282_p2470
mc15_13TeV.361394.Sherpa_CT10_Zee_Pt2000_E_CMS_CFilterBVeto.merge.DAOD_SUSY5.e4133_s2608_s2183_r7326_r6282_p2470
mc15_13TeV.361395.Sherpa_CT10_Zee_Pt2000_E_CMS_BFilter.merge.DAOD_SUSY5.e4133_s2608_s2183_r7326_r6282_p2470
mc15_13TeV.361396.Sherpa_CT10_Zmumu_Pt0_70_CVetoBVeto.merge.DAOD_SUSY5.e3651_s2586_s2174_r7267_r6282_p2470
mc15_13TeV.361397.Sherpa_CT10_Zmumu_Pt0_70_CFilterBVeto.merge.DAOD_SUSY5.e3651_s2586_s2174_r7326_r6282_p2452
mc15_13TeV.361398.Sherpa_CT10_Zmumu_Pt0_70_BFilter.merge.DAOD_SUSY5.e3651_s2586_s2174_r7267_r6282_p2470
mc15_13TeV.361399.Sherpa_CT10_Zmumu_Pt70_140_CVetoBVeto.merge.DAOD_SUSY5.e3651_s2586_s2174_r7267_r6282_p2470
mc15_13TeV.361400.Sherpa_CT10_Zmumu_Pt70_140_CFilterBVeto.merge.DAOD_SUSY5.e3651_s2586_s2174_r7267_r6282_p2470
mc15_13TeV.361401.Sherpa_CT10_Zmumu_Pt70_140_BFilter.merge.DAOD_SUSY5.e3651_s2586_s2174_r7267_r6282_p2470
mc15_13TeV.361402.Sherpa_CT10_Zmumu_Pt140_280_CVetoBVeto.merge.DAOD_SUSY5.e3651_s2586_s2174_r7267_r6282_p2470
mc15_13TeV.361403.Sherpa_CT10_Zmumu_Pt140_280_CFilterBVeto.merge.DAOD_SUSY5.e3651_s2586_s2174_r7267_r6282_p2470
mc15_13TeV.361404.Sherpa_CT10_Zmumu_Pt140_280_BFilter.merge.DAOD_SUSY5.e3651_s2586_s2174_r7267_r6282_p2470
mc15_13TeV.361405.Sherpa_CT10_Zmumu_Pt280_500_CVetoBVeto.merge.DAOD_SUSY5.e4133_s2608_s2183_r7326_r6282_p2470
mc15_13TeV.361406.Sherpa_CT10_Zmumu_Pt280_500_CFilterBVeto.merge.DAOD_SUSY5.e4133_s2608_s2183_r7326_r6282_p2470
mc15_13TeV.361407.Sherpa_CT10_Zmumu_Pt280_500_BFilter.merge.DAOD_SUSY5.e4133_s2608_s2183_r7326_r6282_p2470
mc15_13TeV.361408.Sherpa_CT10_Zmumu_Pt500_700_CVetoBVeto.merge.DAOD_SUSY5.e4133_s2608_s2183_r7326_r6282_p2470
mc15_13TeV.361409.Sherpa_CT10_Zmumu_Pt500_700_CFilterBVeto.merge.DAOD_SUSY5.e4133_s2608_s2183_r7326_r6282_p2470
mc15_13TeV.361410.Sherpa_CT10_Zmumu_Pt500_700_BFilter.merge.DAOD_SUSY5.e4133_s2608_s2183_r7326_r6282_p2470
mc15_13TeV.361411.Sherpa_CT10_Zmumu_Pt700_1000_CVetoBVeto.merge.DAOD_SUSY5.e4133_s2608_s2183_r7326_r6282_p2470
mc15_13TeV.361412.Sherpa_CT10_Zmumu_Pt700_1000_CFilterBVeto.merge.DAOD_SUSY5.e4133_s2608_s2183_r7326_r6282_p2470
mc15_13TeV.361413.Sherpa_CT10_Zmumu_Pt700_1000_BFilter.merge.DAOD_SUSY5.e4133_s2608_s2183_r7326_r6282_p2470
mc15_13TeV.361414.Sherpa_CT10_Zmumu_Pt1000_2000_CVetoBVeto.merge.DAOD_SUSY5.e4133_s2608_s2183_r7326_r6282_p2470
mc15_13TeV.361415.Sherpa_CT10_Zmumu_Pt1000_2000_CFilterBVeto.merge.DAOD_SUSY5.e4133_s2608_s2183_r7326_r6282_p2470
mc15_13TeV.361416.Sherpa_CT10_Zmumu_Pt1000_2000_BFilter.merge.DAOD_SUSY5.e4133_s2608_s2183_r7326_r6282_p2470
mc15_13TeV.361417.Sherpa_CT10_Zmumu_Pt2000_E_CMS_CVetoBVeto.merge.DAOD_SUSY5.e4133_s2608_s2183_r7326_r6282_p2470
mc15_13TeV.361418.Sherpa_CT10_Zmumu_Pt2000_E_CMS_CFilterBVeto.merge.DAOD_SUSY5.e4133_s2608_s2183_r7326_r6282_p2470
mc15_13TeV.361419.Sherpa_CT10_Zmumu_Pt2000_E_CMS_BFilter.merge.DAOD_SUSY5.e4133_s2608_s2183_r7326_r6282_p2470
mc15_13TeV.361420.Sherpa_CT10_Ztautau_Pt0_70_CVetoBVeto.merge.DAOD_SUSY5.e3733_s2608_s2183_r7267_r6282_p2470
mc15_13TeV.361421.Sherpa_CT10_Ztautau_Pt0_70_CFilterBVeto.merge.DAOD_SUSY5.e3733_s2608_s2183_r7267_r6282_p2470
mc15_13TeV.361422.Sherpa_CT10_Ztautau_Pt0_70_BFilter.merge.DAOD_SUSY5.e3733_s2608_s2183_r7267_r6282_p2470
mc15_13TeV.361423.Sherpa_CT10_Ztautau_Pt70_140_CVetoBVeto.merge.DAOD_SUSY5.e3733_s2608_s2183_r7267_r6282_p2470
mc15_13TeV.361424.Sherpa_CT10_Ztautau_Pt70_140_CFilterBVeto.merge.DAOD_SUSY5.e3733_s2608_s2183_r7267_r6282_p2470
mc15_13TeV.361425.Sherpa_CT10_Ztautau_Pt70_140_BFilter.merge.DAOD_SUSY5.e3733_s2608_s2183_r7267_r6282_p2470
mc15_13TeV.361426.Sherpa_CT10_Ztautau_Pt140_280_CVetoBVeto.merge.DAOD_SUSY5.e3733_s2608_s2183_r7267_r6282_p2470
mc15_13TeV.361427.Sherpa_CT10_Ztautau_Pt140_280_CFilterBVeto.merge.DAOD_SUSY5.e3733_s2608_s2183_r7267_r6282_p2470
mc15_13TeV.361428.Sherpa_CT10_Ztautau_Pt140_280_BFilter.merge.DAOD_SUSY5.e3733_s2608_s2183_r7267_r6282_p2470
mc15_13TeV.361429.Sherpa_CT10_Ztautau_Pt280_500_CVetoBVeto.merge.DAOD_SUSY5.e4133_s2608_s2183_r7326_r6282_p2470
mc15_13TeV.361430.Sherpa_CT10_Ztautau_Pt280_500_CFilterBVeto.merge.DAOD_SUSY5.e4133_s2608_s2183_r7326_r6282_p2470
mc15_13TeV.361431.Sherpa_CT10_Ztautau_Pt280_500_BFilter.merge.DAOD_SUSY5.e4133_s2608_s2183_r7326_r6282_p2470
mc15_13TeV.361432.Sherpa_CT10_Ztautau_Pt500_700_CVetoBVeto.merge.DAOD_SUSY5.e4133_s2608_s2183_r7326_r6282_p2470
mc15_13TeV.361433.Sherpa_CT10_Ztautau_Pt500_700_CFilterBVeto.merge.DAOD_SUSY5.e4133_s2608_s2183_r7326_r6282_p2470
mc15_13TeV.361434.Sherpa_CT10_Ztautau_Pt500_700_BFilter.merge.DAOD_SUSY5.e4133_s2608_s2183_r7326_r6282_p2470
mc15_13TeV.361435.Sherpa_CT10_Ztautau_Pt700_1000_CVetoBVeto.merge.DAOD_SUSY5.e4133_s2608_s2183_r7326_r6282_p2470
mc15_13TeV.361436.Sherpa_CT10_Ztautau_Pt700_1000_CFilterBVeto.merge.DAOD_SUSY5.e4133_s2608_s2183_r7326_r6282_p2470
mc15_13TeV.361437.Sherpa_CT10_Ztautau_Pt700_1000_BFilter.merge.DAOD_SUSY5.e4133_s2608_s2183_r7326_r6282_p2470
mc15_13TeV.361438.Sherpa_CT10_Ztautau_Pt1000_2000_CVetoBVeto.merge.DAOD_SUSY5.e4133_s2608_s2183_r7326_r6282_p2470
mc15_13TeV.361439.Sherpa_CT10_Ztautau_Pt1000_2000_CFilterBVeto.merge.DAOD_SUSY5.e4133_s2608_s2183_r7326_r6282_p2470
mc15_13TeV.361440.Sherpa_CT10_Ztautau_Pt1000_2000_BFilter.merge.DAOD_SUSY5.e4133_s2608_s2183_r7326_r6282_p2470
mc15_13TeV.361441.Sherpa_CT10_Ztautau_Pt2000_E_CMS_CVetoBVeto.merge.DAOD_SUSY5.e4133_s2608_s2183_r7326_r6282_p2470
mc15_13TeV.361442.Sherpa_CT10_Ztautau_Pt2000_E_CMS_CFilterBVeto.merge.DAOD_SUSY5.e4133_s2608_s2183_r7326_r6282_p2470
mc15_13TeV.361443.Sherpa_CT10_Ztautau_Pt2000_E_CMS_BFilter.merge.DAOD_SUSY5.e4133_s2608_s2183_r7326_r6282_p2470
mc15_13TeV.361444.Sherpa_CT10_Znunu_Pt0_70_CVetoBVeto.merge.DAOD_SUSY5.e3651_s2608_s2183_r7267_r6282_p2452

```
mc15_13TeV.361445.Sherpa_CT10_Znunu_Pt0_70_CFilterBVeto.merge.DAOD_SUSY5.e3651_s2586_s2174_r7267_r6282_p2452
mc15_13TeV.361446.Sherpa_CT10_Znunu_Pt0_70_BFilter.merge.DAOD_SUSY5.e3651_s2586_s2174_r7267_r6282_p2452
mc15_13TeV.361447.Sherpa_CT10_Znunu_Pt70_140_CVetoBVeto.merge.DAOD_SUSY5.e3651_s2586_s2174_r7267_r6282_p2452
mc15_13TeV.361448.Sherpa_CT10_Znunu_Pt70_140_CFilterBVeto.merge.DAOD_SUSY5.e3651_s2586_s2174_r7267_r6282_p2452
mc15_13TeV.361449.Sherpa_CT10_Znunu_Pt70_140_BFilter.merge.DAOD_SUSY5.e3651_s2586_s2174_r7267_r6282_p2452
mc15_13TeV.361450.Sherpa_CT10_Znunu_Pt140_280_CVetoBVeto.merge.DAOD_SUSY5.e3651_s2586_s2174_r7267_r6282_p2452
mc15_13TeV.361451.Sherpa_CT10_Znunu_Pt140_280_CFilterBVeto.merge.DAOD_SUSY5.e3651_s2586_s2174_r7267_r6282_p2452
mc15_13TeV.361452.Sherpa_CT10_Znunu_Pt140_280_BFilter.merge.DAOD_SUSY5.e3651_s2586_s2174_r7267_r6282_p2452
mc15_13TeV.361453.Sherpa_CT10_Znunu_Pt280_500_CVetoBVeto.merge.DAOD_SUSY5.e4133_s2608_s2183_r7326_r6282_p2470
mc15_13TeV.361454.Sherpa_CT10_Znunu_Pt280_500_CFilterBVeto.merge.DAOD_SUSY5.e4133_s2608_s2183_r7326_r6282_p2470
mc15_13TeV.361455.Sherpa_CT10_Znunu_Pt280_500_BFilter.merge.DAOD_SUSY5.e4133_s2608_s2183_r7326_r6282_p2470
mc15_13TeV.361456.Sherpa_CT10_Znunu_Pt500_700_CVetoBVeto.merge.DAOD_SUSY5.e4133_s2608_s2183_r7326_r6282_p2470
mc15_13TeV.361457.Sherpa_CT10_Znunu_Pt500_700_CFilterBVeto.merge.DAOD_SUSY5.e4133_s2608_s2183_r7326_r6282_p2470
mc15_13TeV.361458.Sherpa_CT10_Znunu_Pt500_700_BFilter.merge.DAOD_SUSY5.e4133_s2608_s2183_r7326_r6282_p2470
mc15_13TeV.361459.Sherpa_CT10_Znunu_Pt700_1000_CVetoBVeto.merge.DAOD_SUSY5.e4133_s2608_s2183_r7326_r6282_p2470
mc15_13TeV.361460.Sherpa_CT10_Znunu_Pt700_1000_CFilterBVeto.merge.DAOD_SUSY5.e4133_s2608_s2183_r7326_r6282_p2470
mc15_13TeV.361461.Sherpa_CT10_Znunu_Pt700_1000_BFilter.merge.DAOD_SUSY5.e4133_s2608_s2183_r7326_r6282_p2470
mc15_13TeV.361462.Sherpa_CT10_Znunu_Pt1000_2000_CVetoBVeto.merge.DAOD_SUSY5.e4133_s2608_s2183_r7326_r6282_p2470
mc15_13TeV.361463.Sherpa_CT10_Znunu_Pt1000_2000_CFilterBVeto.merge.DAOD_SUSY5.e4133_s2608_s2183_r7326_r6282_p2470
mc15_13TeV.361464.Sherpa_CT10_Znunu_Pt1000_2000_BFilter.merge.DAOD_SUSY5.e4133_s2608_s2183_r7326_r6282_p2470
mc15_13TeV.361465.Sherpa_CT10_Znunu_Pt2000_E_CMS_CVetoBVeto.merge.DAOD_SUSY5.e4133_s2608_s2183_r7326_r6282_p2470
mc15_13TeV.361466.Sherpa_CT10_Znunu_Pt2000_E_CMS_CFilterBVeto.merge.DAOD_SUSY5.e4133_s2608_s2183_r7326_r6282_p2470
mc15_13TeV.361467.Sherpa_CT10_Znunu_Pt2000_E_CMS_BFilter.merge.DAOD_SUSY5.e4133_s2608_s2183_r7326_r6282_p2470
```

$t\bar{t}$ samples

```
mc15_13TeV.407012.PowhegPythiaEvtGen_P2012CT10_ttbarMET200_hdamp172p5_nonAH.merge.DAOD_SUSY5.e4023_s2608_r7326_r6282_p2470
mc15_13TeV.410000.PowhegPythiaEvtGen_P2012_ttbar_hdamp172p5_nonallhad.merge.DAOD_SUSY5.e3698_s2608_s2183_r7267_r6282_p2470
mc15_13TeV.410007.PowhegPythiaEvtGen_P2012_ttbar_hdamp172p5_allhad.merge.DAOD_SUSY5.e4135_s2608_s2183_r6869_r6282_p2436
```

single top samples

```
mc15_13TeV.410011.PowhegPythiaEvtGen_P2012_singletop_tchan_lept_top.merge.DAOD_SUSY5.e3824_s2608_s2183_r7326_r6282_p2470
mc15_13TeV.410012.PowhegPythiaEvtGen_P2012_singletop_tchan_lept_antitop.merge.DAOD_SUSY5.e3824_s2608_s2183_r7326_r6282_p2470
mc15_13TeV.410013.PowhegPythiaEvtGen_P2012_Wt_inclusive_top.merge.DAOD_SUSY5.e3753_s2608_s2183_r7326_r6282_p2470
mc15_13TeV.410014.PowhegPythiaEvtGen_P2012_Wt_inclusive_antitop.merge.DAOD_SUSY5.e3753_s2608_s2183_r7326_r6282_p2470
mc15_13TeV.410015.PowhegPythiaEvtGen_P2012_Wt_dilepton_top.merge.DAOD_SUSY5.e3753_s2608_s2183_r7326_r6282_p2470
mc15_13TeV.410016.PowhegPythiaEvtGen_P2012_Wt_dilepton_antitop.merge.DAOD_SUSY5.e3753_s2608_s2183_r7326_r6282_p2470
mc15_13TeV.410025.PowhegPythiaEvtGen_P2012_SingleTopSchan_noAllHad_top.merge.DAOD_SUSY5.e3998_s2608_s2183_r7326_r6282_p2470
mc15_13TeV.410026.PowhegPythiaEvtGen_P2012_SingleTopSchan_noAllHad_antitop.merge.DAOD_SUSY5.e3998_s2608_s2183_r7326_r6282_p2470
```

$t\bar{t}V$ samples

```
mc15_13TeV.410066.MadGraphPythia8EvtGen_A14NNPDF23LO_ttW_Np0.merge.DAOD_SUSY5.e4111_s2608_s2183_r7326_r6282_p2470
mc15_13TeV.410067.MadGraphPythia8EvtGen_A14NNPDF23LO_ttW_Np1.merge.DAOD_SUSY5.e4111_s2608_s2183_r7326_r6282_p2470
mc15_13TeV.410068.MadGraphPythia8EvtGen_A14NNPDF23LO_ttW_Np2.merge.DAOD_SUSY5.e4111_s2608_s2183_r7326_r6282_p2470
mc15_13TeV.410073.MadGraphPythia8EvtGen_A14NNPDF23LO_ttZnnqq_Np0.merge.DAOD_SUSY5.e4111_s2608_s2183_r7326_r6282_p2470
mc15_13TeV.410074.MadGraphPythia8EvtGen_A14NNPDF23LO_ttZnnqq_Np1.merge.DAOD_SUSY5.e4143_s2608_s2183_r7326_r6282_p2470
mc15_13TeV.410075.MadGraphPythia8EvtGen_A14NNPDF23LO_ttZnnqq_Np2.merge.DAOD_SUSY5.e4111_s2608_s2183_r7326_r6282_p2470
```

Bibliography

[1] G. Kane and A. Pierce, *Perspectives on LHC Physics*. World Scientific, 2011.

[2] S. P. Martin, "A Supersymmetry Primer," 1997.

[3] P. Binétruy, *Supersymmetry Theory, Experiment, and Cosmology*. Oxford University Press, 2006.

[4] I. Aitchison, *Supersymmetry in Particle Physics An Elementary Introduction*. Cambridge University Press, 2007.

[5] K. Garrett and G. Duda, "Dark Matter: A Primer." Adv.Astron.2011:968283,2011, 2010.

[6] P. Langacker, "Grand unification," 2012. [Online; accessed 4-April-2016].

[7] O. Pelc and L. P. Horwitz, "Generalization of the Coleman-Mandula Theorem to Higher Dimension." J.Math.Phys. 38 (1997) 139-172, 1996.

[8] LHCb, "LHCb experiment — b is for beauty," 2016. [Online; accessed 10-March-2016].

[9] C. Lefevre, "LHC: the guide (English version)." Feb 2009.

[10] I. Brock and T. Schorner-Sadenius, *Physics at the Terascale*. Wiley, 2011.

[11] CERN, "Restarting the LHC: Why 13 Tev?," 2016. [Online; accessed 11-March-2016].

[12] "LHC Season 2. LHC Saison 2." Mar 2015.

[13] CERN, "CERN Document Server," 2008. [Online; accessed 20-April-2016].

[14] The ATLAS Collaboration, "The ATLAS Experiment at the CERN Large Hadron Collider," *Journal of Instrumentation*, vol. 3, no. 08, 2008.

[15] Y. Takubo, "The pixel detector of the atlas experiment for the run2 at the large hadron collider," 2014.

[16] ATLAS Internal Documentation, "ATLAS coordinate system." https://twiki.cern.ch/twiki/bin/view/AtlasProtected/CcordinateSystemFootnote, Mar. 2016.

[17] Y. Nakahama, "The atlas trigger system: Ready for run-2," *Journal of Physics: Conference Series*, vol. 664, no. 8, p. 082037, 2015.

[18] M. Baak and G. J. Besjes and D. Cote and A. Koutsman and J. Lorenz and D. Short, "HistFitter software framework for statistical data analysis," 2014.

[19] ATLAS Internal Documentation, "SUSY Feynman Diagrams." https://twiki.cern.ch/twiki/bin/view/AtlasProtected/SUSYFeynmanDiagrams, Mar. 2016.

[20] ATLAS Collaboration, "Search for direct top squark pair production in final states with two tau leptons in pp collisions at $\sqrt{s}$ = 8 TeV with the ATLAS detector." Eur. Phys. J. C (2016) 76:81, 2015.

[21] The LEP SUSY Working Group and ALEPH, DELPHI, L3, OPAL experiments, "Combined LEP selectron/smuon/stau results, 183-208 GeV." http://lepsusy.web.cern.ch/lepsusy/www/sleptons_summer04/slep_final.html, Mar. 2016.

[22] W.J. Stirling, "PARTON LUMINOSITY AND CROSS SECTION PLOTS ." http://www.hep.ph.ic.ac.uk/~wstirlin/plots/plots.html, Apr. 2016.

[23] ATLAS Internal Documentation, "LHC SUSY Cross Section Working Group ." https://twiki.cern.ch/twiki/bin/view/LHCPhysics/SUSYCrossSections13TeVstopsbottom, Apr. 2016.

[24] ATLAS Internal Documentation, "NNLO+NNLL top-quark-pair cross sections." https://twiki.cern.ch/twiki/bin/view/LHCPhysics/TtbarNNLO#Top_quark_pair_cross_sections_at, Apr. 2016.

[25] G. Cowan, *Statistical Data Analysis*. Oxford University Press, 1989.

[26] T. Sjöstrand, "Monte Carlo event generation for LHC." 14th CERN School of Computing, 1991.

[27] ATLAS Collaboration, "Search for direct electro-weakino and slepton production in events with at least two hadronic taus and missing transverse momentum at $\sqrt{\text{s}}$ = 13 TeV (supporting INT note)," Tech. Rep. ATL-COM-PHYS-2015-1284, CERN, Geneva, Oct 2015.

[28] ATLAS Collaboration, "Supporting document on electron identification and efficiency measurements using the 2015 LHC proton-proton collision data," Tech. Rep. ATL-COM-PHYS-2016-041, CERN, Geneva, Jan 2016.

[29] ATLAS Collaboration, "Muon reconstruction performance in early $\sqrt{}$ s=13 TeV data," Tech. Rep. ATL-PHYS-PUB-2015-037, CERN, Geneva, Aug 2015.

[30] ATLAS Collaboration, "Identification and energy calibration of hadronically decaying tau leptons with the atlas experiment in pp collisions at $\sqrt{s}$=8 tev." Eur. Phys. J. C75 (2015) 303, 2014.

[31] ATLAS Collaboration, "Reconstruction and Performance of Missing Transverse Momentum in the ATLAS Detector in Proton-Proton Collisions at $\sqrt{s} = 8$ TeV," Tech. Rep. ATL-COM-PHYS-2015-341, CERN, Geneva, Apr 2015.

[32] B. Lindquist, "Dalitz Plots." http://www.slac.stanford.edu/slac/sass/talks/BrianL.pdf, Nov. 2010. SLAC SASS Talk.

[33] K. A. Olive *et al.*, "Review of Particle Physics," *Chin. Phys.*, vol. C38, 2014.

[34] J. Alwall, "Parton showers and MLM matching." http://phys.cts.ntu.edu.tw/workshop/2012/1010525LHC/PDF/NTU-MLM-lectures.pdf, May. 2012. NTU MadGraph school.

[35] M. Alexander, "Calorimeter-Based Triggers At The ATLAS Detector For Searches For Supersymmetry In Zero-Lepton Final States," 2012.

[36] R. D. Cousins, J. T. Linnemann, and J. Tucker, "Evaluation of three methods for calculating statistical significance when incorporating a systematic uncertainty into a test of the background-only hypothesis for a Poisson process." Nuclear Instruments and Methods in Physics Research A 595 (2008) 480–501, 2007.

[37] C. G. Lester and D. J. Summers, "Measuring masses of semi-invisibly decaying particles pair produced at hadron colliders." Phys.Lett.B463:99-103,1999, 1999.

[38] W. Verkerke, "Practical Statistics for Particle Physicists." ESHEP 2014, 2014.

[39] G. Cowan, "Some Prospects for Statistical Data Analysis in High Energy Physics." Terascale Statistics School 2016, 2016.

[40] K. Cranmer, "Practical Statistics for Particle Physics." CERN School HEP, Romania, Sept. 2011, 2011.

[41] R. Camacho, M. Casolino, C. Delitzsch, T. Farooque, K. Hegazy, D. Marley, B. Nachman, P. Nef, H. Resin, A. Schwartzman, M. Solt, M. Swiatlowski, and C. Wanotayaroj, "Jet Re-clustering in ATLAS," Tech. Rep. ATL-COM-PHYS-2014-1117, CERN, Geneva, Sep 2014.

Danksagung

An dieser Stelle noch ein herzlicher Dank für das tolle Jahr, insbesondere an

- den gesamten Lehrstuhl in Garching für die entspannte Atmosphäre und generelle Hilfsbereitschaft, egal bei was man Probleme hat
- Dorothee für ihre Kommentare vor der Abgabe und die Möglichkeit die neuesten Ergebnisse der Teilchenphysik auch weiterhin aus erster Hand zu erfahren
- Alexander, der mir auch gerne alles zweimal (oder noch öfter) erklärt
- Balthasar, der sich meinen Code immer solange anhört, bis ich selber weiss wo der Fehler ist
- Christopher für sein Framework und die daraus resultierende Einfürung in C^{++} templates
- Nikolai für seinen ARRGH Code, die N-1 plotting Skripte und zahllose aber lehrreiche Diskussionen über HistFitter und Statistik
- und natürlich meine Familie die mich während des gesamten Studiums unterstützt hat

Erklärung

Hiermit erkläre ich, die vorliegende Arbeit selbständig verfasst zu haben und keine anderen als die in der Arbeit angegebenen Quellen und Hilfsmittel benutzt zu haben.

München, 04.05.2016

Michael Holzbock